地磁気観測所要報 第28巻 平成12年3月
Memoirs of the Kakioka Magnetic Observatory Vol.28, March 2000

On the Contribution of Global Scale Polar-originating Ionospheric Current Systems to Geomagnetic Disturbances in Middle and Low Latitudes

by

Satoru TSUNOMURA

(Received in final form December 24, 1999)

Polar-originating Ionospheric Current System

Abstract

It is important to examine the characteristics of polar-originating ionospheric current systems for the study of geomagnetic disturbances in middle and low latitudes. The purpose of this paper is to quantitatively clarify the characteristics of polar-originating ionospheric current systems, which concern with geomagnetic disturbances observed in middle and low latitudes. This paper is composed of two main parts. One is for numerical analyses for polar-originating ionospheric current systems including the equatorial enhancement of the ionospheric conductivity and the other is for investigations of the characteristics of geomagnetic sudden commencement (SC) in middle and low latitudes. The latter is aimed to clarify the contribution of the SC-associated polar-originating ionospheric current system for the magnetic variations in middle and low latitudes.

The first part:

At first, the effect of the equatorial enhancement of the ionospheric conductivity for a global, polar-originating ionospheric current is estimated by solving numerically a continuity equation of the ionospheric electric current on a two-dimensional spherical shell, setting some simplifications for a realistic ionospheric conductivity model. Clear daytime equatorial enhancement of the ionospheric current is seen in spite of the reduction of electric field due to the shielding effect of the enhanced equatorial conductivity. The calculated profiles of the ionospheric currents are generally in agreement with the observed characteristics of preliminary impulse (PI) of SC.

Then, a modeling method to derive a two-dimensional ionospheric layer conductivity, which is appropriate for obtaining a realistic solution of the numerical simulation of the polar-originating ionospheric current systems, is developed. The model can be derived modifying the conventional, thin shell conductivity model. It is shown that the modification for $\Sigma_{\theta\varphi}$, one of the non-diagonal terms in the conductivity tensor, near the equatorial region is very important; the term influences the profile of the ionospheric electric field at the equator drastically. The proposed model can well reproduce the results representing the observed electric and magnetic field signatures of SC. Then the new model is applied to examine three matters concerning

polar-originating ionospheric current systems. At first, the latitudinal profile of the DP2 amplitude in the daytime is examined, changing the canceling rate for the dawn-to-dusk electric field by the Region 2 field-aligned current. It is shown that the equatorial enhancement would not be appeared when the ratio of the total amount of the Region 2 field-aligned current to that of the Region 1 exceeds 0.5. Second, the north-south asymmetry of magnetic variations for the summer solstice condition of the ionospheric conductivity is examined calculating the global ionospheric current covering both hemispheres simultaneously. It is shown that the positive relationship between the magnitude of high latitude magnetic field and the conductivity is clearly seen if a voltage generator is give as the source; while the relationship is vague or even reversed for a current generator. Finally, the solar cycle dependence of the equatorial electric and magnetic fields due to the polar-originating ionsopheric current system is examined by comparing the results for the conductivity models corresponding to the solar maximum and minimum periods. The result agrees well with the observed feature in the solar cycle dependence of the local time profile of the equatorial enhancement rate of SC. The new model, being based on the International Reference Ionosphere (IRI) model, can be applied for further investigations in the quantitative analysis of the magnetosphere-ionosphere coupling problems.

The second part:

A statistical analysis is made for the polarity of SC observed at Kakioka, using the routine reports of SC from 1957 to 1992. It is shown that the polarity of the geomagnetically eastward component (D-component) is positive in most cases as well as the geomagnetically northward (H) and vertically downward (Z) components. In the statistics taken on the basis of the magnetic data converted to the geomagnetic dipole coordinate system, there is not a definite shift in the polarity of the D-component for SC; the result agrees well with the polar-originating ionospheric current system model for SC given by Araki (1977). However, correlation coefficients among Memambetsu, Kakioka and Kanoya do not always become higher by the conversion to the geomagnetic dipole coordinate system. It is also found that amplitude ratios of SC at Kakioka and Kanoya to that at Memambetsu reveal an anomalous local time change for the H-component in the morning hours.

A stacking data analysis using routine magnetic observations in middle and low latitudes is made to clarify the characteristics of SC in the H-component in the morning hours. It is found that a negative impulse is usually superposed on main impulse (MI) of SC in the H-component just after its onset, at the stations located in middle and low latitudes in the local time range from the morning to the early afternoon. After case studies and a numerical analysis, it is suggested that this negative impulse is a signature of the magnetic variation due to the polar-originating ionospheric current system responsible for MI of SC. A morphological interpretation that SC-associated preliminary positive impulse (PPI) is the apparent variation, which is visualized by combining the northward magnetic variation due to the magnetospheric compression and the negative impulse, is proposed. A possible interpretation for the variation form of the SC on March 24, 1991 is presented by a numerical calculation giving a high latitude source shifted four hours to the evening side. Finally the availability of the D-component magnetic data in middle latitudes for a rough estimation of the SC-associated magnetosphere-ionosphere coupling process is suggested.

CONTENTS

1. Introduction

1.1 Geomagnetic Disturbances in Middle and Low Latitudes

Time variation of the Earth's natural magnetic field (geomagnetic field) is one of the main matters of geophysical interest. There are many kinds of time variation signatures of the geomagnetic field, time-scales of which are ranging from less than one second to more than one million years. They are attributed to time-varying electric currents inside or outside the Earth and have wavelengths from several km to more than one hundred thousand km. To clarify their properties, it is ideal to observe the time variation of the magnetic field at as many sites as possible including those outside the Earth; however, it is practically impossible.

The observation for the natural geomagnetic field is categorized into two kinds; one is a continuous measurement of the magnetic field with a sampling rate of one minute or second at a fixed place (observatory) and the other is a magnetic survey. In both schemes, components and/or the total intensity of the magnetic field vector are measured, only subtracting a bias or operating a simple high-pass filter; no special modulations in amplitude or frequency are made for the measurement usually. In general, the former is operated in the scope of monitoring global characteristics of the geomagnetic field and the latter to infer the electrical structure under the ground. In this study the signatures of upper atmospheric processes in time variations of geomagnetic fields in middle and low latitudes will be studied.

In most observatories, three components of the magnetic field vector are measured using a three-axis fluxgate magnetometer or similar variation instruments, such as the classical variometer, and the total intensity by a proton precession magnetometer (e. g. Kuwashima, 1990; Tsunomura et al., 1994). Conventionally, the measured data are compiled as horizontal intensity (H), declination (D), vertical intensity (Z) and total intensity (F). In some observatories, the former two are replaced with the geographic northward (X) and eastward (Y) components. The declination is expressed as a dimensionless number expressing the angle while others as the magnetic flux density. To make a data process simpler, the data of H and D are converted to a couple of two components, that is, the local geomagnetic northward and eastward components. At stations operated under special scientific projects such as the 210° magnetic meridian observatory network (Yumoto and the 210° MM Magnetic Observation Group, 1996), the magnetic data in the horizontal plane are reported as these components automatically. In this paper, the abbreviations of H- and D-components are used to denote these.

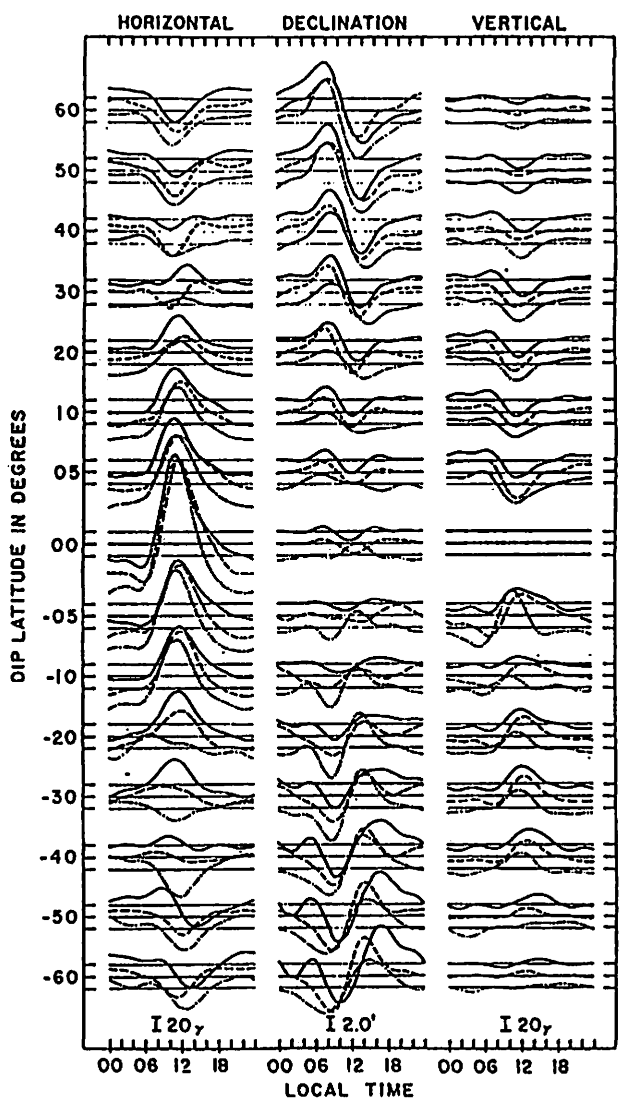

Figure 1-1(a): Solar quiet daily variations of the geomagnetic three components at several dip latitudes from 60° to –60° in zones of the Europe-Africa (solid curves), the Asia-Australia (broken curves), and the North America-South America (chain curves) for equinoctial months (after Matsushita and Maeda, 1965a).

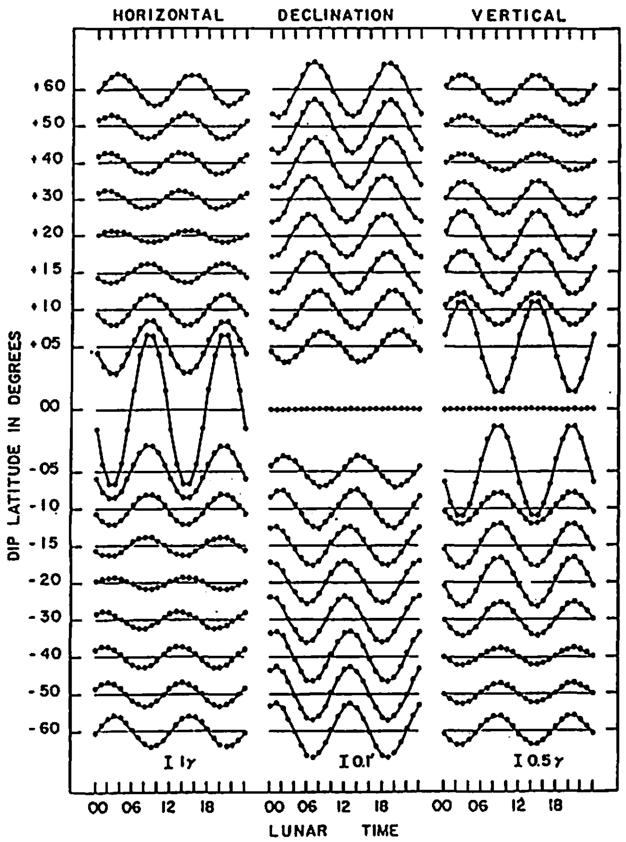

Figure 1-1(b): Lunar semidiurnal variations of the geomagnetic three components at several dip latitudes from 60° to −60° for equinoctial months (after Matsushita and Maeda, 1965b).

For a time varying magnetic field the origin of which is located far outside the Earth (external origin), the Z-component suffers the shielding effect of the conducting Earth. Meanwhile, the secondary Z-component magnetic field is produced by electromagnetically induced Earth-currents, which flow under the ground. This Z-component variation appears if the distribution of the Earth-current is inhomogeneous due to the anomaly of the electrical conductance under the observation site (e. g. Rikitake and Honkura, 1985, pp. 201 or 297). The information of the time variation pattern of the external origin is more clearly displayed in the H- and D-components.

Daily records of the magnetic field in middle and low latitudes are usually composed of gradual time variations; the dominant period of the variations is nearly one day. The gradual time variation is called "geomagnetically quiet diurnal variation" as a whole. The dominant portion of the quiet diurnal variation is the solar quiet diurnal variation (Sq) which is attributed to the global ionospheric current system caused by the tidal winds driven by the thermal effect of the solar radiation (e. g. Matsushita and Maeda, 1965a). The average variation forms of the Sq in the equinoctial months are shown in Figure 1-1(a). The Sq observed on the ground is the apparent magnetic variation when the observatory passes the stationary current vortex in the dayside hemisphere according to the Earth's rotation. The amplitude of the Sq is in the range from 10 to 100 nT in middle and low latitudes. Variations due to the tidal force of the moon (L), whose amplitudes are about 1/30 of the Sq (Matsushita and Maeda, 1965b) is also included in the quiet diurnal variations. The dominant part of the L is the semi-diurnal variation as shown in Figure 1-1(b). Superposed on the quiet diurnal variation, which exists all the year round, there often appear irregular time variations with periods ranging from several minutes to several days. The irregular variations are usually called "geomagnetic disturbances" because of their irregular forms of time variation and sporadic occurrences (e. g. Chapman and Bartels, 1940, pp. 194). Phenomenologically, geomagnetic storm, storm sudden commencement (SSC), sudden impulse (SI), DP2, bay disturbance and solar flare effect are classified as geomagnetic disturbances. Geomagnetic disturbances are caused by time varying electric currents flowing in the upper atmospheres, that is, the ionosphere, magnetosphere, magnetopause and magnetotail (Figure 1-2). The energy sources for the electric currents responsible for geomagnetic disturbances are essentially originated in the solar wind or the radiation from the solar flares. Various solar wind parameters such as the dynamic pressure, the electric and magnetic fields and others are related with the magnitudes and/or the time variation forms of geomagnetic disturbances.

The inputted energy from the solar wind or the radiation associated with solar flare is processed so as to yield complicated systems of electric currents inside the magnetosphere and the ionosphere; and then magnetic fields with characteristic spatial distributions and time variation forms are observed on the ground. In general, geomagnetic disturbances observed in middle and low latitudes show less spatial irregularities and complexities in time variation forms than those in high latitudes. Figure 1-3 is a correlation plot of magnetic records for a geomagnetic storm with an SSC

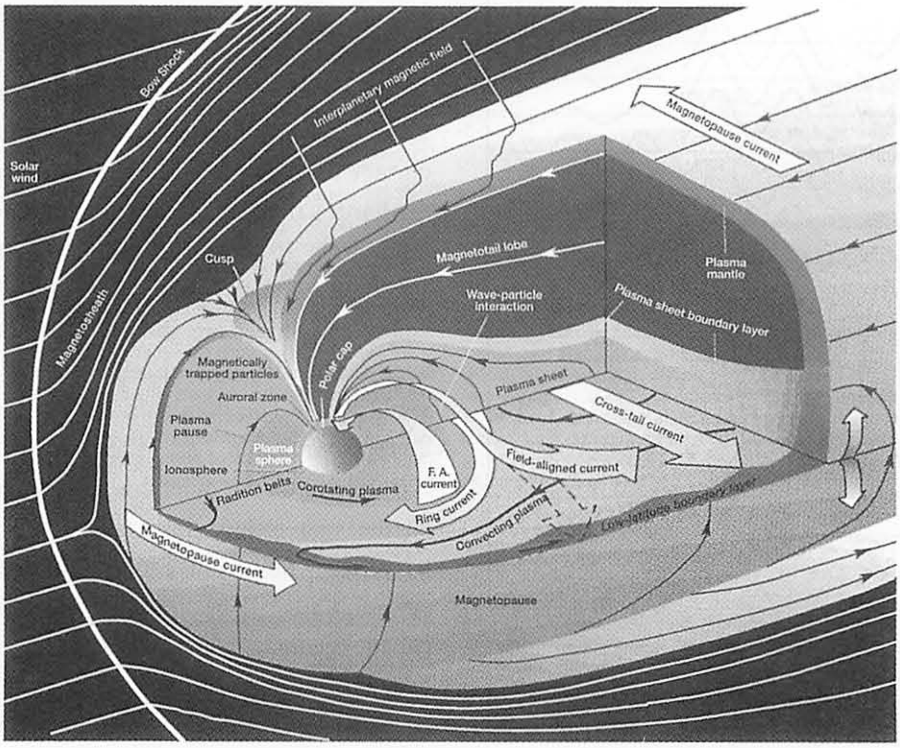

Figure 1-2: A schematic cut-away drawing of the magnetospheric cavity (after Williams et al., 1992).

of 0139UT of September 09. The time variation forms are very irregular and incoherent at the stations in high latitudes (LRV, NAS, PBQ, FCC, RES, YKC, CMO, BRW), whereas those at the stations from middle to low latitudes (VAL, SJG, BOU, HON, KAK, LNP, HER) look simple and coherent. Magnitudes of the variations are much larger in high latitudes than other latitudes. This is because ground observation sites in middle and low latitudes are basically very distant from the origin of disturbances. As the variation pattern looks simple, qualitative models or theories for geomagnetic disturbances in middle and low latitudes were constructed from the last century and almost established in the two decades after the International Geophysical Year (IGY) which was operated from 1957 to 1958. In 1980's, interests of scientists have been mainly directed to the phenomena in the interplanetary space, the inner and outer magnetosphere and the polar region.

Nevertheless, it is far from the truth that geomagnetic disturbances in middle and low latitudes are fully understood quantitatively. Although many qualitative studies have been developed since the IGY using analogue data, precise discussions or statistical studies on the basis of digital data have not been completed. They show rather complicated time changes and/or spatial variations when they are examined precisely. There might be a possibility that some geomagnetic phenomena are not recognized because of the masking by the established "usual" variations in observed data or in the scientist's subconscious.

Recently, the number of studies for geomagnetic disturbances in middle and low latitudes is increasing as magnetic data have been accumulated in wide area. On the basis of high time resolution magnetic data, new findings and/or confirmations for the existing models of geomagnetic disturbances in middle and low latitudes have been obtained (e. g. Russell et al., 1992, 1994a, b; Yumoto et al., 1992, 1994, 1996; Yumoto and the 210° MM Magnetic Observation Group, 1995, 1996; Itonaga et al., 1992, 1995). On the other hand, some statistical results have been obtained using long-term data obtained at routine observatories (e. g., Takahashi et al., 1992; Tsunomura, 1995). Quantitative studies have been and will be further

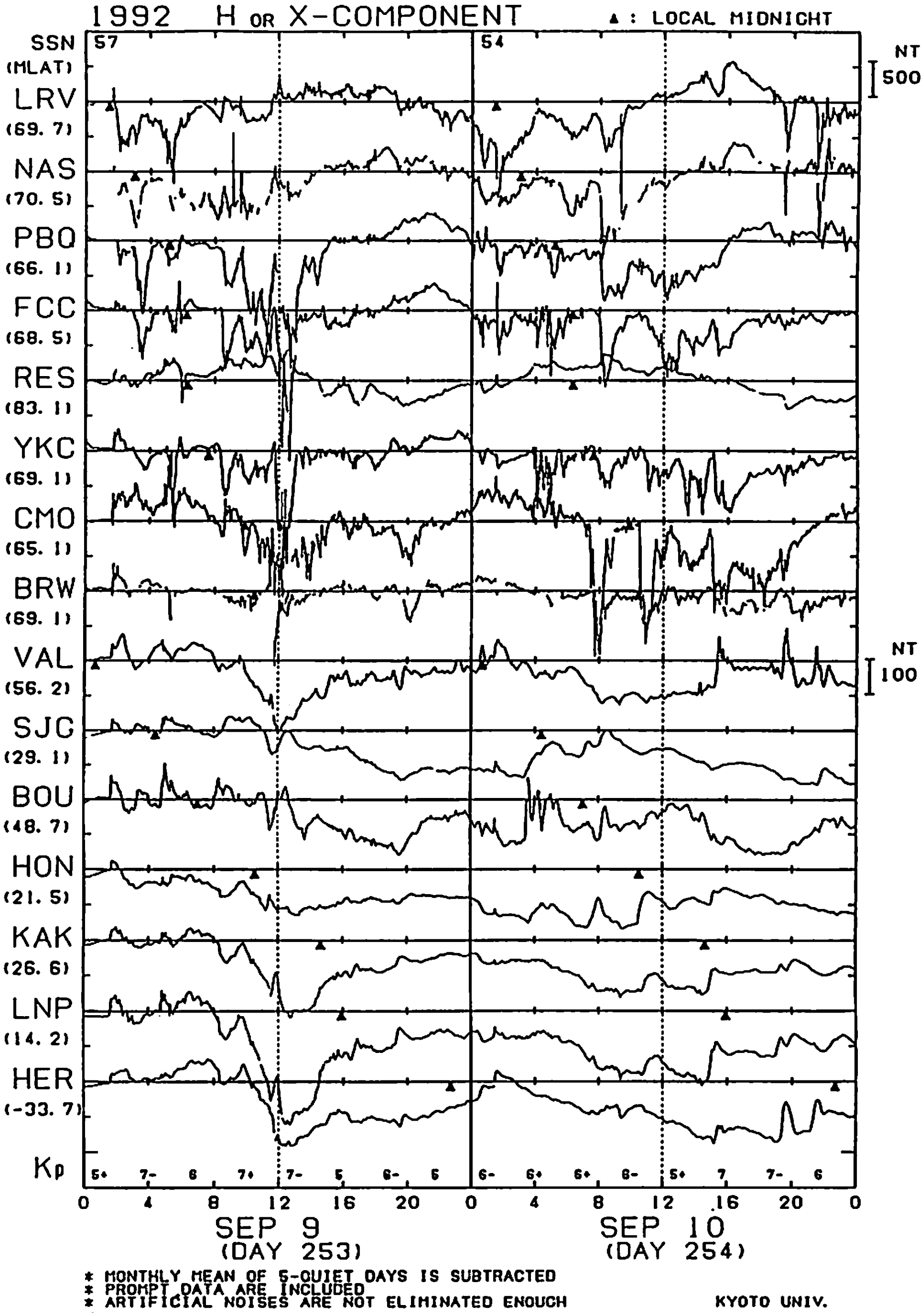

Figure 1-3: Correlation plot of magnetic records for the geomagnetic storm of September 9-10, 1992 at the stations located from high to low latitudes. The numbers in the parentheses under the station codes are the geomagnetic latitudes of the stations. Note that the scale values are different for the stations in high latitudes from those in middle and low latitudes (after 'PROVISIONAL GEOMAGNETIC DATA PLOTS No.7 (July-December)', Data Analysis Center for Geomagnetism and Space Magnetism, Faculty of Science, Kyoto University, 1993).

developed in the Solar Terrestrial Energy Program (STEP) and STEP-Results, Applications, and Modeling Phase (S-RAMP) periods, respectively, to clarify more precisely geomagnetic disturbances in middle and low latitudes, because the research is important as one of the subjects of the magnetosphere-ionosphere coupling problem.

Before developing the quantitative analysis, it is useful to quantitatively check whether existing theories can explain the recognized characteristics of the observational results. Among many matters concerning geomagnetic disturbances in middle and low latitudes, the quantitative evaluation of the contribution of ionospheric current systems to the ground magnetic observation is one of the very important ones.

Global scale ionospheric current systems, the driving sources of which are located in the polar region (polar-originating ionospheric current system) appear in various geomagnetic disturbances, such as SSC, SI, DP2, polar magnetic substorm and others. The current systems are categorized two kinds, DP1 and DP2 types, according to the location and spatial extent. The DP1 type is localized in a narrow region around the auroral oval and contributes to the auroral electrojet (e. g. Obayashi and Nishida, 1968). The DP2 type ionospheric current system, being primarily the equivalent current system of DP2, has a wider spatial extension than that of DP1 and extends to the equatorial region beyond middle and low latitudes (Nishida et al., 1966, Nishida, 1968a, b). The time variation form of DP2 has a relationship with that of the north-south component of the interplanetary magnetic field (IMF-B_z); thus DP2 is probably related with the time variation of the solar wind electric field. It is thought that the solar wind electric field imposed to the magnetosphere propagates to the polar ionosphere along highly conducting magnetic lines of force and causes a global scale ionospheric current.

A global scale electromotive force is expected to occur at the period of SSC and/or SI and drives a global scale DP2 type ionospheric current system. The equivalent current systems of preliminary impulse (PI) and disturbance diurnal variation (DS) part of main impulse (MI) (Obayashi and Jacons, 1957) of SSC and/or SI can be categorized in DP2 type ionospheric current systems (Araki, 1977, 1994). Figure 1-4 shows the equivalent current system for PI obtained by Nagata and Abe (1955) as an example of DP2 type ionospheric current system. It can be seen that the current system consists of two vortices in the morning and the evening hemispheres and that they extend to low latitudes from the polar region. It is necessary to exactly understand the characteristics of the DP2 type ionospheric current system for the discussion of geomagnetic disturbances in middle and low latitudes.

SSC and/or SI are good phenomena for the investigation because of their clear causality and variation form. Indeed, the characteristics of SSC and/or SI are subjects of many scientists' interest. In this paper the terminology 'SC (sudden commencement)' will be used to denote the SSC and/or SI, unless the classification is needed, because the physical mechanisms to cause them are essentially the same. The term 'PI' will be used on behalf of 'PRI (preliminary reverse impulse)' of SC* (suffix '*' is accompanied to denote that the SC is preceded by PRI) as the precursory impulse before the MI (Araki et al., 1985). Here, PI is distinguished from PPI (preliminary positive impulse) introduced by Kikuchi and Araki (1985).

There is an interaction between the ionosphere and the magnetosphere as a response to the impressed electric field. Generally, the magnetospheric electric field is reduced in the low latitude ionosphere by the shielding effect due to the electric charge produced by the ring current at the Alfvén layer (Vasyliunas, 1972; Kikuchi et al., 1996). The shielding effect depends on the time scale of the phenomenon (Senior and Blanc, 1984). The typical time scale is about half an hour (Senior and Blanc, 1984). However, as the investigation of the initial response of the ionosphere against the electric field impressed from the magnetosphere, the examination of the spatial characteristics of the steady state DP2 type ionospheric current system is very important to discuss geomagnetic disturbances in middle and low latitudes.

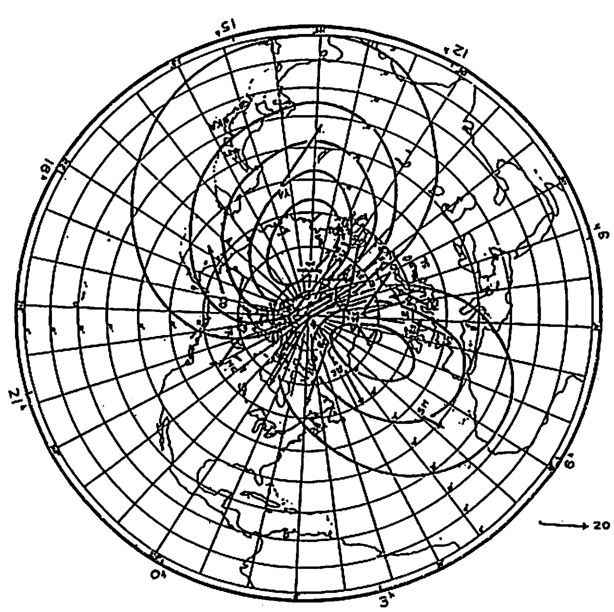

Figure 1-4: Distribution of the equivalent current arrows and current system of preliminary reverse impulse of SC* at 6h 25m UT on May 29, 1933 (after Nagata and Abe, 1955).

The ionosphere, having the wide horizontal expansion compared to its vertical thickness, is usually treated as a thin conducting spherical shell. It has been established that the global distribution of the ionospheric layer conductivity is a very important parameter for deciding the distribution of polar-originating ionospheric currents, along with the characteristics of their origin (field-aligned currents, the solar wind electric field or others). The horizontal distribution of the ionospheric layer conductivity shows complicated characteristics. In the auroral region, there appear frequently very irregular distributions and time variations of the conductivity due to the precipitation of energetic particles from the magnetosphere (e. g. Brekke and Moen, 1993). Meanwhile, the ionospheric layer conductivity, depending on the geometric feature of magnetic lines of force, increases with decreasing latitude gradually from high to low latitudes and is quite steeply enhanced in the limited area near the equator with the latitudinal width less than 10°. This is called the equatorial anomaly or the equatorial enhancement of the ionospheric conductivity.

Since geomagnetic phenomena are usually

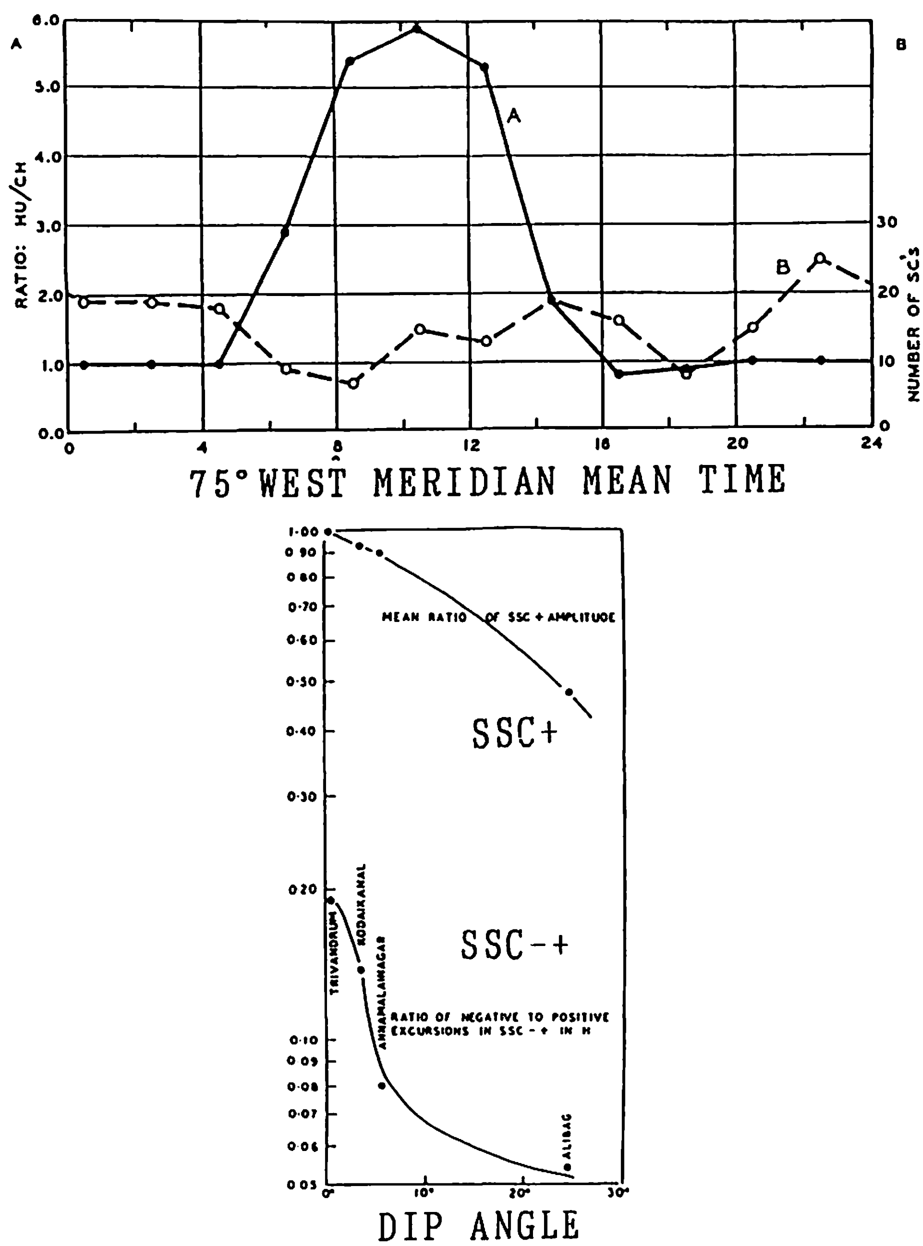

Figure 1-5: Upper panel: Diurnal variation of the normalized amplitude of SC at Huancayo near the dip equator [Sugiura, 1953]. Lower panel: Latitudinal variation of the normalized amplitude of MI (denoted as SSC+) and PI (denoted as SSC−+) at Indian stations [Rastogi and Sastri, 1974] (after Araki, 1994).

expected as symmetric or anti-symmetric with respect to the geomagnetic equator, the geomagnetic equator is regarded as a boundary of a hemisphere for ionospheric currents. In the following discussions, the geomagnetic equator will be abbreviated as the equator. The electromagnetic condition at the equator is characterized by its high conductance in the very narrow region around the dayside equator. It is thought that the characteristics of geomagnetic disturbances in middle and low latitudes cannot be discussed comprehensively without examining the effect of the equatorial enhancement on the polar-originating ionospheric currents. The characteristics of the equatorial enhancement of the ionospheric conductivity and currents will be briefly introduced in the next section.

1.2 Equatorial Enhancement of Polar-originating Ionospheric Current Systems

The high conductance at the equatorial ionosphere is attributed to the effects of the geometry of magnetic lines of force and the Hall conductance of the ionospheric conductivity (Hirono, 1952; Baker and Martyn, 1953; Fejer, 1953); the high conductivity at the dayside equator is often called Cowling conductivity. The intensity of polar-originating ionospheric currents, which decreases with decreasing latitude, grows up very high just near the equator. Because of this effect, geomagnetic disturbances are often observed with large amplitudes at the dayside equator. On reverse, the feature whether the geomagnetic phenomenon shows the feature of the equatorial enhancement or not is often used for the assessment of the mechanism of the phenomenon, that is, the ionospheric contribution exists or not.

DP2 is observed in both the polar region and the dayside equator simultaneously and coherently (Nishida et al., 1966). The time variation form of DP2 is well correlated with that of the north-south component of the IMF-B_z (Nishida, 1968a, b), which is related with the solar wind electric field; therefore, DP2 in the equatorial region has a relationship with the solar wind electric field and associated magnetospheric processes. Kikuchi et al. (1996) showed a clear equatorial enhancement for a DP2 event at the equatorial stations in the dayside in spite of the reduction of the dawn-to-dusk electric field by the Region 2 field-aligned current. There were also many articles discussing electric field variation at the equator associated with the magnetospheric processes (e. g. Fejer, 1986, 1991, 1997; Rastogi, 1997; Sastri et al., 1997 and references therein). These observational facts reveal that the electric field impressed on the high latitude ionosphere is transmitted instantaneously and drives the intense ionospheric current at the dayside equator.

The amplitudes of magnetic variations of MI of SC at the equator become large in the daytime (Sugiura, 1953; Forbush and Vestine, 1955; Maeda and Yamamoto, 1960; Matsushita, 1962) and rapidly increase with decreasing latitude near the equator (Obayashi and Jacobs, 1957; Araki, 1977; Kane, 1978; Rastogi, 1993; Araki, 1994), as shown in Figure 1-5. Jacobs and Watanabe (1963) tried to explain the equatorial enhancement of MI of SC by the conductivity increase in the ionosphere due to the downward motion of charged particles driven by the westward electric field on the wavefront of the compressional wave which propagates earthward in the dayside magnetosphere. However, the appearance of eastward electric fields associated with MI of SC in low latitudes (Kikuchi et al, 1985; Figure 1-6) and the equator in the dayside are evidenced by HF Doppler observations (Rastogi, 1976; Reddy et al., 1981; Kikuchi, 1986; Sastri et al., 1993). It is most probable that the polar-originating dawn-to-dusk

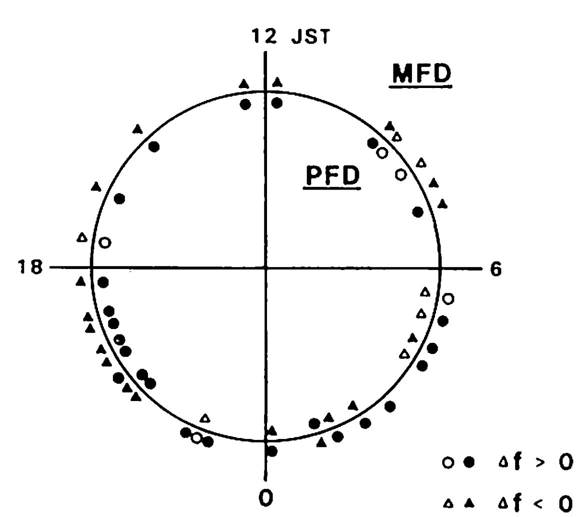

Figure 1-6: Local time features of the signs of preliminary frequency deviations (PFD's) and main frequency deviations (MFD's) of SCF's; SCF is the frequency deviation associated with SC. The SCF(+ −) appears in the daytime and evening sectors and

electric field is transmitted to the low-latitude ionosphere instantaneously from high latitudes at the period of MI of SC.

PI of SC shows clear equatorial enhancement (Matsushita, 1962; Nishida and Jacobs, 1962; Araki and Ishizaki, 1973; Rastogi and Sastri, 1974; Araki, 1977). The amplitude of PI which frequently appears in the afternoon-side high latitudes (Matsushita, 1960, 1962) decreases with decreasing latitude and becomes almost zero at latitudes around 20° geomagnetic latitude, but grows again to the observable strength at the dayside equator (Nagata, 1952; Matsushita, 1960; Araki, 1977). Figure 1-7 shows the distribution of PI observation. Because of its clear variation form, PI is a good phenomenon for the investigation of the ionospheric response to the electric field impressed in high latitudes.

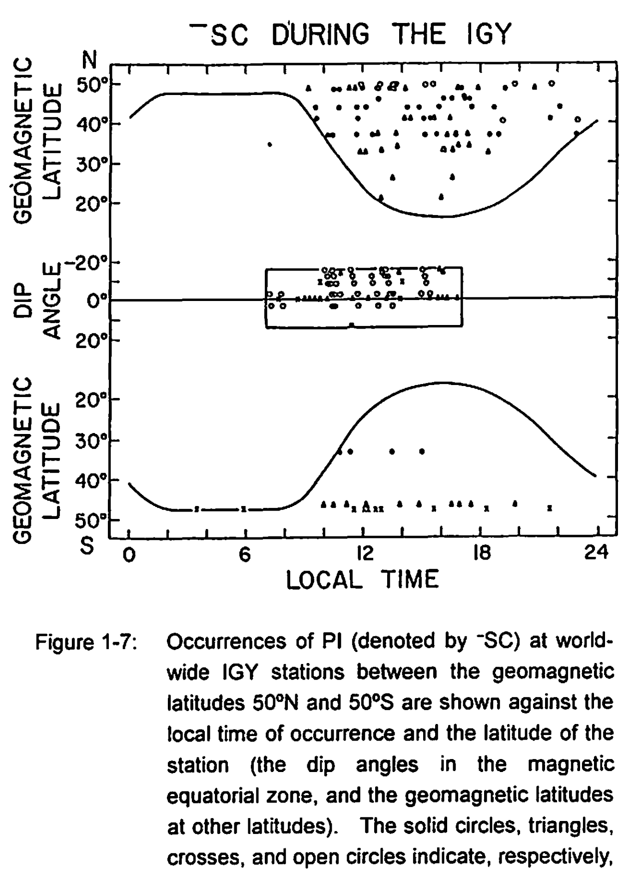

Figure 1-7: Occurrences of PI (denoted by ⁻SC) at world-wide IGY stations between the geomagnetic latitudes 50°N and 50°S are shown against the local time of occurrence and the latitude of the station (the dip angles in the magnetic equatorial zone, and the geomagnetic latitudes at other latitudes). The solid circles, triangles, crosses, and open circles indicate, respectively, the following four longitude zones: Europe and Africa (geomagnetic 50°E-140°E); Asia and Australia (geomagnetic 140°E-230°E); northwest America and New Zealand (geomagnetic 230°E-320°E), and northeast America and South America (320°E-50°E). No Indian data are available. Ibadan (geographic 7°26′N, 3°53′E), near the magnetic equator, showed no PI because of frequent lack of data. Two curves and one square indicate the regions of predominant occurrence of ⁻SC (after Matsushita, 1962).

Because of the isolated appearance of PI at the dayside equator, some investigators tried to interpret the equatorial PI in terms of special mechanisms independent of that for the high latitude PI (Tamao, 1964; Sugiura, 1971). Kikuchi and Araki (1979a), however, showed that direct incidence of the hydromagnetic wave into the dayside equatorial ionosphere cannot cause PI. On the basis of a detailed data analysis about the relationship between the polar and equatorial PI, Araki (1977) concluded that the global distribution of PI may be explained by the model based on polar-originating ionospheric currents as suggested by Nishida et al. (1966). Araki (1977) attributed the equatorial enhancement of PI to the enhanced ionospheric current due to the Cowling conductivity. Simultaneous magnetic observations above the ionosphere (MAGSAT) and on the ground reveal the ionospheric contribution for PI's (Araki et al., 1982, 1984).

The most probable mechanism for PI in high latitudes is as follows; westward electric field along the compressional wave front propagating earthward in the dayside magnetosphere is transmitted along magnetic lines of force to the polar ionosphere and produces twin-vortex type ionospheric currents (Tamao, 1964). Figure 1-8 illustrates this situation. It is thought that the PI at the dayside equator is caused by the afternoon counterpart of the ionospheric current vortex extending to the dayside equator (Figure 1-4).

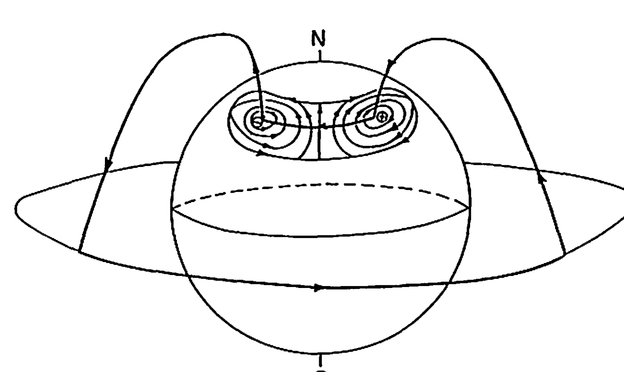

Figure 1-8: A sketch illustrating the current in the magnetosphere due to the pure transverse mode (thick line) and the ionospheric Hall-current caused by the incidence of the mixed transverse mode into the ionosphere, viewed from the solar side (after Tamao, 1964).

In order to establish the interpretation of PI in terms of the polar-originating ionospheric current, however, two problems should have been theoretically solved. One is the existence of the instantaneous propagation mode of electromagnetic waves, which can globally transmit the effects of large-scale field-aligned currents flowing into (away from) the polar ionosphere from (to) the magnetosphere. If we assume that the transmission took place in an unbounded uniform ionosphere, the propagation time from the pole to the equator would be several tens of minutes (Jacobs et al., 1965; Rostoker, 1965). Observations show, however, that PI appears almost simultaneously in both high latitudes and the equatorial region (Araki, 1977). This contradiction was solved by a theory of the transmission of the zeroth-order TM (transverse magnetic) mode in the wave guide between the Earth and the ionosphere (Kikuchi et al., 1978; Kikuchi and Araki, 1979b). They showed that the large-scale horizontal electric filed impressed on the polar ionosphere penetrates instantaneously to low latitudes by the mode. The mechanism is illustrated in Figure 1-9. Applying this solution, the transmission of the polar-originating electric fields to low latitudes can be explained in the same manner for other phenomena (MI of SC and DP2). Thus, the examination of PI contributed to create a general solution applicable to all the phenomena concerning olar-originating ionospheric current systems.

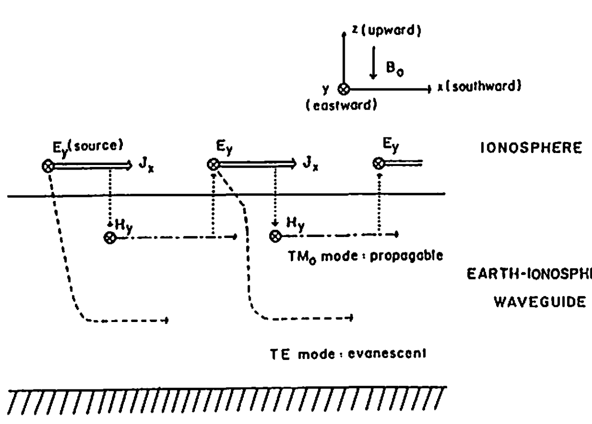

Figure 1-9: A schematic picture of southward transmission of the polar ionospheric field. The zeroth-order TM mode excited by the source TE field in the Hall-dominated ionosphere propagates instantaneously and in turn produces TE fields

The morphology of magnetic fields of SC observed on the ground was systematically investigated by Araki (1977) and upgraded by Araki (1994). The disturbance electric and/or magnetic fields for SC are decomposed to *DL* and *DP*; the *DP*-field is further decomposed to DP_{pri} (or more generally DP_{pi}) and DP_{mi}. The *DL*-field is made by the compressional mode of hydromagnetic waves, which is driven by a magnetospheric compression and propagates in the equatorial plane in the magnetosphere; that is a direct effect by the magnetospheric compression. The DP_{pi}- and DP_{mi}-fields are the ones due to polar-originating ionospheric current systems responsible for PI and MI, respectively. A rough sketch representing the *DL*- and *DP*-fields is shown in Figure 1-10. In the following discussion, this schematic model for SC is called Araki's model. Figure 1-11 shows the observed local time profile of the rate of the equatorial DP_{mi}- to DL-fields (Papamastorakis et al., 1984).

The other problem remained to be solved is the theoretical demonstration of the distribution of ionospheric currents, which is consistent with the observed distribution of the magnetic variations. The distribution of PI, being regarded as the most pure manifestation of the polar-originating ionospheric current contribution, should be explained at first. Especially, the disappearance of PI around Honolulu and its clear enhancement in the dayside equator should be proved quantitatively. As a simple speculation, there is a possibility that polar-originating ionospheric currents are not sufficiently amplified at the dayside equator, since, in general, the polar-originating electric field is reduced in the region of enhanced conductivity by the resulting counter polarization electric field (Figure 1-12).

There were some simulation studies discussing horizontal distribution of polar-originating ionospheric current systems concerning magnetospheric substorm (Maeda and Maekawa, 1973; Yasuhara et al., 1975; Nisbet et al., 1978; Nopper and Carovillano, 1978; Kamide and Matsushita, 1979a, b) in late 1970's. Most of them (except for Nopper and Carovillano, 1978) are interested in the behavior of the ionospheric electric and magnetic fields in high latitudes. Nopper and Carovillano (1978) discussed difference of the longitudinal variation of the electric field at the equator between different models of the source currents, but did not mention whether the equatorial enhancement of the ionospheric currents occurs or not. This is because the calculation is hardly converged with the rapidly changing conductivity near the equator.

Since 1980', there have been some studies discussing the electric or magnetic field variations at the equator associated with substorm (Senior and Blanc, 1984; Denisenko and Zamay, 1992). These studies do not show latitudinal profiles of the magnetic variations. Furthermore they have some confinements in the treatment of the equatorial enhancement of the ionospheric conductivity or need a sophisticated numerical technique. Takeda (1982) presented another type of two-dimensional calculations including the equator and showed the equatorial enhancement pattern. His model is useful to obtain the vertical structure of the ionospheric current, however, there remain some ambiguities in the current strength along magnetic lines of force. Tsunomura and Araki (1984) operated a two-dimensional

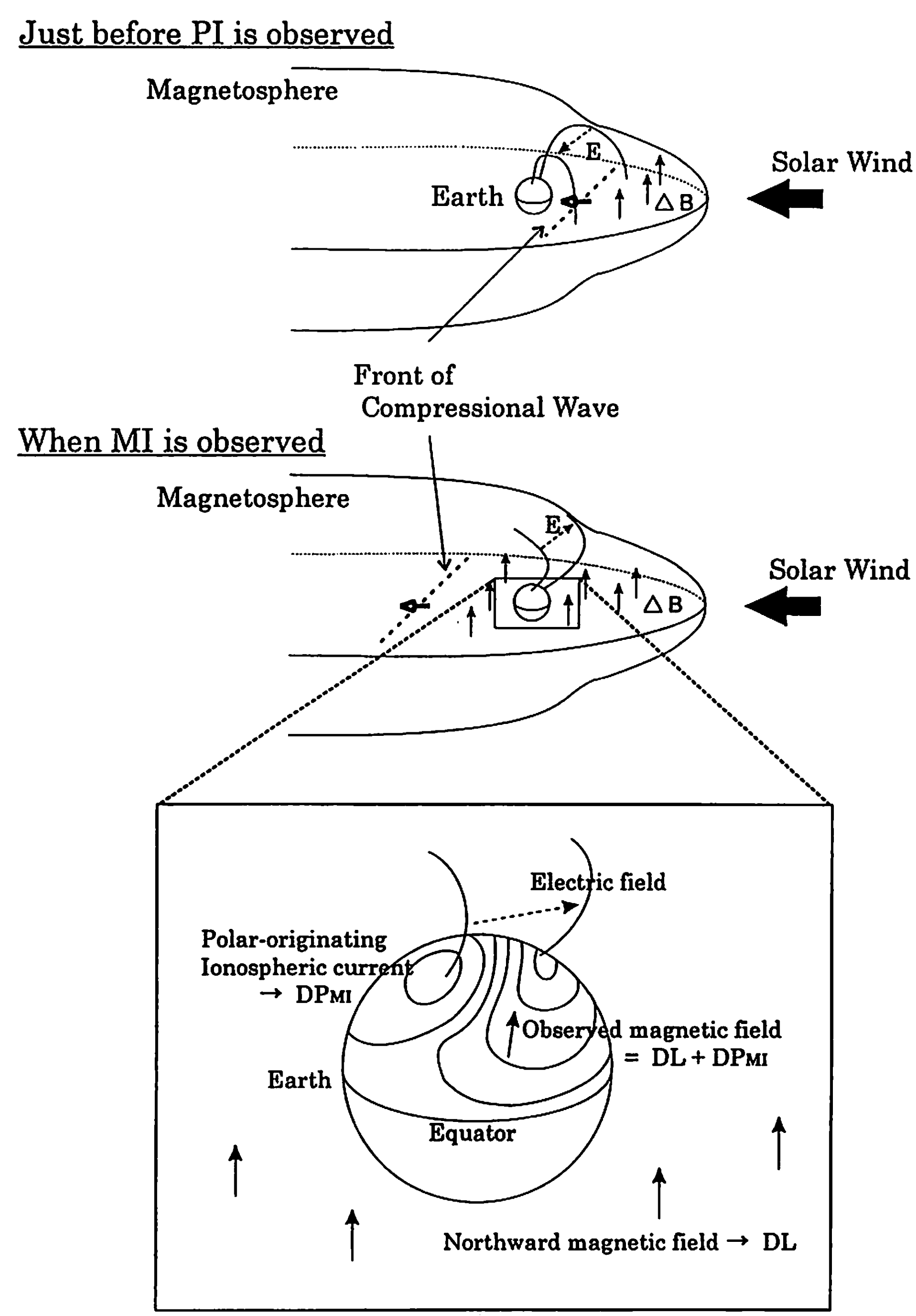

Figure 1-10: A sketch illustrating the electromagnetic process when a shock or a discontinuity of the solar wind dynamic pressure passes the Earth's magnetosphere. E and ΔB denote electric field and magnetic field variation, respectively.

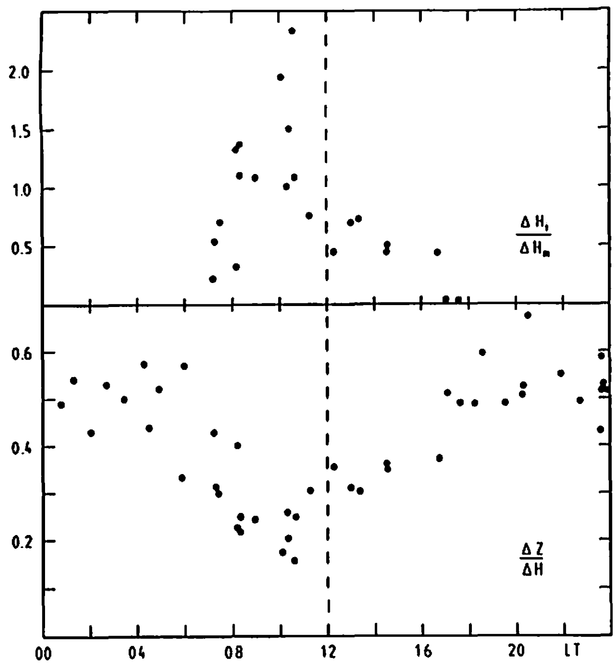

Figure 1-11: Lower panel: Local time dependence of ΔZ/ΔH for 44 SC's observed at Annamalainagar. Upper panel: Local time dependence of the calculated amplitude ratio $\Delta H_i/\Delta H_m$ (ionospheric to magnetospheric part) for 21 daytime SC's (after Papamastorakis et al., 1984).

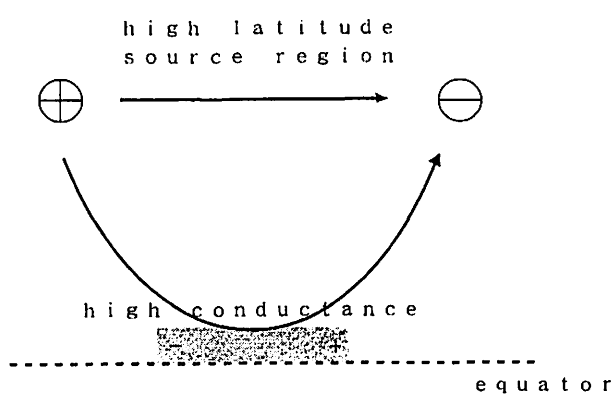

Figure 1-12: An illustration describing the extension of the polar-originating ionopheric current to the equator.

calculation in the horizontal plane with a nearly realistic ionospheric conductivity model and obtained the equatorial enhancement of the ionospheric current. They ignored the anti-symmetry of the non-diagonal terms of the ionospheric conductivity tensor with respect to the equator. Recent HF Doppler observations by Sastri et al. (1993) during SC's show the different local time dependence of the electric field at the equator from the result of Tsunomura and Araki (1984). Their model should be improved to compare with the observational results more exactly. For this reason and for making it possible to calculate the ionospheric current covering both hemispheres simultaneously, the numerical model based on the ionospheric conductivity model with the anti-symmetric non-diagonal term should be developed.

It is thought that the improvement of Tsunomura and Araki (1984)'s model above mentioned is one of the most efficient ways to develop the simulation scheme for the polar-originating ionospheric current system including the equatorial region. Recently Tsunomura (to be published) tried the improvement and succeeded to obtain a self-consistent, two-dimensional model.

Meanwhile, versatility of the numerical model, such as the variability in the conductivity distribution, will be desired for the quantitative investigation of the magnetosphere-ionosphere coupling problems. For example, the effect of the ionospheric current system should be examined when one discusses SC events quantitatively. The effect of the *DL*-field, which depends primarily on the variation of the solar wind dynamic pressure, can be estimated from one of the mathematical models of the magnetosphere. The distribution of the magnetic variations due to the *DL*-field is successfully reproduced giving various solar wind parameters and/or the magnetospheric conditions (Russell et al., 1992, 1994a, b). Whereas, for the *DP*-fields, it is not in the stage to accurately predict the magnetic effects from the solar wind parameters. The development in the estimation method of the DP_{pi}- and/or DP_{mi}-fields is needed to proceed the investigation of SC. That will be applicable for the analysis of other phenomena, such as DP2.

It is one of the purposes of this study to construct a realistic and versatile modeling method of the two-dimensional ionospheric layer conductivity, useful for the numerical simulation of the polar-originating ionospheric current system. A modeling method for the ionospheric conductivity will be proposed after some discussions. By making numerical calculations using the newly developed model, various geomagnetic phenomena concerning the polar-originating ionospheric current system will be discussed as test cases.

1.3 Some Unsolved Matters Concerning SC in Middle and Low Latitudes

In middle and low latitudes, the effect of the *DL*-field is dominant. The *DL*-field causes the increase in the H-component in middle and low latitudes without severe local time dependence. The characteristics of the DP_{pi}- and DP_{mi}-fields in middle and low latitudes, being superposed on the *DL*-field, have not been examined sufficiently because of their small amplitudes. Moreover, the mechanism to generate the electric field for the DP_{mi}-fields at the magnetopause has not been definitely explained yet as pointed out by Kikuchi (1986). This is one of the fundamental problems concerning the process of SC and should be clarified in the future studies. Before setting about such fundamental studies, it is important to check how exactly the existing theory can explain the observed features; indeed that has not been sufficiently examined yet.

The equivalent current systems of PI (MI) is basically composed of two vortices; a counterclockwise (clockwise) one on the morning side and a clockwise (counterclockwise) one on the day and evening sides, viewed from the outside of the Earth. The senses of the vortices for PI are reverse to those for MI; an example of the equivalent current system of a PI was shown in Figure 1-4. The variations of the MI in the D-component is expected to be positive (eastward) in the morning and negative (westward) in the evening, respectively in middle and low latitudes. However, the D-component variation for the MI of SC is eastward at Kakioka in many cases by several

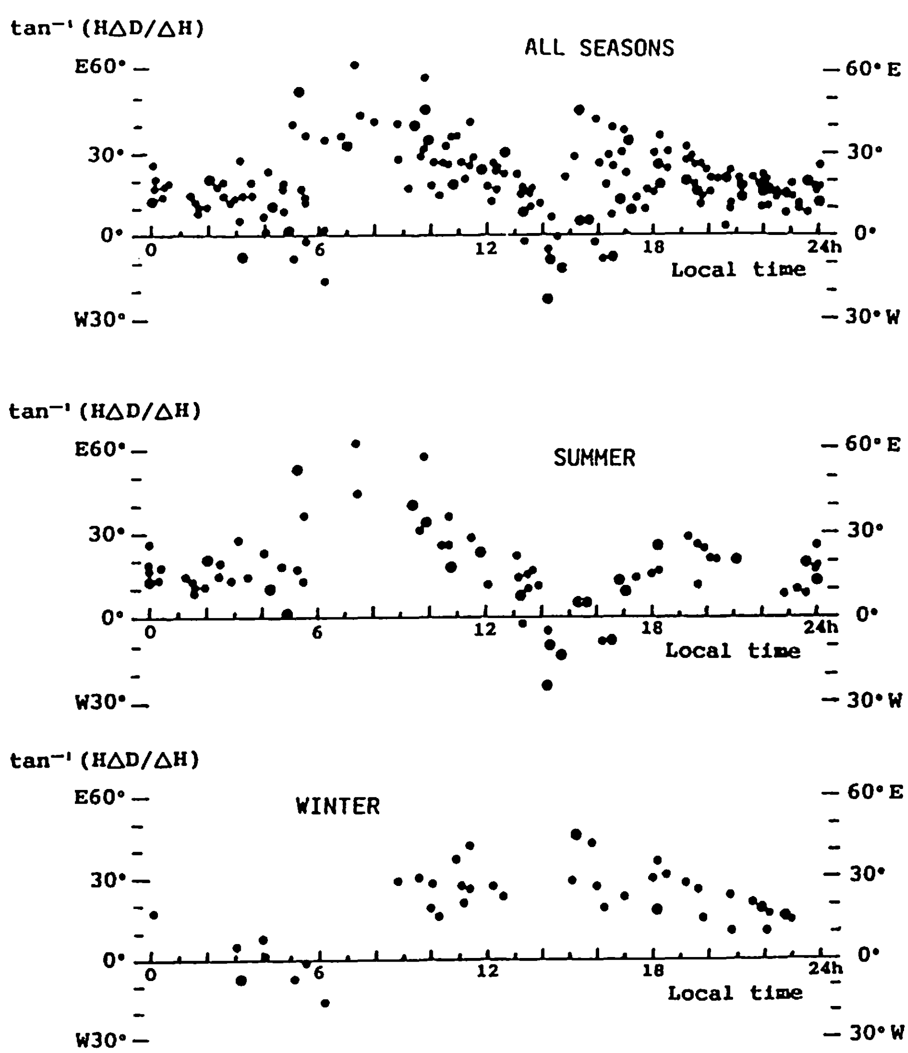

Figure 1-13: Local time dependence of the deviation angle of horizontal SC vectors from the local magnetic meridian, for SC's observed at Kakioka, Japan, during 1950-1964 in the summer months, winter months, and all seasons (after Fukushima, 1994).

minutes of arc (Fukushima, 1994) as shown in Figure 1-13. Fukushima (1994) proposed that this eastward shift of the D-component polarity of SC is attributable to the observational situation.

Figure 1-14 shows a rough sketch of the situation of the routine magnetic observation in Japan; note that the sign of the D-component output of the magnetometer is assigned as plus for the westward variation in Japan because of the westward shift of the local declination as the base. The H-component axis of the magnetometer is usually aligned to the local direction of the local geomagnetic field, to adjust the output of the D-component nearly zero on geomagnetically quiet days. In usual, the D-component roughly pointing the local geomagnetic east-west direction is used for scientific studies without converted to other universal coordinate systems.

The *DL*-field variation of SC, which is caused by a magnetospheric compression by the solar wind dynamic pressure increase, is most probably aligned to the geomagnetic dipole axis, which is a little different from the direction of the local declination. Therefore the observed D-component should includes an apparent variation due to the projection of the magnetic field variation of the magnetospheric compression. As the magnetospheric compression makes the increase in the direction of the geomagnetic dipole meridian at any local time, this will result in the eastward bias for the D-component. Then the rate of the eastward variation of the D-component for SC increases.

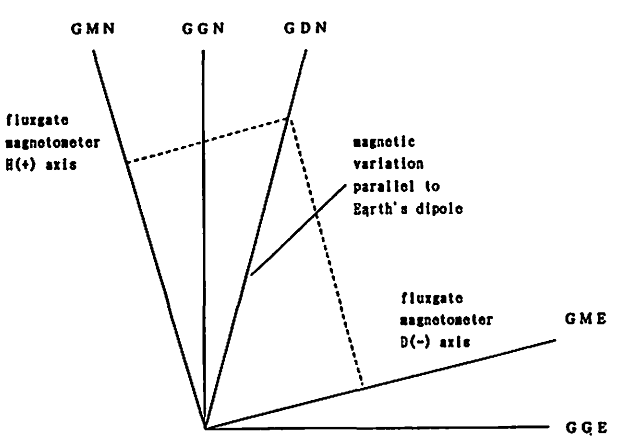

Figure 1-14: A sketch of the situation of routine magnetic observation in Japan. GGN and GGE are geographic north and east, GMN and GME, geomagnetic north and east, and GDN, geomagnetic dipole north, respectively.

After considering this observational situation, Fukushima (1994) presented a model of the image dipole in the solar wind to explain the eastward shift of the declination change. However, it is thought to be difficult to explain the complex local time profile of the declination change by his model, especially for the large eastward change usually observed in the morning. It is necessary to examine the possibility whether the Araki's model can explain the matter; that can be checked converting the data to the geomagnetic dipole coordinate system. Tsunomura (1995) showed that the conversion of the magnetic data to the geomagnetic dipole coordinate system reduces the percentage of the positive variation of SC in the D-component.

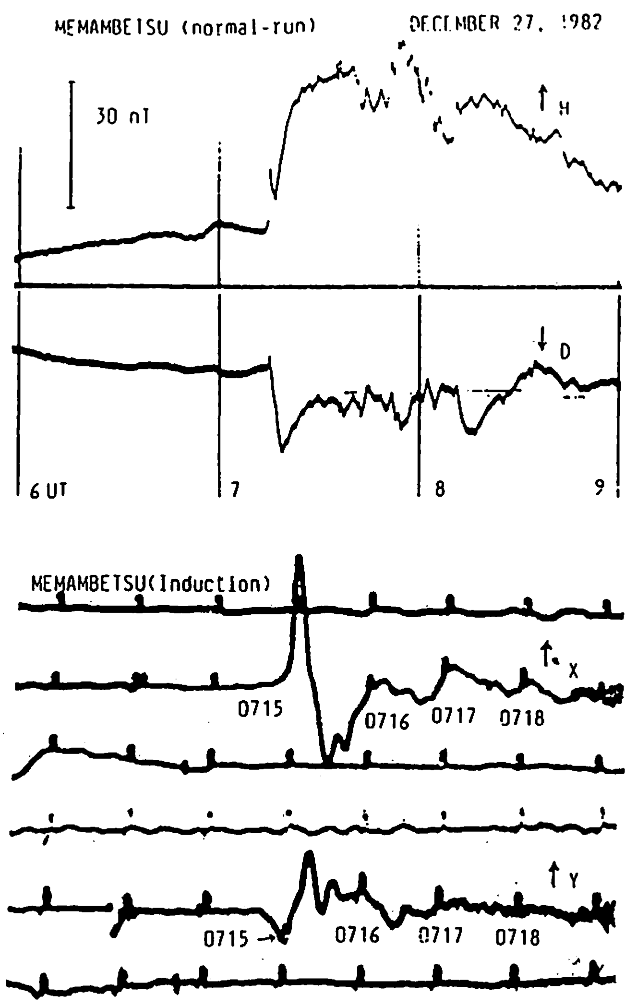

Figure 1-15: An example of a typical preliminary positive impulse (PPI) of SC in the geomagnetic H-component recorded on the normal-run magnetogram (top) from Memambetsu at 0715 UT, December 27, 1982. The induction magnetogram is given in the bottom part (after Kikuchi and Araki, 1985).

Another unsolved matter concerning SC is the occurrence of preliminary positive impulse (PPI), which was introduced by Kikuchi and Araki (1985) as a preceding positive impulse before the MI of SC (Figure 1-15). They showed that PPI is often observed in the dayside middle latitudes and mentioned that PPI is different from PI. Comparing the observations of magnetic fields and HF Doppler observations, they deduced that PPI is caused by the compressional wave excited by the magnetospheric compression. However, their explanation cannot explain sufficiently the local time distribution of the occurrence frequency, especially the disappearance in the nightside. Some other mechanisms are needed to explain the characteristics of PPI. At least, the relationship of the PPI with the existing model of SC should be examined. On the basis of data analyses using the routine magnetic data in middle and low latitudes and the numerical analysis, Tsunomura (1998) suggested that PPI is a signature of the DP_{mi}-field in this area.

It is also difficult to explain simply the fact that several SC's with enormously large amplitude such as those on February 11, 1958 and March 24, 1991, show a steep pulse-like structure just after the onset. They are far from the usual step-like variation form of SC. It is necessary to check whether these events can be explained by the existing theories. The morphology of the variation form of the SC on March 24, 1991 was precisely examined by Araki et al. (1997). Araki et al. (1997), using as many data as possible, investigated the SC on March 24, 1991 qualitatively and showed that the event can be explained by the Araki's model. Tsunomura (1998) examined the effect of the conversion to the dipole coordinate system for the SC event and operated a numerical analysis shifting the source current region to the evening side; he succeeded to obtain the local time profile of the magnetic variation of the event.

In another aspect, it is imagined that the magnetic data in middle and low latitudes have a potential as a useful indicator to estimate the whole magnetosphere-ionosphere coupling process. This is because the magnetic variations in middle and low latitudes are not suffered from local irregularities, comparing with those in the polar region and the equator. Since there are not magnetic observatories more than enough in the world, an efficient utilization on the basis of the limited number of the magnetic data is important for the scientific and routine works in the solar-terrestrial phenomena.

1.4 Composition of the Following Chapters

In Chapter 2, the effect of the equatorial enhancement for the global structure of the polar-originating ionospheric current system is evaluated operating a numerical calculation setting some simplifications for a realistic conductivity model at first. And then a method to construct a realistic two-dimensional ionospheic conductivity model is proposed after the discussion of the effect of the ionospheric conductivity in the equatorial region. Numerical calculations will be performed to demonstrate the reality and the versatility of the model.

Chapter 3 is devoted for the examination of SC in middle and low latitudes. A statistical analysis using one-minute magnetic data at Kakioka will be operated at first. It is aimed to check the effect of the conversion of the magnetic data to the geomagnetic dipole coordinate system and to examine the possibility of the Araki's model to explain the observational results. Data analysis for SC's in middle and low latitudes will be developed for the newly recognized feature in the H-component in middle and low latitudes in the local time range from the morning to the afternoon hours. The discussion will be extended to propose a possibility to understand the PPI morphology. The results of the data analysis are compared with a numerical solution including the equatorial enhancement, which is based on the discussion in Chapter 2. A quantitative examination will be given for the SC on March 24, 1991. Finally, the availability of the D-component for the use of monitoring the magnetosphere-ionosphere coupling problem will be discussed.

2. Numerical Analysis for Polar-originating Ionospheric Current Systems Including the Effect of the Equatorial Enhancement of the Ionospheric Conductivity

2.1 Basic Equations

The simulation scheme assuming the ionosphere as a conducting thin sheet is used by many authors to derive the ionospheric current system (e. g. Fejer, 1953; Tarpley, 1970; Maeda and Maekawa, 1973; Yasuhara et al., 1975; Kamide and Matsushita, 1979a, b; Forbes and Lindzen, 1976a, b; Maekawa and Maeda, 1978; Nisbet et al., 1978; Nopper and Carovillano, 1978; Maekawa, 1980; Harel et al., 1981a, b,; Kamide et al., 1981; Senior and Blanc, 1984; Ahn et al., 1986; Spiro et al., 1988). Since the thickness of the ionosphere is much smaller than its horizontal expanse and/or the size of the magnetosphere, it can be assumed that the net electric current in the vertical direction is negligibly small in the ionosphere. Assuming that the vertical component of electric current is zero entirely in the ionosphere, Ohm's law of the electric current, $j = \sigma \cdot E$ (j is electric current density vector, σ ionospheric conductivity tensor, E electric field vector, respectively) at each point in the ionosphere can be described as follows;

$$\begin{pmatrix} j_\theta \\ j_\varphi \end{pmatrix} = \begin{pmatrix} \sigma_{\theta\theta} & \sigma_{\theta\varphi} \\ \sigma_{\varphi\theta} & \sigma_{\varphi\varphi} \end{pmatrix} \cdot \begin{pmatrix} E_\theta \\ E_\varphi \end{pmatrix}, \qquad (2\text{-}1)$$

where θ and φ are colatitude and longitude, respectively. Since the ionosphere takes the form of spherical shell, the polar co-ordinate system (θ , φ , z) is usually used to describe the physical processes. Here, z directs vertically upward. The non-diagonal components in the conductivity tensor are caused by the existence of the Hall conductance in the ionosphere. The components of the ionospheric conductivity tensor are derived by a simple algebraic calculation on the assumption of the null vertical current. The forms of $\sigma_{\theta\theta}$, $\sigma_{\theta\varphi}$ and $\sigma_{\varphi\varphi}$ are

$$\sigma_{\theta\theta} = \frac{\sigma_0 \sigma_1}{\sigma_0 \sin^2 I + \sigma_1 \cos^2 I}, \qquad (2\text{-}2)$$

$$\sigma_{\theta\varphi} = \frac{\sigma_0 \sigma_2 \sin I}{\sigma_0 \sin^2 I + \sigma_1 \cos^2 I}, \qquad (2\text{-}3)$$

and

$$\sigma_{\varphi\varphi} = \sigma_1 + \frac{\sigma_2^{\,2} \cos^2 I}{\sigma_0 \sin^2 I + \sigma_1 \cos^2 I}, \qquad (2\text{-}4)$$

where σ_0, σ_1 and σ_2 are longitudinal, the Pedersen and the Hall conductivities and I dip angle, respectively. $\sigma_{\theta\varphi}$ is exactly minus of $\sigma_{\varphi\theta}$. Clearly seen from the equations, $\sigma_{\theta\theta}$ and $\sigma_{\varphi\varphi}$ asymptotically approach to σ_1 and $\sigma_{\theta\varphi}$ to σ_2 in high latitudes, respectively. There were some simulation studies assuming this relationship in high latitudes (e. g. Fejer, 1953; Kamide et al.,1981, Ahn et al., 1986); however the assumption cannot be applicaable for low latitudes.

Another important assumption is that vertical variations of horizontal components of electric field are small. This assumption makes it possible to put the electric field outside the height-integration of the electric current, that is,. $\int j\,dz = \int \sigma \cdot E\,dz = E \cdot \int \sigma\,dz$ According to this separation of variables, the equivalent, two-dimensional layer conductivity of the ionosphere can be independently obtained by only integrating σ with height. The equation of Ohm's law for the height-integrated ionospheric current is finally written as

$$J = \Sigma \cdot E = -\begin{pmatrix} \Sigma_{\theta\theta} & \Sigma_{\theta\varphi} \\ \Sigma_{\varphi\theta} & \Sigma_{\varphi\varphi} \end{pmatrix} \cdot \nabla \psi, \qquad (2\text{-}5)$$

where J is the height-integrated current density vector, Σ height-integrated conductivity tensor, E electric field vector, and ψ electric potential, in the two-dmensional layer model of the ionosphere, respectively. Each component of Σ is the height-integrated values of $\sigma_{\theta\theta}$, $\sigma_{\theta\varphi}$, $\sigma_{\varphi\theta}$ and $\sigma_{\varphi\varphi}$. This model, based on a thin shell approximation of the ionosphere, is called 'thin shell model' (same as 'thin shell' dynamo model of Forbes and Lindzen (1976a) in essence).

When a field-aligned current flows into or away from the polar ionosphere, there appear horizontal electrostatic fields in the ionosphere and drive ionospheric currents globally. The resulting ionospheric current distribution can be obtained by solving the equation of current continuity,

$$\nabla \cdot J = \sin I \cdot j_{\parallel}, \qquad (2\text{-}6)$$

where $j_{\parallel}$ is the density of the field-aligned current (positive for downward). This type of the external source is regarded as a current generator. The equation can be solved putting certain values for the potentials at some points as if they are boundary conditions. This case corresponds to an external source of a voltage generator. The solutions for the both kinds of generators become basically different because of the inhomogeneity and the non-diagonal components in the ionospheric conductivity.

Combining the equations (2-5) and (2-6) yields the following partial differential equation of elliptic type for electric potential, Ψ.

$$A\frac{\partial^2 \psi}{\partial \theta^2} + B\frac{\partial \psi}{\partial \theta} + C\frac{\partial^2 \psi}{\partial \varphi^2} + D\frac{\partial \psi}{\partial \varphi} = E, \qquad (2\text{-}7)$$

where

$$A=\sin^2\theta\,\Sigma_{\theta\theta},\quad B=\sin\theta\left\{\frac{\partial}{\partial\theta}\left(\sin\theta\,\Sigma_{\theta\theta}\right)+\frac{\partial\Sigma_{\varphi\theta}}{\partial\varphi}\right\},\quad C=\Sigma_{\varphi\varphi},$$

$$D=\sin\theta\frac{\partial\Sigma_{\theta\varphi}}{\partial\theta}+\frac{\partial\Sigma_{\varphi\varphi}}{\partial\varphi},\quad E=-\mathrm{Re}^2 j_{\|}\sin^2\theta\sin I,$$

$$\sin I=\frac{2\cos\theta}{\left(1+3\cos^2\theta\right)^{1/2}}, \tag{2-8}$$

and the Re is the mean distance of the ionosphere from the center of the Earth. The equation (2-7) is converted to the difference equation to solve numerically. Putting spatially, two-dimensional distribution of $j_{\|}$ into it, Ψ can be obtained through iteration method of numerical calculation. Height-integrated current is obtained from the calculated potential as,

$$\begin{pmatrix} J_\theta \\ J_\phi \end{pmatrix}=-\begin{pmatrix} \Sigma_{\theta\theta} & \Sigma_{\theta\varphi} \\ \Sigma_{\varphi\theta} & \Sigma_{\varphi\varphi} \end{pmatrix}\cdot\begin{pmatrix} \dfrac{\partial\psi}{\mathrm{Re}\,\partial\theta} \\ \\ \dfrac{\partial\psi}{\mathrm{Re}\sin\theta\,\partial\varphi} \end{pmatrix}. \tag{2-9}$$

The distribution of $j_{\|}$ can be a realistic two-dimensional configuration based on the observations or artificial patterns as the approximation of the Region 1 or 2 field-aligned currents.

2.2 Evaluation of the Effect of the Equatorial Conductance

In this section, the effect of the equatorial conductance on the global scale ionospheric current system is evaluated making the calculation assuming some simplicities for a realistic conductivity model as shown in Figure 2-1. The profile of $\Sigma_{\theta\varphi}$ is not shown for $\theta > 89°$ because it decreases from a finite value at $\theta = 89°$ to zero at $\theta = 90°$. The model is constructed from $\sigma_{\|}$, σ_1 and σ_2 calculated every 5km in the height range from 80km to 400km and every 5° latitudes in the noon-midnight meridian, using IRI-76 and CIRA-72 models. It can be seen that all conductivity components grow high with decreasing latitude. The model is different from Kamide and Matsushita (1979a)'s model, where $\Sigma_{\varphi\varphi}$ was completely reduced at the equator. This profile is a nearly realistic model of the two-dimensional ionospheric conductivity.

Among all components, the gradient of $\Sigma_{\theta\theta}$ near the equator is most steep. It varies almost three

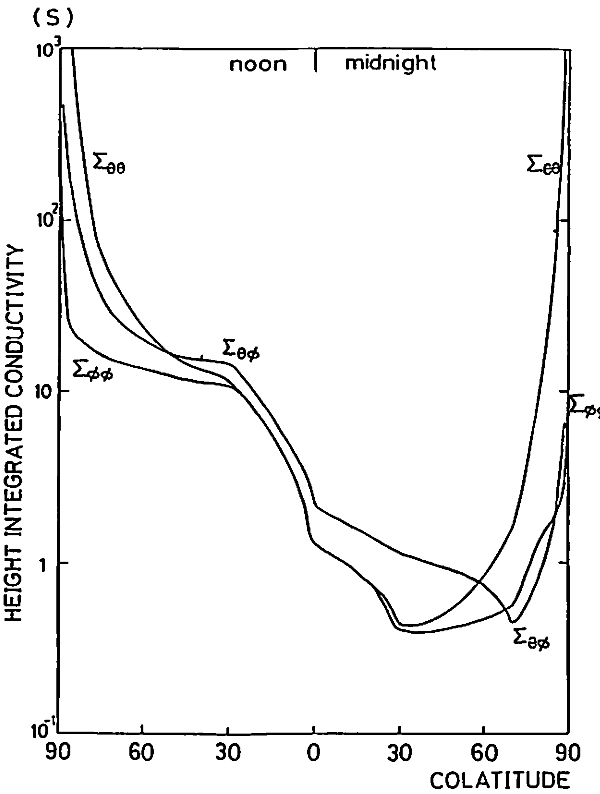

Figure 2-1: Noon-midnight profile of the ionospheric height-integrated conductivity used in Section 2.2. The extremely large values of $\Sigma_{\theta\theta}$ and zeros of $\Sigma_{\theta\varphi}$ in the equatorial region are not plotted in the figure (after Tsunomura and Araki, 1984).

orders of magnitude with only one degree of latitude from 1° latitude to the equator. If one operate a calculation with this condition, the calculation cannot be converged. Here, the artificial treatment that $\Sigma_{\theta\theta}$ at the equator is twice as large as that at 1° latitude is applied. This procedure is not thought to be far from the actual situation because the magnetic field lines of force may not be perfectly aligned horizontal for the whole height range of the ionosphere in reality.

Treatments are also made for $\Sigma_{\theta\varphi}$. One is making $\Sigma_{\theta\varphi}$ at 1° latitude equal to that at 2° and the other is to make $\Sigma_{\theta\varphi}$ symmetric with respect to the equator. The latter is inconsistent with the real nature because $\Sigma_{\theta\varphi}$ and $\Sigma_{\varphi\theta}$ are anti-symmetric with respect to the equator and is an important simplification from the realistic model; therefore, the calculation in this section is called "quasi-realistic".

Diurnal variation form of conductivity is

$$\Sigma_{ij}=const.=\Sigma_{ij0}\,, \tag{2-10}$$

from φ=270° (1800 LT) to φ=90° (0600 LT) and

$$\Sigma_{ij} = \frac{1}{2}\left(\Sigma_{ijn} - \Sigma_{ij0}\right)\left\{1 - \cos 2(\varphi - 90°)\right\} + \Sigma_{ij0}\ , \tag{2-11}$$

from φ=90° to, φ=270° ,where i and j represent θ or φ, Σ_{ij0} the value at midnight and Σ_{ijn} the value at noon, respectively. The field-aligned current pattern is given as $j_{\parallel} = -j_0 \sin\varphi \cos\{18(\theta - 15°)\}$, where $j_0 = 1.0 \times 10^{-7}$ (A/m^2) for θ = 10° - 20°. The sense of the field-aligned current is set to create a dusk-to-dawn electric field in the polar region, corresponding to PI of SC. This is because PI is thought to be purely ionospheric current origin and good for the first evaluation of the effect of the polar-originating ionospheric current system. The magnitude of $J_{\parallel}$ is taken so that the magnetic variation at the dayside equator becomes about 10 nT. It is much smaller than the Region 1 field-aligned currents for the most quiet times ($j_{max} \geqq 6.0 \times 10^{-7}$ A/m for Kp = 0 (Iijima and Potemra, 1976)).

Under these conditions, successive over relaxation (SOR) method is operated for the difference equation extended horizontally with the grids of 1° for θ and 7.5° for φ. The relaxation coefficient is 1.5. In the calculation, difference between the geographic and the geomagnetic poles and those between local time (LT) and magnetic local time (MLT) are not taken into account. This is same for all the calculations in the following sections.

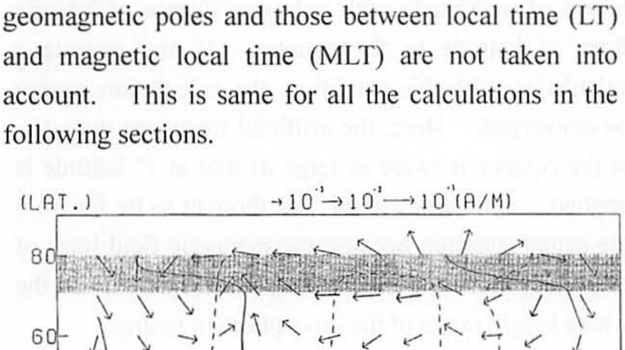

Figure 2-2: Global distribution of the ionospheric currents for the quasi-realistic model. The dashed zone is the source-current region (after Tsunomura and Araki, 1984).

Global distribution of ionospheric current vectors is presented in Figure 2-2. Although the conductivity model and source currents are symmetric and anti-symmetric with respect to the noon-midnight meridian, respectively, the current pattern is asymmetric. Approximately, the θ-components of the Pesersen and the Hall currents are antisymmetric and symmetric and the φ-components of them are symmetric and antisymmetric with respect to the noon-midnight meridian, respectively. Both components of resulting currents are, therefore, basically asymmetric with respect to the meridian.

The shaded zone between 70° and 80° latitudes indicates the source current region where the field-aligned current flows into the ionosphere in the afternoon side and away from it in the morning side. The ionospheric current diverges from the source region in the afternoon side rotating its direction clockwise and converges to the one in the morning side counterclockwise. The rotation of the current vector is due to the Hall conductivity and especially notable in high latitudes where $\Sigma_{\theta\varphi}$ is larger than $\Sigma_{\theta\theta}$ and $\Sigma_{\varphi\varphi}$.

The sense of the rotation is roughly consistent with the equivalent current system shown by Nagata and Abe (1955) (Figure 1-4). In high latitudes, the magnetic field at the ground produced by that due to the field-aligned currents and the pattern of ionospheric currents effective for the magnetic variations at ground will be more like the equivalent current system which closes in the ionosphere.

Solid and dashed curves in the figure are the demarcation lines for the reversal of the signs of the east-west and the north-south components. The latter changes its sign four times a day in the latitude region between 30° and 70°. This is roughly consistent with the statistical analysis of the diurnal variation of the sign of SC* (Sano, 1963). The fact that amplitude of the north-south component is largest in the morning hour is consistent with observations that SC* in the D-component is more easily detected in the morning than in the afternoon (Matsushita, 1962). In the early morning hours, the φ-component of the currents is eastward in the region from the equator to the source current region. The increase of the H-component should be produced by the currents in this region but sometimes it might be masked by larger increase of the *DL*-field of SC (Araki, 1977). In high latitudes where the amplitude of the *DL*-field is small, the currents may contribute to the inverted SC* which frequently appears in the morning hours (Matsushita, 1957, 1960).

At the equator where $\Sigma_{\theta\varphi} = 0$ and $E_\theta = 0$ (due to the boundary condition), the current direction is exactly east-west. The currents from the higher latitudes flow into the equator in the afternoon and away from it in the morning. Throughout whole latitudes, the region of the westward current is wider in local time than that of the eastward current. This is due to the dayside enhancement of the conductivity (especially at the equator). If there is no diurnal variation for the conductivity, the width of both region will be the same.

The latitudinal variation of the total current density, J and the total electric field, E are shown as curves noted by 'b' in Figure 2-3. For comparison, results of the calculation for the uniform distribution of the conductivity are also given (curves noted by 'a'), in which $\Sigma_{\theta\theta}$, $\Sigma_{\theta\varphi}$ and $\Sigma_{\varphi\varphi}$ are 10 S and $\Sigma_{\varphi\theta}$ is −10 S everywhere except the equator ($\Sigma_{\theta\varphi} = \Sigma_{\varphi\theta} = 0$ at the equator). The value 10 S (or −10 S) is nearly equal to the dayside conductivity around 60° latitude in the quasi-realistic model.

In the uniform conductivity model, E and J decrease monotonously with decreasing latitude showing the simple geometrical attenuation. A local steep decrease of J at the equator is caused by zero dropping of $\Sigma_{\theta\varphi}$ there. The latitudinal decrease of E for the quasi-realistic model is steeper than that for the uniform model. This is because the latitudinal increase of the conductivity toward the dayside equator produces a distribution of counter polarization charges and shields the primary electric field. In spite of the reduction of the elctric field, the ionospheric current in the quasi-realistic model shows a clear equatorial enhancement.

Figure 2-4 shows the latitudinal variation of the θ- and φ-components of the electric field at 12 LT. Subscripts a and b are the same as used in Figure 2-3. A clear difference between two models is seen in the behavior of E_θ. $E_{\theta a}$ is smaller than $E_{\theta b}$ in high and middle latitudes, increases slowly with decreasing latitude and drops zero suddenly at the equator, while $E_{\theta b}$ decreases monotonously from the higher value at high latitudes to zero at the equator.

If the conductivity is uniform, there is no accumulation of charges anywhere and the electric field lines simply connect two source-current regions

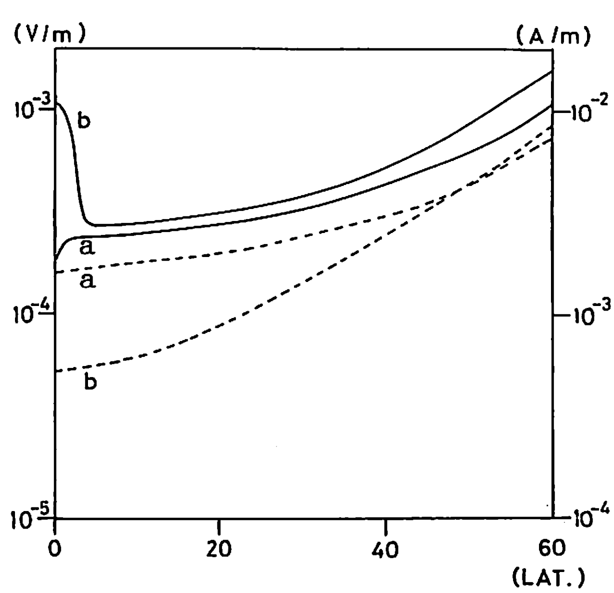

Figure 2-3: Latitudinal variation of the total current density (solid lines) and the total electric field (broken lines) at 12 LT for the uniform model (a) and the quasi-realistic model (b) (after Tsunomura and Araki, 1984).

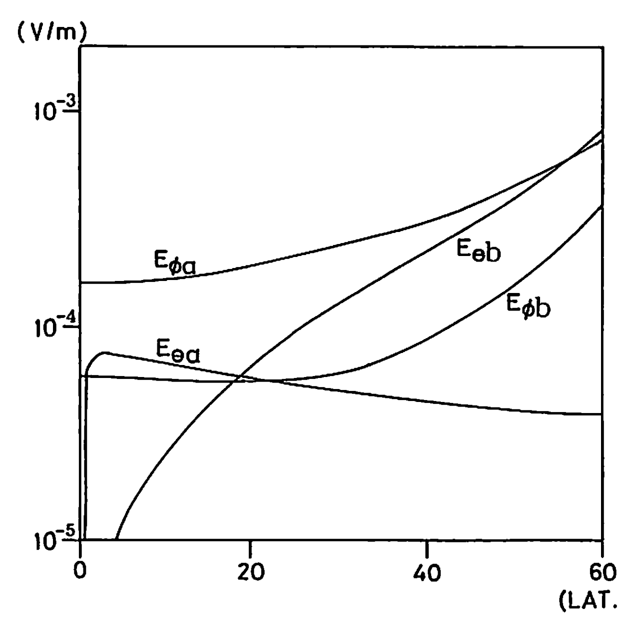

Figure 2-4: Latitudinal variation of the north-south component of electric field (E_θ) and the east-west component (E_φ) at 12 LT for the uniform model (a) and the quasi-realistic model (b) (after Tsunomura and Araki, 1984).

without being modified by the existence of a medium. Since the source currents flow into and away from the ionosphere symmetrically with respect to the noon-midnight meridian, the θ-component of the electric field should be vanished along the noon-midnight meridian if there is no effect of the medium. In the uniform model, $\Sigma_{\theta\theta}$ and $\Sigma_{\varphi\varphi}$ are perfectly uniform everywhere but the non-diagonal terms, $\Sigma_{\theta\varphi}$ and $\Sigma_{\varphi\theta}$ contribute the deformation of the symmetric distributionof the electric field with respect to the noon-midnight meridian and the resulting finite E_θ along the meridian. It makes a skewness of the electric potential contours and causes E_θ in higher latitudes in the meridian. The sudden drop of $E_{\theta a}$ to zero at the equator is due to the boundary condition.

Since the charge accumulation due to the non-uniform conductivity occurs everywhere in the quasi-realistic model, the θ-component of the electric field, $E_{\theta b}$, in high and middle latitudes is larger than that for the uniform model which is non-uniform only near the equator. A large $E_{\theta b}$ cannot be retained in low latitudes of the dayside, however, because of the great enhancement of $\Sigma_{\theta\theta}$ and $E_{\theta b}$ simply converges to zero at the equator. The effet of large $\Sigma_{\theta\theta}$ is also reflected on the latitudinal variation of $E_{\varphi b}$ in low latitudes, where $E_{\varphi b}$ is almost constant up to 20° from the equator. This is because the short circuit effect of the large $\Sigma_{\theta\theta}$. $E_{\varphi b}$ near the equator is almost half of $E_{\varphi a}$. It means that the electric field is reduced even in the quasi-realistic model because of the daytime enhancement of conductivity. It is noteworthy that $E_{\varphi b}$ in low latitudes is not so much reduced due to the counterpolarization at the equator.

Figure 2-5 shows the longitudinal variation of the total current density along six latitude circles. The current density decreases with decreasing latitude at most local times but is greatly enhanced at the dayside equator. The peak values at the equator is higher than that at 45° and is nearly equal to the level at 60°.

When an SC* occurs, the PI is superimposed by the increase of the horizontal component (MI) in low and middle latitudes. The magnitude of MI takes the maximum at the equator (Araki, 1977) and decreases with increasing latitude gradually (Rastogi and Sastri, 1974). Hence, the decrease of the H-component of the PI due to the westward current will be vanished by the masking effect of the MI in the ground observation in the dayside low latitudes where the overhead

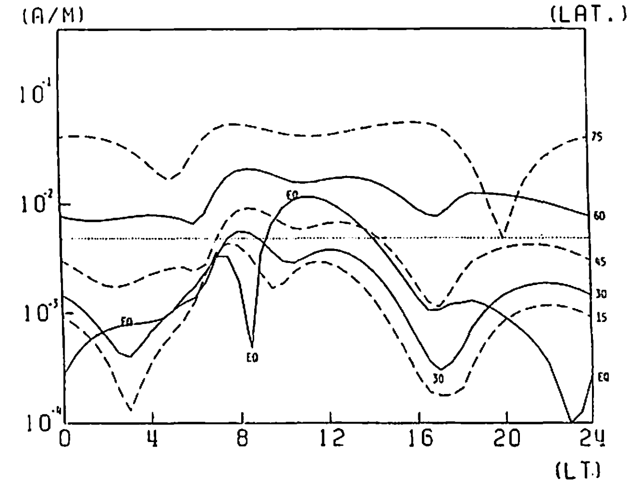

Figure 2-5: Longitudinal variation of the total current densities at 75, 60, 45, 30, 15° latitudes and the equator for the quasi-realistic model. The dotted line denotes an assumed threshold for detection of a PI (after Tsunomura and Araki, 1984).

ionospheric current is not enhanced sufficiently. If the horizontal dotted line is assumed to be the magnitude of the MI in low latitudes, a station at 15° latitude cannot observes the ionospheric current effect which can be detected at the stations in higher latitudes and at the dayside equator. This can well explain why a PI of SC* is hardly observed at low latitude stations off the equator (Honolulu, for example), while it is detected simultaneously in high latitudes in the afternoon-side and the dayside equator.

The longitudinal variation of the eastward component of the current density (J_φ) and that of the electric field (E_φ) at the equator are given in Figure 2-6, which shows clearly the daytime enhancement of J_φ as well as the daytime reduction of E_φ due to shielding by enhanced $\Sigma_{\varphi\varphi}$ (Cowling conductivity). The westward current density takes the maximum value just before noon, that is, the curent flows into (away from) the equator from (toward) higher latitudes in the afternoon (morning). The result roughly presents the observed feature but the recent observational results of the equatorial electric field associated with SC* show somewhat different features from this result (Sastri et al., 1993). The quasi-realistic model is not sufficient to produce the realistic fields at the equator exactly. Seeing the above results, however, it is thought that the two-dimensional calculation based on the thin shell

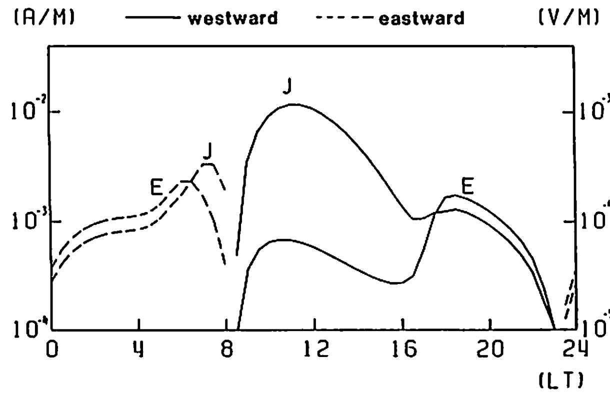

Figure 2-6: Longitudinal variation of E_φ and J_φ at the equator for the quasi-realistic model. Solid lines denote westward and broken lines eastward (after Tsunomura and Araki, 1984).

model can reproduce a realistic solution when the conductivity model is appropriate.

Simulation studies of polar-originating ionospheric currents including the equatorial enhancement of the ionospheric conductivity were developed by Takeda (1982), Senior and Blanc (1984) and recently by Denisenko and Zamay (1992). Although Takeda (1982)'s model may be the overcoming among these, the treatment is more complicated than the thin shell model and not versatile always. Senior and Blanc (1984)'s model treats the equator differently from other region; the equatorial region is assumed as a conducting belt. Their model is succesful in presenting the local time profile of the electric field and current at the equator but cannot show the latitudinal profile of the electric field and current. Denisenko and Zamay (1992) presented a new geometrical structure based on the high conductance along the magnetic lines of force to describe the ionospheric condition. The model needs some complicated techniqes in coding programs and they did not show the latitudinal profiles of the electric and magnetic fields. Hence, so long as the horizontal distribution of the electric field and current are concerned, it is certainly useful to improve the thin shell model so as to be capable of yielding the realistic results and to be versatile for various needs. The improved model will be proposed in the following sections.

2.3 Estimate of the Realistic Conductivity Model

2.3.1 Modeling of the Diagonal Terms ($\Sigma_{\theta\theta}$ and $\Sigma_{\varphi\varphi}$) of the Conductivity Tensor near the Equator

The distribution of the conductivity should be set as realistic as possible. The base of the ionospheric conductivity σ_0, σ_1 and σ_2 are obtained in the noon and midnight meridian using IRI-90 (electron density) and CIRA-72 models (density of neutral particles). Collision frequencies are the average of collision frequencies for five kinds of the positive ions; collision frequencies are calculated using masses and gyro frequencies derived from IRI-90 and CIRA-72 and coefficients deduced from the Table of Banks and Cockarts (1973). And then $\sigma_{\theta\theta}$, $\sigma_{\theta\varphi}$ and $\sigma_{\varphi\varphi}$ are integrated with height from 80 to 400 km.

The enhancement of the conductivity in the auroral region is added using the model presented by Reiff (1984). This process is necessary; otherwise the resulting potential drop in high latitudes becomes too large compared with the values deduced from observations. As the base model for geomagnetically quiet period, the conductivity in the auroral region is calculated putting zero to the AE parameter in the model of Reiff (1984). The derived Pedersen conductivity is superposed on $\Sigma_{\theta\theta}$ and $\Sigma_{\varphi\varphi}$ of the IRI model and Hall conductance on $\Sigma_{\theta\varphi}$. $\Sigma_{\varphi\theta}$ is given as $-\Sigma_{\theta\varphi}$ at this stage.

For $\Sigma_{\theta\theta}$ which increases very rapidly, the value at the equator is reduced such that the gradient of $\sigma_{\varphi\varphi}$ at 1° latitude becomes equal to that at 2° latitude. This procedure is similar to that of the previous section.

Second, the modification of $\Sigma_{\varphi\varphi}$ is made. Untiedt (1967) and Richmond (1973) made calculations of an equatorial meridional current system driven by external eastward electric field and showed that the strength and width of the height-integrated eastward ionospheric current are increased compared to $\sigma_{\varphi\varphi}$ model (equivalent to the thin shell model) of Sugiura and Cain (1966). Being based on the same conductivity profiles in height and the same eastward electric field strength, this result means that the height-integrated conductivity is enhanced equivalently by the existence of the meridional current system. Both of the meridional current system models of Untiedt (1967) and Richmond (1973) yielded more realistic solutions than those of $\sigma_{\varphi\varphi}$ model. The existence of the meridional current system was evidenced by the observations by rocket measurements (Musmann and Seiler, 1978) and MAGSAT (Maeda et al., 1982). By making a three-dimensional calculation in the equatorial region, Forbes and Lindzen (1976a, b) showed that the equatorial electrojet strength is nearly doubled and the jet region is widened. Hence, it is strongly suggested that the strength and the width of $\Sigma_{\varphi\varphi}$ should be enhanced and broadened, respectively more than those in the thin shell model.

To understand this mechanism clearly, the mechanism of the meridional current system should be discussed. The secondary, upward electric field perpendicular to the magnetic field line of force is appeared as a polarization electric field near the equator due to the downward Hall current driven by the external eastward electric field impressed to the equatorial region. The strength of the polarization field is assumed such that the Pedersen current driven by the field cancels the Hall current driven by the original eastward field in the thin shell model; it becomes nearly thirty times as large as that of the original field (Figure 2-7). The polarization electric field also drives the secondary eastward Hall current. The resulting eastward electric current becomes very large at the equator. This is the basic mechanism to yield large value of $\Sigma_{\varphi\varphi}$ at the equator (Hirono, 1952; Baker and Martyn, 1953).

In reality, a meridional current system will be appeared as shown above. The sense of the meridional current is clockwise (counterclockwise) viewed from the east when eastward (westward) external electric field of global scale is impressed. At the equator the upward (downward) current should exist ($J_z>0$) under this condition. Then the magnitude of the vertical electric field E_z (= $\sigma_2 E_\varphi / \sigma_1$, which is obtained under the assumption that $J_z = \sigma_1 E_z - \sigma_2 E_\varphi = 0$) should become larger. Forbes and Lindzen (1976b) gave an similar explanation to enhance $\Sigma_{\varphi\varphi}$ by the effect of vertical current flow. The vertical electric field and/or the resulting eastward (westward) Hall current at the equator is highest in the altitude range from 100 to 105 km (Untiedt, 1967, Sugiura and Poros, 1969, Richmond, 1973).

A speculation for the production mechanism of the meridional current system is presented as follows. Figure 2-7 illustrates the electrical situation in the meridional plain in the equatorial region. Suppose an electrical circuit noted as 'ABCD' in the left figure. The electric field perpendicular to magnetic lines of force may basically show similar height variation with that of the thin shell model at first. Then the low altitude portion off the equator ('DC') and the high altitude one at the equator ('AB') act as batteries with strong and weak voltages, respectively. Hence, the total electromotive force is not cancelled in the circuit 'ABCD' and there flows an electric current as shown by thick arrows in the figure. Similar discussion was given by Reddy and Devasia (1978). In this sense, the meridional current system is regarded as the redistribution process of electric field, driven by the unbalance of the polarization electric fields aligned on the same magnetic lines of force.

As Maeda et al. (1982) showed, the horizontal

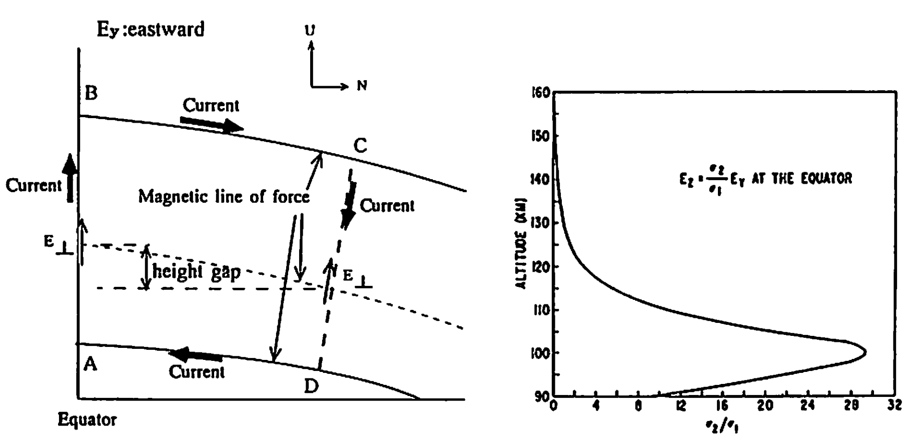

Figure 2-7: Left: Illustration of the electrical circuit analogy in the meridional plane near the equator. Thick arrows denote the meridional currents. Ey is the east-west component of the electric field. Right: The ratio σ_2/σ_1 (for 280E longitude) as a function of height, representing the E_z in the thin shell model (after Sugiura and Cain, 1966).

scale of the meridional current system in the north-south direction may be nearly 20° in latitude. Similar enhancement mechanism for $\Sigma_{\varphi\varphi}$ is expected to be efficient for the region near the equator; thus the width of the electrojet becomes broad as pointed out by Untiedt (1967).

The comparison of the meridional current and the $\sigma_{\varphi\varphi}$ models for the eastward height-integrated current is presented by Untiedt (1967) (Figure 2-8). The result is used to decide the multiplication factor for $\Sigma_{\varphi\varphi}$ of the thin shell model. According to Figure 2-8, $\Sigma_{\varphi\varphi}$ in the equatorial region is multiplied as follows; 1.2 times at the equator, 1.8 times at 1° latitude, twice at 2° latitude. For higher latitudes than 2°, the multiplication factor is linearly decreased with increasing latitude to the unity at 25° latitude.

Figure 2-9 shows the two-dimensional height-integrated conductivity in the noon-midnight meridian obtained for the conditions of the equinox, the sunspot number = 50 and 0° geographic longitude for IRI-90 parameters after the procedures for $\Sigma_{\theta\theta}$ and $\Sigma_{\varphi\varphi}$ mentioned above. The pattern is almost same as the conductivity model of the previous section except for the slight enhancement in the auroral region. The enhancement in the region becomes large when AE parameter is increased.

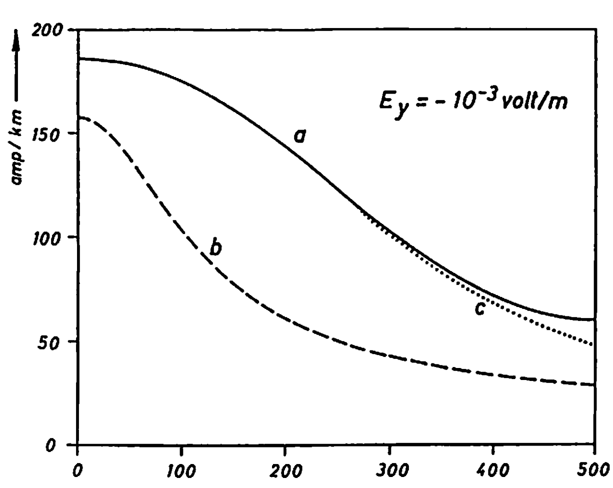

Figure 2-8: The height-integrated current density of the electrojet as a function of x for the new model (curve a), for the corresponding σ_{yy} model (curve b), and for the new model in the case of the modified boundary condition, $\Psi = 0$ at x = 500 km (curve c) (after Untiedt, 1967). Here, x is the distance from the equator and Ey is the westward component of the electric field. Thus, the σ_{yy} model is the same as the $\sigma_{\varphi\varphi}$ model in essence.

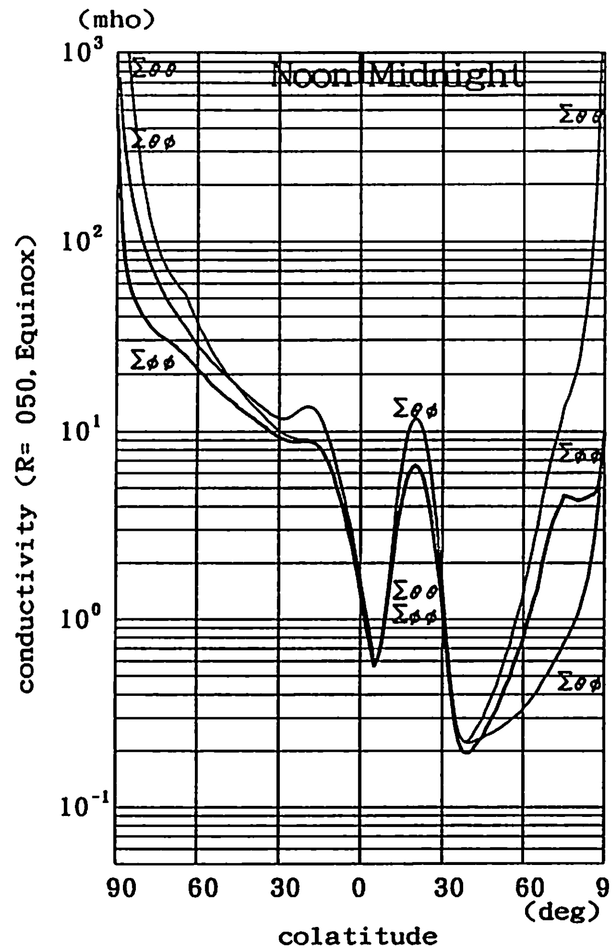

Figure 2-9: Noon-midnight profile of $\Sigma_{\theta\theta}$, $\Sigma_{\theta\varphi}$ and $\Sigma_{\varphi\varphi}$ of the ionospheric height-integrated conductivity tensor for the condition on equinox with sunspot number = 50 for the IRI parameters. The extremely large values of $\Sigma_{\theta\theta}$ and zeros of $\Sigma_{\theta\varphi}$ in the equatorial region are not plotted in the figure (after Tsunomura, 1999).

2.3.2 Modeling of the Non-diagonal Terms ($\Sigma_{\theta\varphi}$ and $\Sigma_{\varphi\theta}$) of the Conductivity Tensor near the Equator

The treatment of $\Sigma_{\theta\varphi}$ is more complicated and important to discuss the structure of the electric field at the equator. In the thin shell model, $\Sigma_{\theta\varphi}$ becomes maximum at the neighbor of the equator, reduced to zero at the equator and changes its sign anti-symmetrically beyond the equator. The quasi-realistic model assumes $\Sigma_{\theta\varphi}$ at 1° latitude equal to that at 2° latitude and ignores its gradient at the equator. The modeling of the $\Sigma_{\theta\varphi}$ near the equator should be discussed to make the physical base more definite. Besides, the quasi-realistic model cannot be applied to the calculation covering both hemispheres simultaneously.

Before the discussion of $\Sigma_{\theta\varphi}$, the original equations to derive equation (2-3) should be examined. The equation for j_θ is written as follows;

$$j_\theta = (\sigma_0 \cos^2 I + \sigma_1 \sin^2 I)\cdot E_\theta + \sigma_2 \sin I \cdot E_\varphi + (\sigma_0 - \sigma_1)\sin I \cos I \cdot E_z \tag{2-12}$$

E_z is written as,

$$E_z = \frac{-(\sigma_0 - \sigma_1)\sin I \cos I \cdot E_\theta + \sigma_2 \cos I \cdot E_\varphi}{\sigma_0 \sin^2 I + \sigma_1 \cos^2 I}. \tag{2-13}$$

The contributions of the original east-west component of electric field to the north-south component of electric current as shown in the second term of the right side of the equation (2-12) appears explicitly as long as E_φ exists. The contribution through the vertical field, E_z as described in the second term of the numerator of the right side of the equation (2-13), and then the third term of the right side of the equation (2-12) should be examined.

In the thin shell model, the algebraic calculation is operated under the assumption that the vertical current is zero (Figure 2-10). This procedure yields the vertical electric field as an algebraic product. The vertical component includes the parallel component with respect to the magnetic field line of force off the equator and then contributes the north-south component of ionospheric current through the longitudinal conductivity, σ_0. This is the mechanism for bearing large values of $\sigma_{\theta\varphi}$ near the equator.

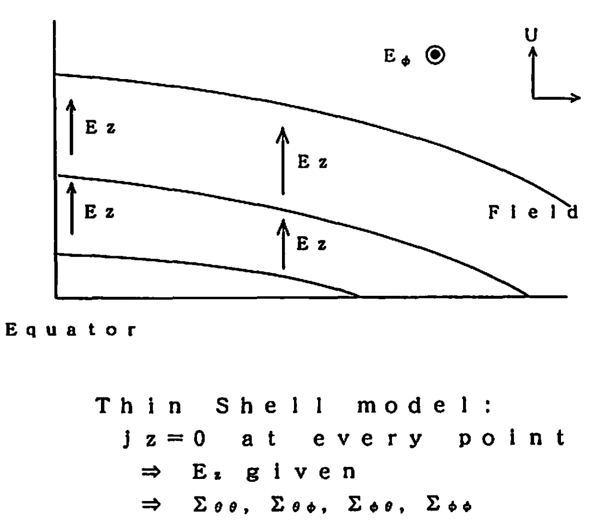

Figure 2-10: Illustration of the vertical component of electric field for the thin shell model.

Note that this discussion is applied for the polarization field, E_z. It is not necessary to modify the first term of the right side of equation (2-12) which is directly related with the external north-south component of electric field. The situation that the polarization electric field in the north-south direction is weak is confirmed by the numerical analysis of the meridional current system by Richmond (1973). The potential contour in the meridional plane, which is produced by giving the eastward electric field as the driving source, was almost parallel to the magnetic field line in his result. The thin shell model does not consider this situation and then leads large value of $\sigma_{\theta\varphi}$ just near the equator.

Therefore, the contribution of the parallel component by E_z in the thin shell model as described in the second term of the numerator of the right side of the equation (2-13) should be reduced to get the more realistic values of $\Sigma_{\theta\varphi}$ near the equator. This process can be understood as another effect of the meridional current system.

As the reduction factor cannot be decided theoretically, the trial and error method is performed to find the solution. First, the contribution of the second term of the numerator of equation (2-13) is decreased from the equation (2-3) in the course of height integration by the rate of 0.0, 0.5, 0.75 and 1.0. In each model the rate is maximum at 1° latitude and decreased linearly with increasing latitude to zero at 30° latitude. The noon-midnight profiles of $\Sigma_{\theta\varphi}$ with the maximum reduction rate, 0.0, 0.5, 0.75 and 1.0 are shown in Figure 2-11. The model 0.0 corresponds to the original profile. Note that $\Sigma_{\theta\varphi}$ shows the maximum just neighboring the equator (1° latitude in the figure) except for the full reduction model (the reduction rate is 1.0). The latitudinal gradient of $\Sigma_{\theta\varphi}$ at 1° latitude is zero for the models of the 0.0, 0.5 and 0.75 reduction rates. Standing on the viewpoint that the parallel component of electric field with respect to the magnetic field line should be small, the full reduction model is expected to be most realistic. It is noteworthy that the pattern of $\Sigma_{\theta\varphi}$ of the full reduction model is similar to that of Fejer (1953) except for the difference in the peak latitude.

The above discussion was devoted to the feature

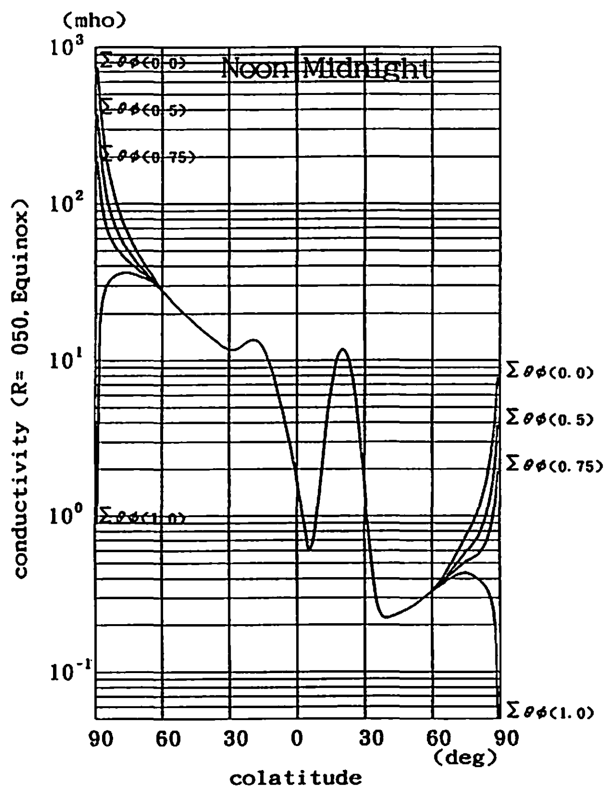

Figure 2-11: Noon-midnight profiles of $\Sigma_{\theta\varphi}$'s with maximum reduction rates of 0%($\Sigma_{\theta\varphi(0.0)}$), 50%($\Sigma_{\theta\varphi(0.5)}$), 75%($\Sigma_{\theta\varphi(0.75)}$) and 100%($\Sigma_{\theta\varphi(1.0)}$) for the E_z contribution in the longitudinal direction. The IRI parameters and the plot style are the same as those for Figure 2-9 (after Tsunomura, 1999).

of polarization electric field (E_z) driven by the external east-west component of the electric field (E_φ); the modification of E_z thus influences the conductivity components associated with E_φ, that is, $\Sigma_{\theta\varphi}$ and $\Sigma_{\varphi\varphi}$. The reduction of $\Sigma_{\theta\varphi}$ and the enhancement and broadening of $\Sigma_{\varphi\varphi}$ from the thin shell model are the products obtained by allowing the vertical current which forms the meridional current system.

It is difficult to decide whether a meridional current system is driven by the north-south component of the electric field (E_θ). Untiedt (1967) briefly discussed this matter and showed that E_θ does not drive meridional current so much as a result of numerical calculation. This means that the modulation of $\Sigma_{\theta\varphi}$ from the thin shell model is not appropriate. Therefore, the similar procedure as $\Sigma_{\theta\varphi}$ is not operated for $\Sigma_{\varphi\theta}$. In reality, the calculated results of the ionospheric electric field and current were not so much changed by the modulation of $\Sigma_{\varphi\theta}$ because of the smallness of E_θ.

2.3.3 Intercomparison of the Results for the Different Models of $\Sigma_{\theta\varphi}$

With the four conductivity models designed in the previous subsection, the electric fields and currents are calculated giving the current source in high latitudes. The diurnal variation form of conductivity is assumed as a sine curve from 04-20 LT; the form is basically equivalent to that of Tarpley (1970) or Richmond et al. (1976).

The distribution of the field-aligned current of Gaussian type is given similarly as that of Kamide and Matsushita (1979a). Its functional form is

$$j_{\parallel} = \pm j_0 \exp\left[-\frac{(\theta-\theta_0)^2}{D_\theta^{\ 2}} - \frac{(\varphi \mp \varphi_0)^2}{D_\varphi^{\ 2}}\right], \qquad (2\text{-}14)$$

where the upper and lower signs of j_0 and φ_0 are taken for the currents flowing into and away from the ionosphere, respectively. The parameters, θ_0, φ_0, D_θ, D_φ and j_0 are 15°, 105°, 2°, 59° and 10^{-6} A/m^2, respectively. In this case the total amount of the current becomes 1.13×10^6 A. The result is linearly changed by the strength of j_0. The boundary condition for the electric potential at the equator is $d\Psi/d\theta = 0$, and at the pole Ψ= (the mean of Ψ at 89° latitude circle).

The equation is solved by SOR method. The relaxation coeeficient is gained to 1.7 to have a rapid conversion. The basic grid spacing is 1° for the direction of θ and 7.5° for φ. Since the conductivity changes very rapidly near the equator, the grid spacng in θ direction is set 0.5° in the region from the equator to 10° latitude. The narrowing of the grid spacing in this region is primarily important to obtain the true result. Figure 2-12 shows the difference in the results for the equatorial electric fields by changing the grid spacing in the equatorial region. Drastic change of the numerical solution is seen with narrowing the grid spacing from 2° to 1°; the sense of the electric field at the equator was reversed. The change of the solution from 1° to 0.5° is not so large, accompanying slight enhancement of the electric field strength at the equator. The solution becomes constant for the narrower spacing than 0.5°. I checked it down to 0.1° setting (not shown here). In this study, 0.5° spacing was adopted.

The narrowing of the grid spacing in other region is not so important since the result obtained setting the grid spacing 0.5° for the whole space is almost the

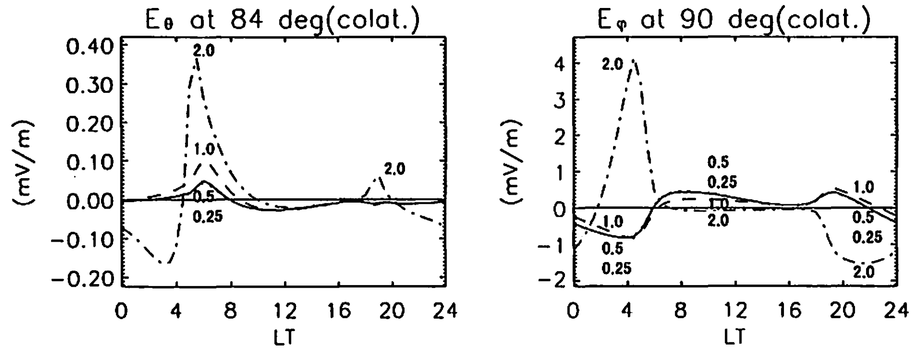

Figure 2-12: Electric and magnetic fields for the calculated results setting the grid spacing as 2° (dot-dashed lines), 1° (dashed lines), 0.5° (dotted lines) and 0.25° (solid lines) for θ direction in the equatorial region.

same with that obtained limiting the narrowing area in the equatorial region. Note that the latitude at which $\Sigma_{\theta\varphi}$ and $\Sigma_{\varphi\theta}$ take maxima (except for $\Sigma_{\theta\varphi}$ in the full reduction model) is 0.5°, that is, just at the neighbour of the equator.

Electric field and current are calculated in each thousand calculation to monitor the convergence of calculation. Figure 2-13 shows the time change of the magnetic field at every 10° in latitude in the noon meridian calculated for each thousand iteration. The magnetic field is increased at the early stage of the iteration in high latitudes, whereas that at the equator delays very much. The real time constant for this process cannot be estimated exactly but it should be kept in mind when discussing the phase of the equatorial magnetic phenomena precisely that the development of DC electric field can yield some phase lag due to the electric conductance. Figure 2-14 is the similar plot for the electric field at the equator for every two LT's. It is noteworthy that the time

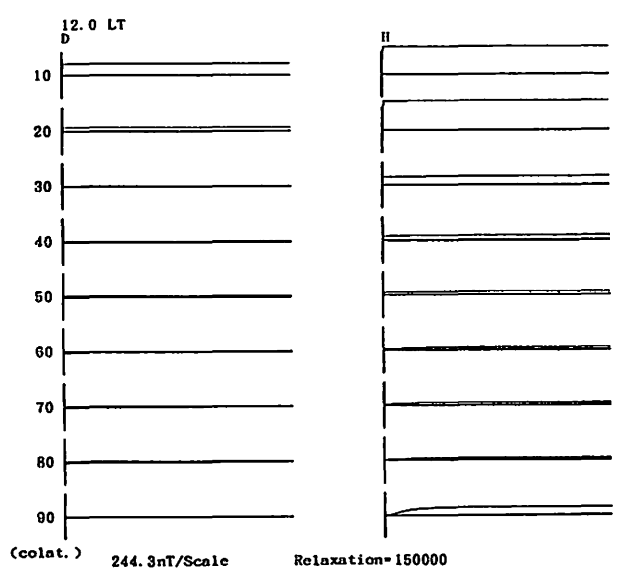

Figure 2-13: Latitudinal profile of the time change of the electric currents (in unit of nT) corresponding to the D- and H- component magnetic fields obtained for every 1000 times iteration at 80°, 70°, 60°, 50°, 40°, 30°, 20°, 10° latitudes and the equator.

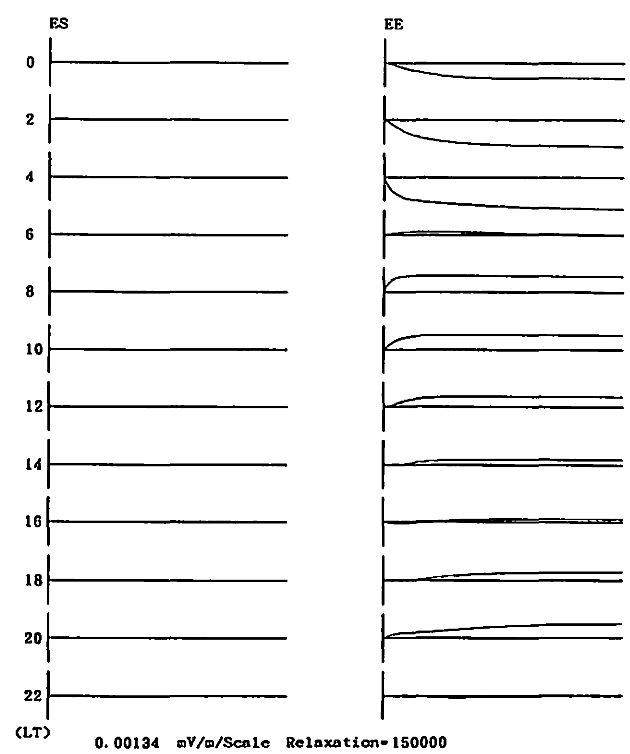

Figure 2-14: Local time profile of the time change of the southward component of electric field (ES) at 1° latitude and the eastward one (EE) at the equator obtained for every 1000 times iteration at every 2 hour in LT. ES is not apparent because of the very small amplitude.

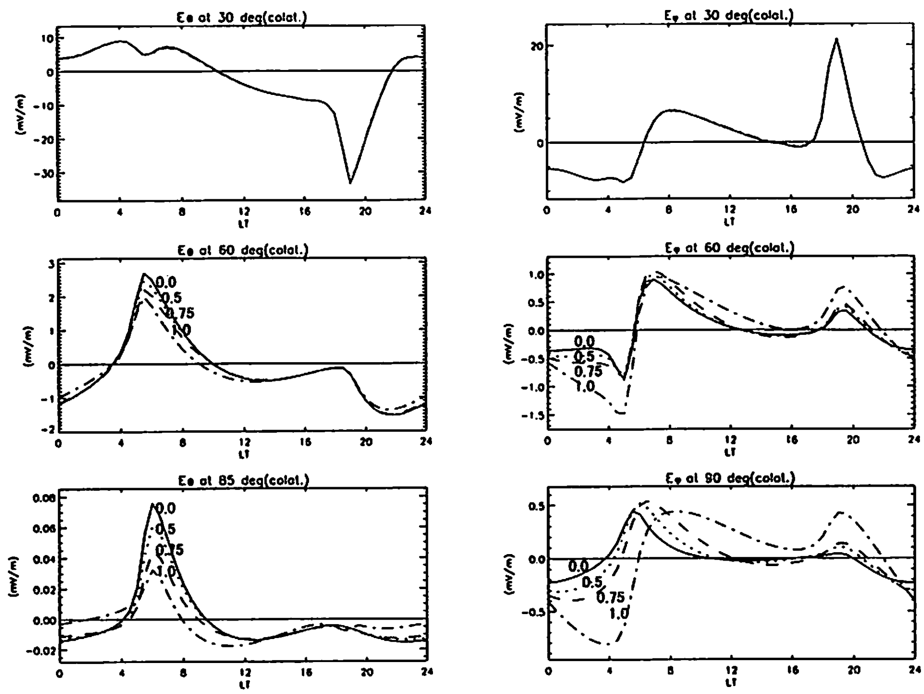

Figure 2-15(a): Local time variations of southward (E_θ, left panels) and eastward (E_θ, right panels) components of the ionospheric electric fields at 60°, 30° latitudes and the equator calculated for the four conductivity models. Solid, dotted, dashed and dot-dashed lines are the results with $\Sigma_{\theta\varphi}$ of 0.0, 0.5, 0.75 and 1.0 reduction, respectively; numbers labeled on the curves mean the reduction rate. Note that four curves are almost the same in the uppermost panels (after Tsunomura, 1999).

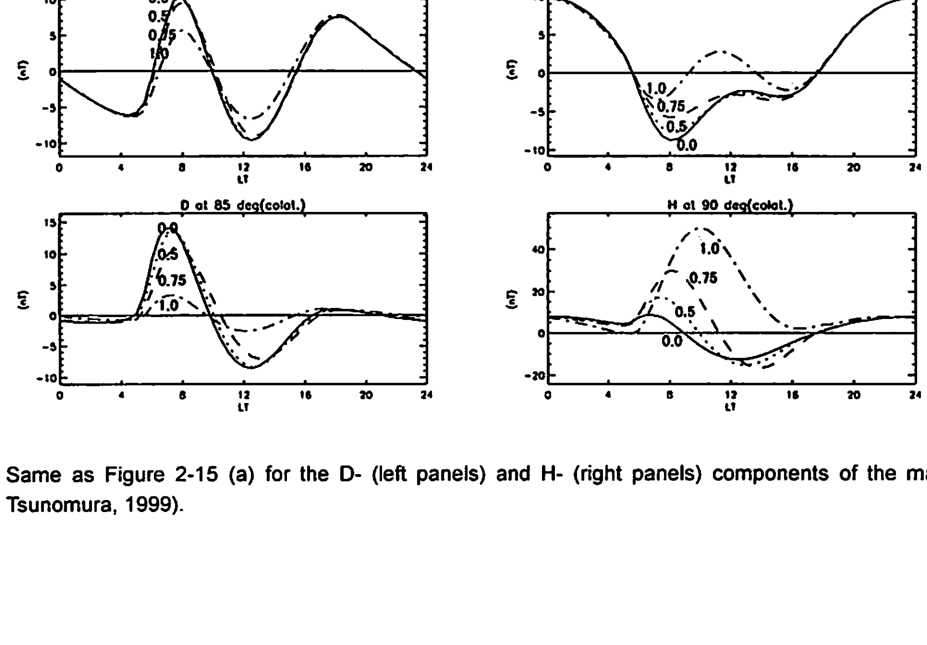

Figure 2-15(b): Same as Figure 2-15 (a) for the D- (left panels) and H- (right panels) components of the magnetic fields (after Tsunomura, 1999).

constant for the convergence of calculation is different for different LT. Viewing this figure, the calculation is expected to converge after about 120000 iteration.

Local time profiles of electric fields and magnetic fields at 60°, 30° latitudes and the equator for the four models are shown in Figures 2-15(a) and (b), respectively. For the north-south components near the equator, the data at 5° latitude are shown because they are almost vanished near the equator. The magnetic fields are derived from the equivalent currents, that is, the magnetic field due to the field-aligned current, obtained numerically assuming the geomagnetic dipole configuration of the magnetic line of force is added to that of the overhead, ionospheric current. Near the equator, the magnetic fields are calculated using Biot-Savart's law for the ionospheric currents in the range of 5° north and south, because the electrojet current flows in the narrow region and the approximation of the overhead current sheet is broken. Ground induction effect is neglected.

It is clearly seen that electric and magnetic fields at 60° latitude are not affected by the $\Sigma_{\theta\varphi}$ modulation in the equatorial region. The variation pattern of the magnetic field in 60° latitude is almost identical with the local time distribution of the variation sense of SC's as shown by Matsushita (1962). Although the full reduction model shows brief difference from other models at 30° latitude in the dayside, the profiles in 60° and 30° latitudes are in general similar to the results of the quasi-realistic model. The profile of the eastward component of electric field (E_φ) at 30° is consistent with the local time profile of the polarity of MFD of SCF in the observations of HF Doppler frequencies associated SC as shown by Kikuchi et al. (1985) (Figure 1-6).

At the equator, the E_φ varies very much by the modification of $\Sigma_{\theta\varphi}$, resulting in the drastic change of magnetic variations. It can be seen that the southward component (E_θ) of the electric field in the morning gradually decreases with increasing the reduction rate, whereas the E_φ increases. The E_φ's in the dayside equator for the models except for that of the full reduction are small and negative. The curves of the E_φ for the models of 0.0, 0.5 and 0.75 cross the zero line twice in the afternoon; it means that there appears a singular point in the afternoon for the potential at the equator in these models. This feature of E_φ at the equator is attributed to the situation that $\Sigma_{\theta\varphi}$ takes the sharp maximum just at the neighbor of the equator.

In order to examine the electric field configuration more clearly, the potential contours in low latitudes are shown for the full and zero reduction models in Figure 2-16. In the figure only the potential pattern in low latitudes are shown. The density of potential contour in the latitude range from 30° latitude to the equator becomes sparse for the zero reduction model. This can be explained as follows. Large $\Sigma_{\theta\varphi}$ causes the southward current just near the equator and gives charge accumulation at the equator. This charge makes northward electric field and current.

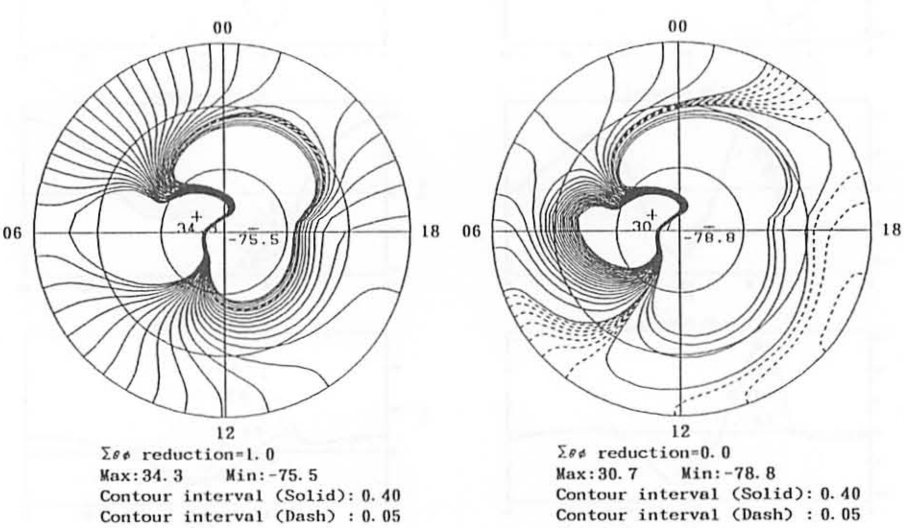

Figure 2-16: Potential contours in low latitude region obtained for the conductivity models with $\Sigma_{\theta\varphi}$ of 1.0 (left) and 0.0 (right) reduction. Solid lines are written for –5.0 to +5.0 kV and Dashed lines for –3.8 to –3.4 kV.

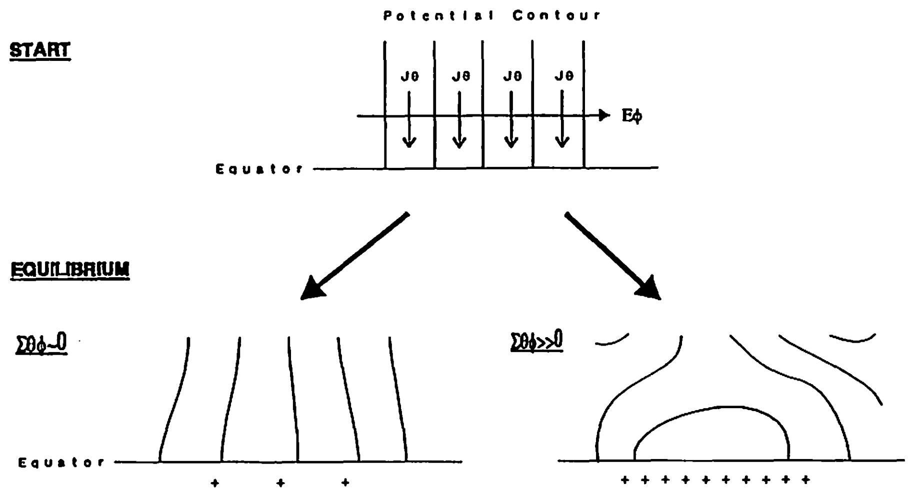

Figure 2-17: Illustration for the effect of $\Sigma_{\theta\varphi}$ near the equator to the potential contour changes in the equatorial region.

The existence of this secondary, northward electric field, though it cannot be large because of high $\Sigma_{\theta\theta}$, makes the inclination of potential contours to produce the north-south component of electric field near the equator. The inclination angle depends on the amount of accumulated charge. The amount of charge accumulation differs with local time and then the secondary electric field in the east-west direction is produced. The direction of the secondary electric field is reverse to that of the original field. The situation is illustrated in Figure 2-17.

The fact that negative variations of the H-component in the evening hours are seen in the models except for the full reduction model is interesting in

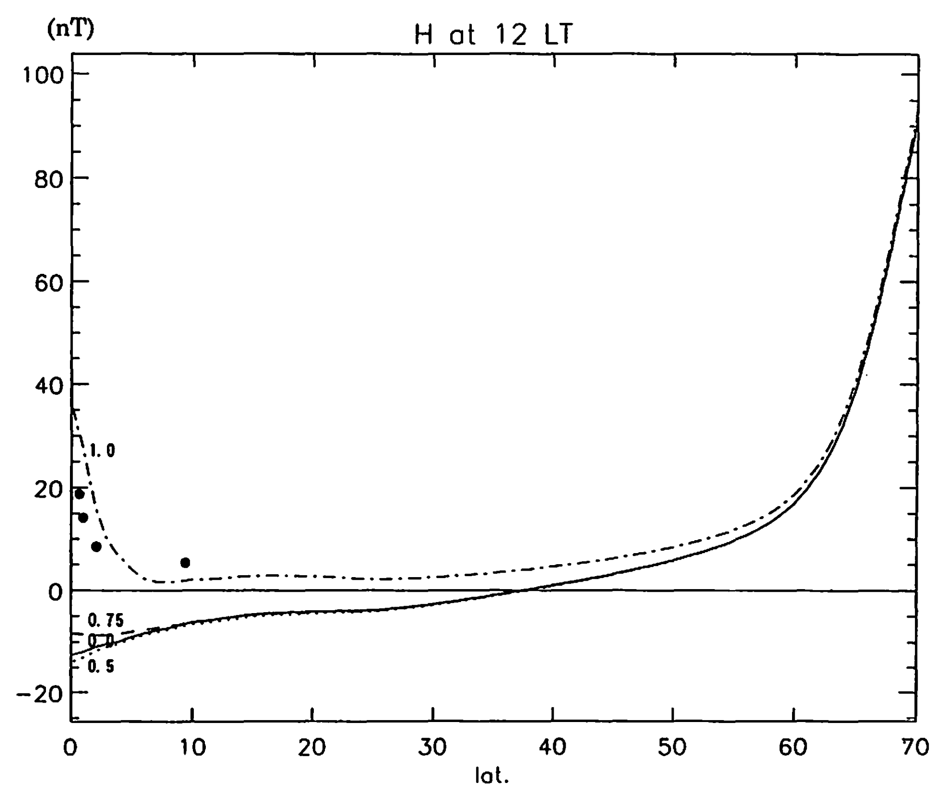

Figure 2-18: Latitudinal variations of the H-component of magnetic fields in the 12 LT meridian calculated for the four models of $\Sigma_{\theta\varphi}$. Meanings of the labels are the same as those of Figure 2-15. Closed circles near the equator are the observed results for 08-16 LT at the Indian stations (Rastogi and Sastri, 1974) fitted to the curve of 1.0.

relation with counter electrojet often observed at the equator in the evening hours. Although the counter electrojet has been so far attributed to the wind dynamo systems (Marriott et al., 1979, Hanuise et al., 1983) and supporting observational results were obtained (Somayajulu et al., 1993), the conductivity condition can be added as one of the parameters to discuss the matter. If the electrical condition of the full reduction is broken near the equatorial ionosphere, resulting in the model corresponding to $\Sigma_{\theta\varphi}$ of 0.0 to 0.5 reductions, the westward currents in the evening may be produced with certain wind dynamo modes. To make such values for $\Sigma_{\theta\varphi}$, however, it is necessary to discuss the decrease of the reduction rate for $\Sigma_{\theta\varphi}$ by some mechanisms. Since the discussion of the counter electrojet is not the main purpose of this paper, I would like to only suggest the possibility.

Latitudinal profiles of the H-component of magnetic field at 12 LT are shown in Figure 2-18. The curves except for the full reduction model do not show the equatorial enhancement pattern. The profile of the full reduction model is in good agreement with the mean latitudinal profile of the SC amplitude shown by Rastogi (1993) and that of SC* shown by Rastogi and Sastri (1974) (Figure 1-5). The latitudinal profile from high latitudes to the equatorial region for the full reduction model shows similar profile as that of Pi2 shown by Yumoto et al. (1994) and Yumoto and the 210° MM Magnetic Observation Group (1995).

The results except for the full reduction model are far from the observed result. The full reduction model may be the nearest to the realistic condition among the four models. In the next subsection, comparisons with other models or observational results of SC will be made for the full reduction model.

2.3.4 Comparison with Other Models and Observations

In Figure 2-19, local time profiles of the equatorial electric field and current of the full reduction model and those of the quasi-realistic model and 'the initial phase' of Senior and Blanc (1984) are compared because they are calculated for a similar composition of the high latitude source. These are arranged so as to equalize the sign and total amount of the input source current or potential drop in the polar region to the present calculation. As Senior and Blanc (1984) treated the equator as a conducting belt

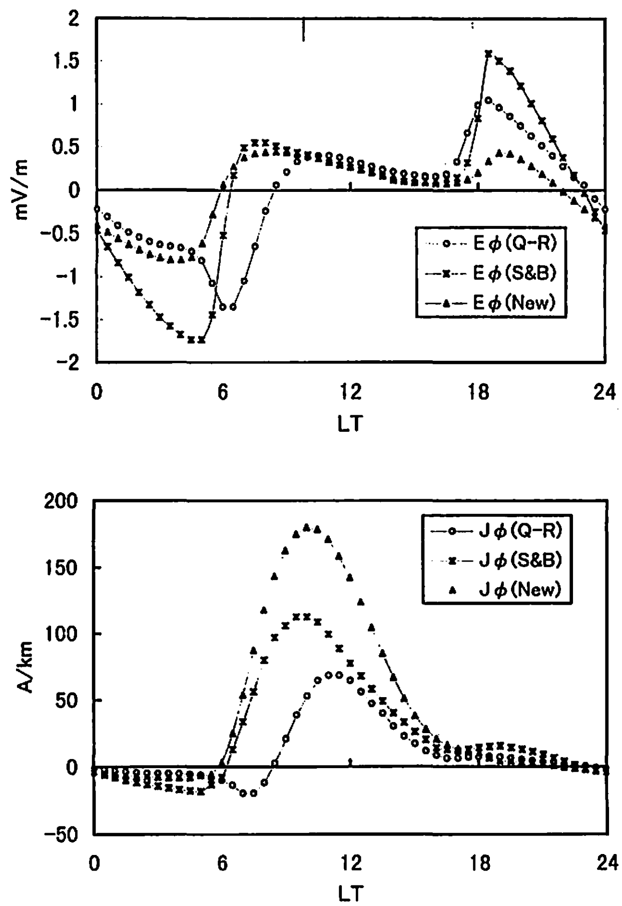

Figure 2-19: Comparison of the local time variations of eastward electric field (upper) and current (lower) at the equator of the full reduction model (noted as 'New') with those of Senior and Blanc (1984) (noted as 'S&B') and the quasi-realistic model (noted as 'Q-R') (after Tsunomura, 1999).

with 10° latitude width, the electric current shown here is the average of their result. As the main purpose of Senior and Blanc (1984)'s study is the time development of the magnetosphere-ionosphere coupling process, they did not discuss the latitudinal profile of electric current in low latitudes. Therefore, the exact comparison of the current magnitude or latitudinal profile with their result is impossible.

It is seen that the present result and that of Senior and Blanc (1984) take the maximum and minimum at the similar local times. The local time of the morning minimum for them is nearer than that of the quasi-realistic model to the observational result of Sastri et al. (1993) that the magnitude of SC-associated electric field becomes highest near 03 LT. The local time profile of the electric field in the present model is in good agreement with that of prompt penetration zonal

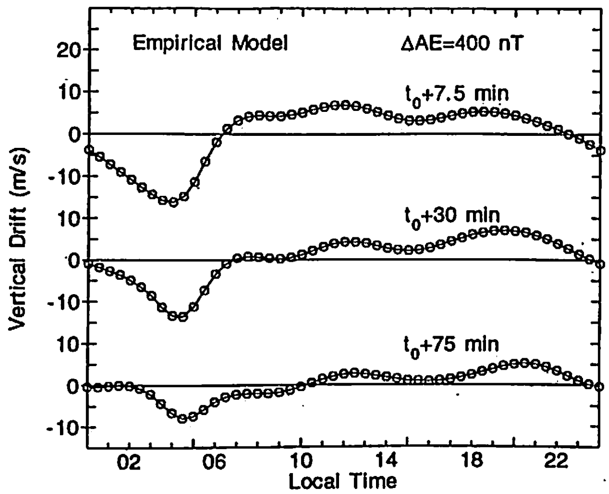

Figure 2-20: Empircal prompt penetration vertical drift patterns at three storm times following a step function increase in the AE index by 400 nT (after Fejer and Scherliess, 1997).

electric fields obtained by the radar observation at Jicamarca and the prediction by the Rice Convection Model shown by Fejer and Scherliess (1997) (Figure 2-20). Thus, the model shows some improvement in deriving the equatorial electric field from that of the quasi-realistic model.

The peak electric field intensity in the morning and evening is smaller in the present model than Senior and Blanc (1984)'s result. It cannot be decided which model fits the observations better. It is noted that the similar electric field pattern with sharp maximum in the evening as those of the quasi-realistic model and Senior and Blanc (1984) is also derived using the present model setting the grid spacing 1° in the equatorial region (Figure 2-12). However, as noted in the last section, the grid spacing of 1° is not sufficient to get the true solution.

The electric field intensities in the daytime are nearly same for all models. Since the ionospheric conductivity is the highest in the present model, the electric current intensity in the dayside is strongest for the present model than others. The validity of the current intensity of the present model should be clarified in future by the global magnetic and radar observations. At the actual comparison with observations, the geomagnetic latitude of the magnetic observation point should be checked carefully because of the rapid latitudinal change of the current intensity near the equator.

Reddy et al. (1981) showed the relationship between the electric and magnetic fields for some SC events. It is difficult to exactly compare the present result with theirs because the relationships between the electric and magnetic fields should be examined extracting the DP_{mi}-field contribution from the magnetic observations. The local time profile of the mean ratio of the DP_{mi}- to DL-fields, presented by Papamastorakis et al. (1984) (Figure1-11) can be used for this purpose. Applying it to the magnetic data of Reddy et al. (1981), the DP_{mi}-field contributions in the events are roughly extracted. Also assuming that the SC-associated DP_{mi}-electric field is proportional to the deviation of the Doppler frequency, the ratio of the magnetic variation (nT unit) to the electric field variation (mV/m unit) for each event of their study can be derived. The ratios calculated for the SC events on 1979 Dec. 27, 1980 Feb. 14 and 1979 Mar. 12, which were analyzed by Reddy et al. (1981), are in the range of 70-130, 50-120 and 30-280, respectively. The corresponding values derived from the present model are about 110, 80 and 80, respectively. The values for the present result are near the medians of those inferred from the events analyzed by Reddy et al. (1981).

Sastri et al. (1993) evaluated the equatorial electric fields associated with two events of SC in the pre-midnight hours. In this local time range, the local time variation of the electric field is expected to be rapid as shown by Figures 2-15(a) or 2-19. It is also very difficult to compare their results with the present one because the derivation of pure DP_{mi}-field from the magnetic observation is very difficult for their event. Roughly comparing the present result with the Jan. 01, 1992 event of theirs, the intensity of the electric field in the present result seems to be same as or a little smaller than their observational result.

An intense electric field was observed near the equator in the premidnight hours associated with a sudden expansion event as shown by Sastri et al. (1995). Although the comparison of the event with the present result is also difficult, the observed value is roughly estimated to be several times as large as that of the present result. However, the local time variation of the electric field is very sharp in this local time. If the input source current pattern in the polar region is somewhat shifted to the morning side, the more intense electric field can be expected from the present calculation as can be seen in Figure 2-15(a) or 2-19.

The local time variation of the equatorial enhancement pattern of magnetic field for SC shown by Sarma and Sastry (1995) is different from the present result. Their result shows the peak at 12 LT. However, a similar investigation by Papamastorakis et al. (1984) shows almost identical result with the present one. As the analysis by Sarma and Sastry (1995) deals with the enhancement rate without subtracting the contribution of the *DL*-field, it can not be decided whether the difference between the present result and theirs is exact or not. For the local time profile of the magnetic field, it can be said that the present result basically agrees with the observations.

Viewing the above results, it is thought that the full reduction process of $\Sigma_{0\varphi}$ primarily gives the realistic two-dimensional conductivity distribution in the equatorial region. Some applications using the full reduction model will be presented in Section 2.5.

2.4 Efficiency of the Two-dimensional Model Calculation

It was shown that the two-dimensional model calculation can principally provide similar solutions as the three-dimensional model as long as the external electric field does not vary with height very much. Although it is desirable to confirm this by the observations of the vertical profile of SC-associated electric field, it is practically impossible to obtain the height profile of the electric field just at the time of SC. As a matter of fact, the speculation that the external electric field of distant origin does not vary with height so much in low latitudes may not be far from the nature. On the other hand, the effect of the difference of height profile of E_z from that of the thin shell model due to the meridional current system was included in the derivation of the conductivity discussed in the subsections 2.3.1 and 2.3.2.

Three-dimensional models may give the ultimate solutions in the fidelity to simulate the real ionospheric current system. However, the complete three-dimensional model has not been developed so far because it needs tremendous memory and calculation time of the computer. A quasi-three-dimensional calculation was performed by Forbes and Lindzen (1976b); in their model, the three-dimensional calculations were limited to the equatorial region giving the solution of the two-dimensional calculation as the boundary condition.

Takeda (1982) obtained a three-dimensional electric structure by making a two-dimensional calculation assuming that the magnetic line of force is equipotential. The model is regarded as one of the two-dimensional calculations; the treatment of the indefinite current along the magnetic lines of force, which is inevitably included in the numerical scheme, may become the problem in deriving the current system.

Merits of the thin-shell, two-dimensional model are the easiness in changing parameters and the intuitiveness of the results. For example, the effect of the auroral conductivity enhancement can be given simply using the published two-dimensional models, whereas the three-dimensional structure of the auroral region conductivity needed for other models are hardly obtained at present. Global distribution of the horizontal electric field and current are more intuitively understood with the planer conductivity distribution. The three-dimensional model, having much more parameters concerned, it is difficult to take an outlook for the process, that is, the insight of the effectiveness of the various physical parameters in the calculation scheme. The versatility must be useful in the sense that the numerical simulation is one of the physical experiments to understand the physical phenomena.

Hence, I would like to mention that the 'modified' thin shell model developed here for the numerical calculation of the ionospheric current system is useful in the study of the magnetosphere-ionosphere coupling problems unless the vertical structure is needed.

2.5 Applications of the Realistic Model of the Ionospheric Conductivity to Some Matters of Polar-originating Ionospheric Current Systems

2.5.1 Canceling Effect by the Region 2 Field-aligned Current for DP2

Kikuchi et al. (1996) discussed the equatorial enhancement of a DP2 event as a case study and showed that the equatorial enhancement was recognized at the daytime equator, even the Region 2 field-aligned current, causing as a canceling effect for the dawn-to-dusk electric field of the DP2, was expected to exist to some extent. Several authors theoretically estimated the canceling effect of the Region 2 field-aligned current on the equatorial electric field (Nopper and Calovillano, 1978; Senior

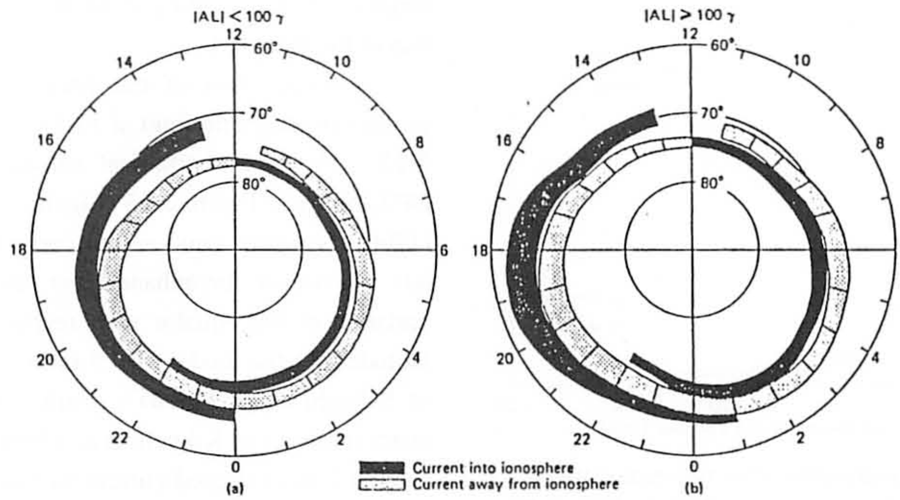

Figure 2-21: A summary of the distribution and flow directions of large-scale field-aligned currents determined from (a) data obtained from 439 passes of Triad during weakly disturbed conditions (|AL|<100 nT) and (b) data obtained from 366 Triad passes during active periods (|AL|≧100 nT) (after Iijima and Potemra, 1978).

and Blanc, 1984; Denisenko and Zamay, 1992). However, these authors did not discuss the latitudinal profile of magnetic fields. It is worth to examine the degree of the equatorial enhancement in the latitudinal profile, giving the canceling effect of the Region 2 field-aligned current.

Calculations changing the ratio of total amount of the Region 2 field-aligned current to the Region 1 are performed for this purpose. The distribution of the Region 1 field-aligned current is same as the previous section. That for the Region 2 field-aligned current is different from it only in the peak latitude and the sign

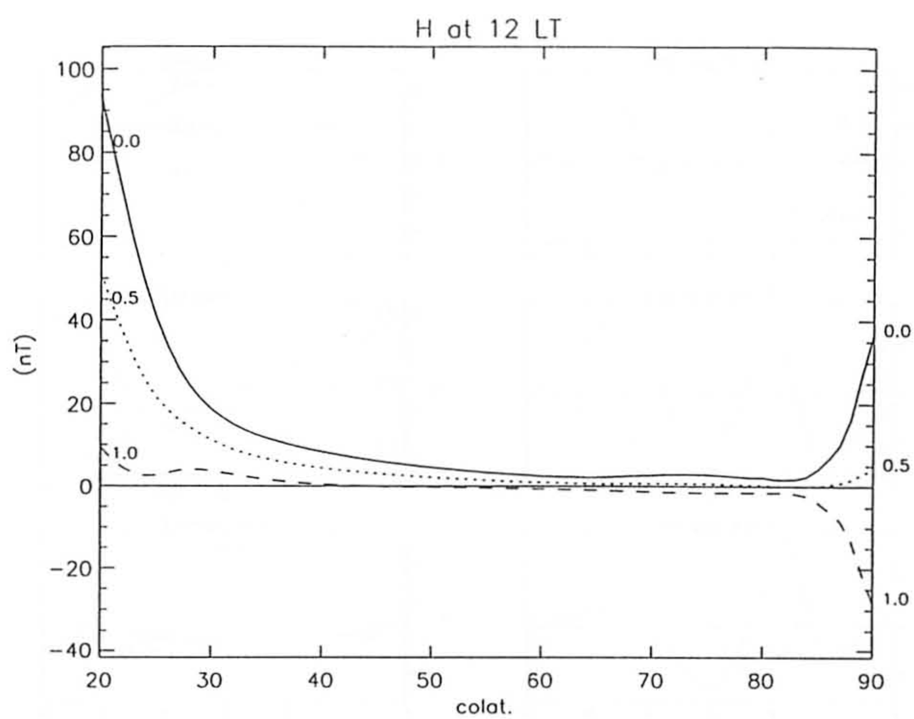

Figure 2-22: Latitudinal variations of the H-component magnetic fields in the 12 LT meridian calculated for the three models of source current composition. Solid, dotted and dashed lines are for the results with the ratio of Region 2 current intensity 0.0, 0.5 and 1.0 to that of Region 1 current, respectively as labeled on each curve. The abscissa is arranged for colatitude to compare with Figure 2-23 (after Tsunomura, 1999).

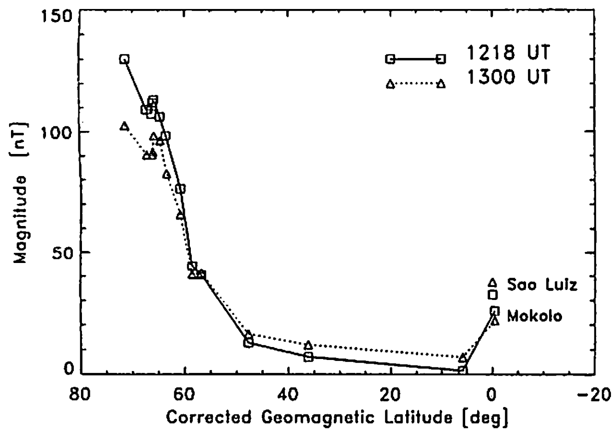

Figure 2-23: Latitudinal profiles of the magnitude of the DP 2 fluctuations recorded on April 20, 1993, at the IMAGE stations and the European and African chain stations. Two profiles are depicted for the peaks at 1218 and 1300 UT with solid and dashed curves, respectively. The magnitude at Sao Luiz is also plotted to indicate the remarkable equatorial enhancement at the dip equator. Here the magnitude is comparable to that at subauroral latitudes (after Kikuchi et al., 1996).

(Figure 2-21). The peak latitude and sign of the Region 2 field-aligned current are 65° and reversed to that of the Region 1.

A Comparison of the three cases in latitudinal profiles of magnetic field at 12 LT is shown in Figure 2-22. The basic latitudinal variation profile of the DP2 shown in Figure 2-23 (Figure 7 of Kikuchi et al. (1996)) is nearly same as the curve for the model of 0.0. However, the enhancement rate of the magnetic variation at the equator with respect to that in high latitudes for the model of 0.0 ratio is higher than that of Kikuchi et al. (1996)'s result. Therefore, at the event analyzed by Kikuchi et al. (1996), the ratio of the Region 2 field-aligned current to that of the Region 1 is thought to be between 0.0 and 0.5 and may be near 0.0.

In this case, the equatorial enhancement ratio, that is the ratio of the magnetic field strength at the equator to that in high latitudes, becomes a good measure to evaluate the ratio of the magnitude of the Region 1 field-aligned current to that of the Region 2. It should be kept in mind, however, that the local time profile of

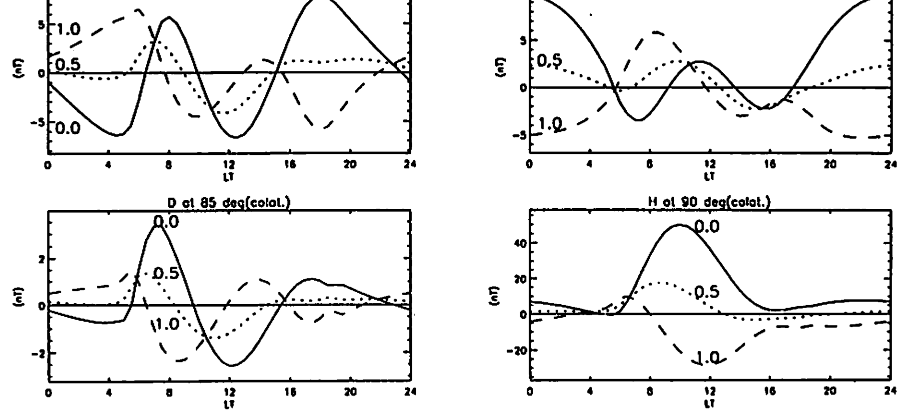

Figure 2-24: Local time variations of the D- (left panels) and H- (right panels) components of the magnetic fields at 60°, 30° latitudes and the equator calculated for the three models of the source current composition. Meanings of the labels are the same as those of Figure 2-22 (after Tsunomura, 1999).

magnetic variations in high latitudes is very complicated as seen in Figure 2-24. Because of the limited number of the station distribution, the idealized station pairs cannot be always obtained. The equatorial enhancement rate can be changed very much for events or local time and not a stable parameter to use as the indicator of the mixing ratio of the Region 1 and 2 field-aligned currents. The polarities of the H-component in middle latitudes in the nightside and/or that of the H-component at the equator in the dayside are the better indicators for this purpose.

2.5.2 North-south Asymmetry of Ionospheric Current Systems in the Solstitial Period

When the observational data are accumulated for long years, the relationship of amplitudes, phases and other parameters for geomagnetic phenomena between the north and south hemispheres becomes one of the important matters to examine the characteristics of the origin of the magnetic variations. For example, if the magnetic variation in the summer hemisphere is larger than that in the winter one, it is primarily expected that the driving force have some relationships with the ionospheric currents, because the background ionospheric conductivity due to solar radiation is higher in the former. However, the dependence on the conductivity may be different between the voltage generator and the current one, as discussed for the quiet time geomagnetic variations by Fujii et al. (1981) and Fujii and Iijima (1987). The north-south asymmetry is not expected for the current generator, as discussed by Vickrey et al. (1986) for Birkeland currents of the intermediate scale size. Therefore, the difference of the asymmetry characteristics for the voltage generator and the current one should be examined or confirmed by a numerical analysis at least.

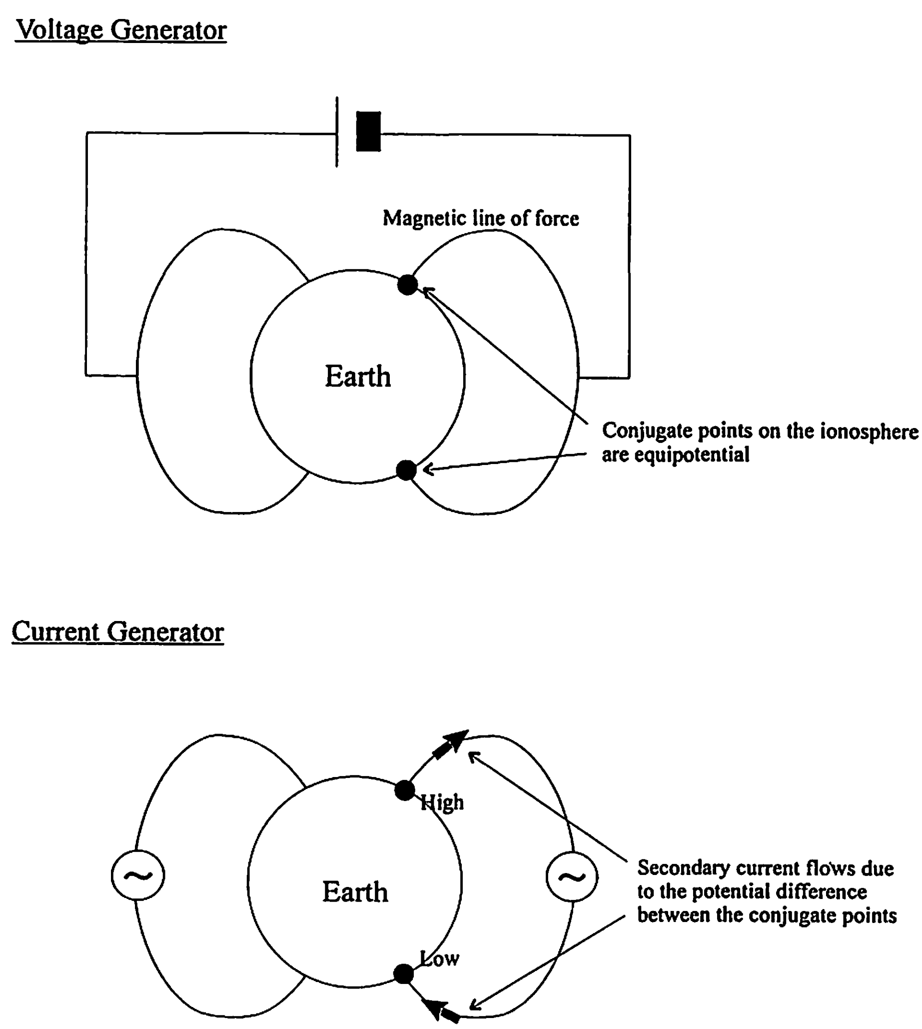

Figure 2-25: Illustration of the voltage (upper) and current (lower) generators of the magnetospheric source for the ionospheric current system..

Kamide and Matsushita (1979a) and Nisbet et al. (1978) calculated the ionospheric current system driven by a current generator for one hemisphere independently setting the summer or winter solstice conditions for the ionospheric conductivity. In this paper, after making the universal conductivity model, numerical calculations of the ionospheric currents covering both hemispheres simultaneously can be operated regarding the equator as an intermediate point.

The types of the source are varied two kinds, that is, the voltage and the current generators (Figure 2-25). For the voltage generator, the potentials at 75° latitude are given as a sinusoidal form, the peaks of which are located at 06 and 18 LT. The total potential drop is 100 kV, giving +50 kV at 06LT and -50kV at 18LT. The property of the current generator is the same as that of Section 2.3. As the peaks of the calculated potentials for the current generator are situated near 06 and 18 LT, the results can be easily compared.

The calculation does not include any feedback to equalize the potentials of conjugate points at first. In the actual state, the potential difference between the conjugate points may drive the secondary field-aligned currents to equalize the potentials. As the process is completed after the transition time of the signal through the magnetic lines of force, there may be some delay of the order of a few minutes after the impression of the original field or current. The following result is used to infer the instantaneous response of the ionosphere to the external driver.

Conductivity profiles in the north and south hemispheres are given as the summer and winter conditions of ionospheric conductivity derived from IRI-90 model with the sunspot number = 50 (Figure 2-26). Here, the northern hemisphere is set as the summer one. Conductivity enhancements in the auroral region are the same as those in Section 2.3 for both hemispheres. Since the conductivity at the equator for the summer and the winter conditions are not so different, the averaged values are used at the equator.

Figure 2-27(a) shows potential contours of the voltage generator. The potential profiles are almost symmetric with respect to the equator as if both hemispheres are connected electrically. It is noted that the potential contours are skewed at the source latitude as if dragged by an external force.

The potential contours for the current generator are shown in Figure 2-27(b). The total potential drops are 69.3 kV and 148.4 kV in the summer and the winter hemispheres, respectively. The average of

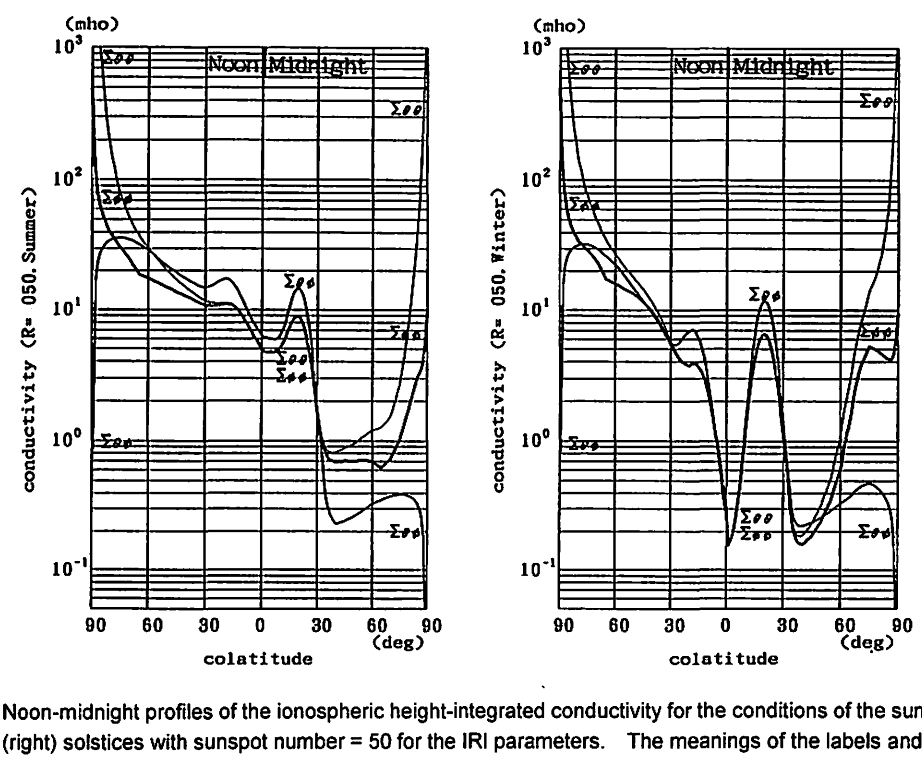

Figure 2-26: Noon-midnight profiles of the ionospheric height-integrated conductivity for the conditions of the summer (left) and winter (right) solstices with sunspot number = 50 for the IRI parameters. The meanings of the labels and the plot style are the same as those of Figure 2-9 (after Tsunomura, 1999).

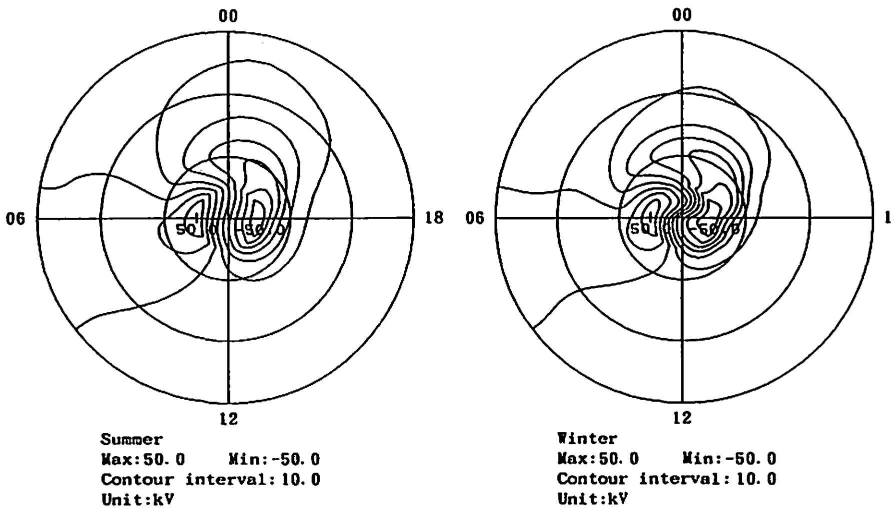

Figure 2-27(a): Potential contours in the summer (left) and winter (right) hemispheres for the voltage generator. Circles are 60° and 30° latitudes and the equator from the inside, respectively. The interval of the potential contours is 10 kV (after Tsunomura, 1999).

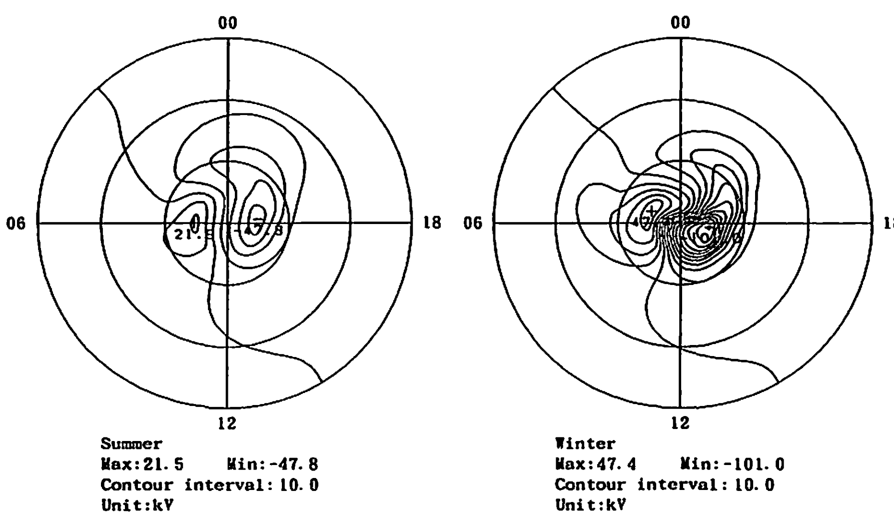

Figure 2-27(b): Same as Figure 2-27(a) for the current generator (after Tsunomura, 1999).

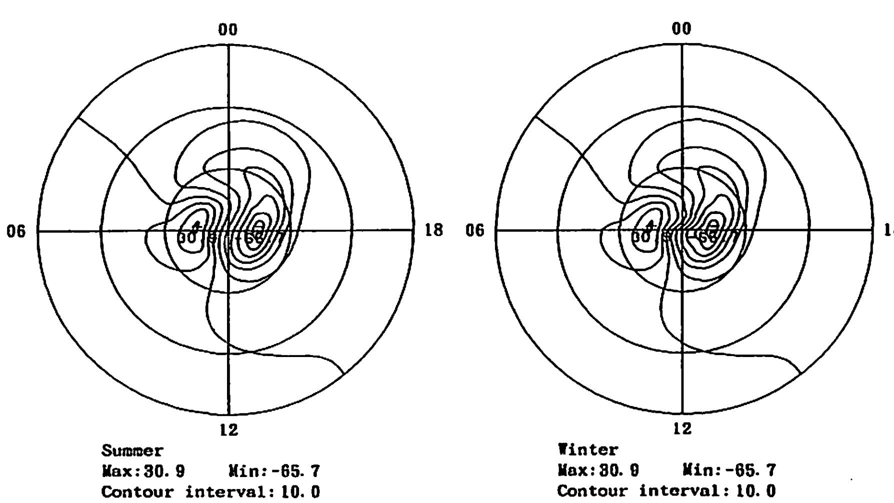

Figure 2-27(c): Same as Figure 2-27(a) for the current generator including the feedback process between the conjugate points.

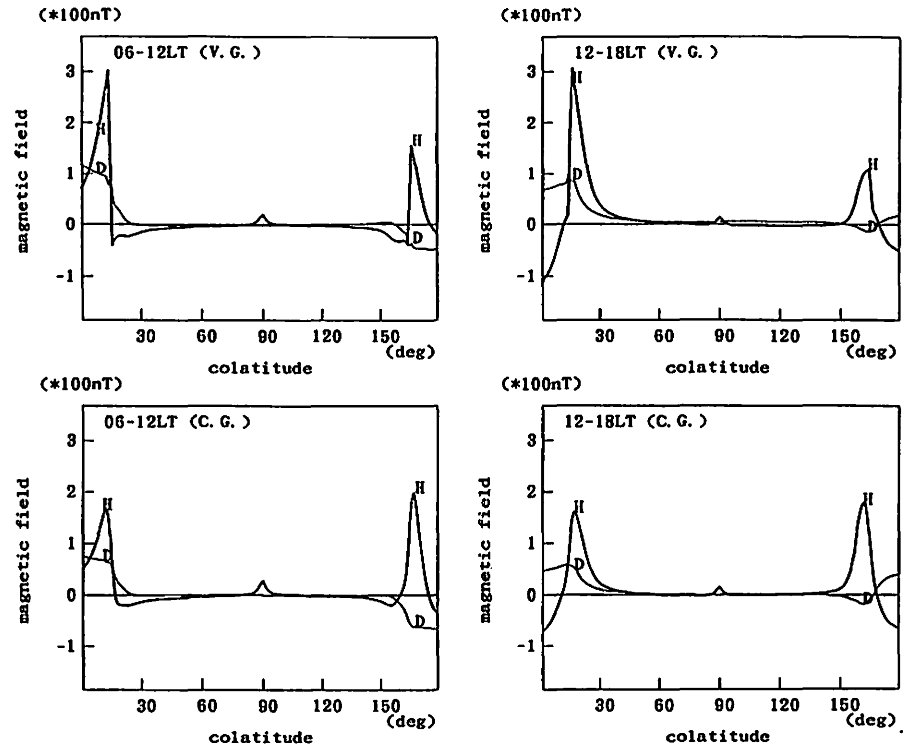

Figure 2-28: Average latitudinal variations of the H- (thick lines) and D- (thin lines) component magnetic fields of the voltage (upper panels) and current (lower panels) generators, for two local time blocks.

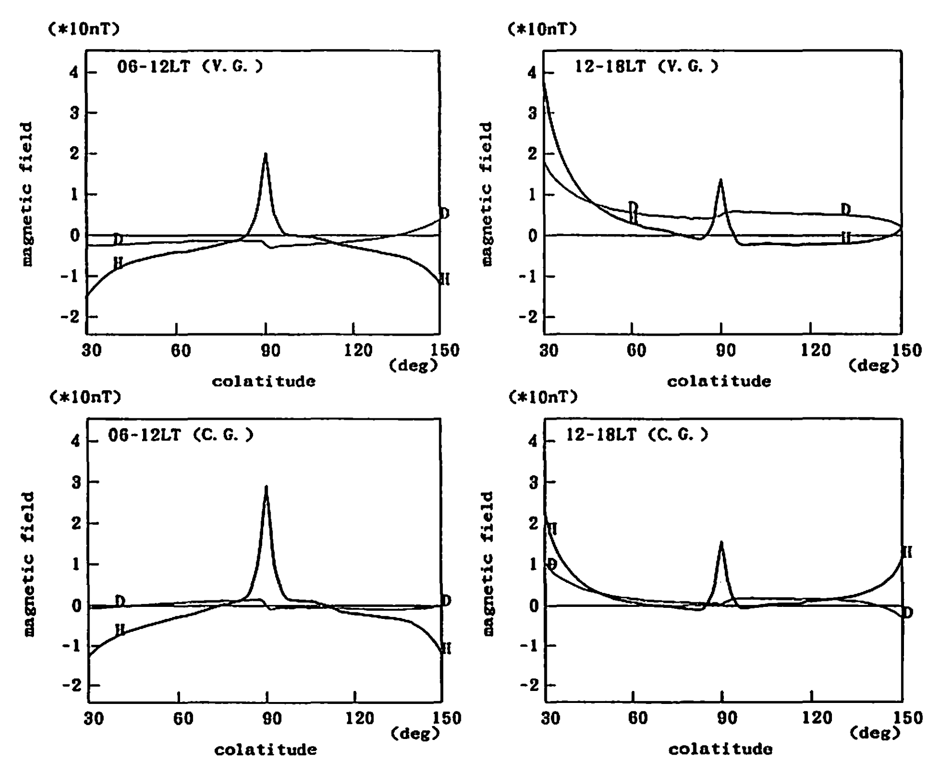

Figure 2-29: Same as Figure 2-28 for the latitude range from 60° to –60°.

them (108.85 kV) is a little larger than that of the voltage generator. The peak potential values are almost same as those calculated for each hemisphere independently setting the conductivity models on the summer or winter solstice. The peak positions of the potential are not shifted to the nightside because the slight enhancement of the auroral conductivity is included in this model and the contrast of the day-night conductivity in high latitudes is reduced. The difference in the calculation schemes, simultaneous for both hemispheres or independently for each hemisphere, does not make much difference in the electrical conditions in high latitudes.

As the potentials between the geomagnetically conjugate points are quite different especially in high latitudes for the current generator, it may lead secondary field-aligned currents along the highly conductive magnetic field lines as mentioned above. Figure 2-27(c) is the result of the calculations for the current generator including the feed backs of the secondary field-aligned currents. The feed back process was made as follows; the electric current with the strength corresponding to reduce the difference of the electric potentials between conjugate point pairs by one-thousandth are additionally put in for the point of smaller potential and flown away from the other one in each one-hundred iteration. The feed back process was not made for the polar region (from the pole to 80° latitude), because the magnetic lines of force are open in the region. Although the gross pattern of the potential is similar to that of the voltage generator, the contour lines are much smoother (without a skewing) than those of the voltage generator.

In Figure 2-28, the average latitudinal profiles of magnetic fields of both generators are compared for 06-12 and 12-18 LT blocks. Generally the magnetic fields are larger for the voltage generator than the current generator in high latitudes in summer. The magnetic fields in the polar region are larger in the summer than the winter for the voltage generator, whereas the contrast is not clear and even in a little reversed situation for the latter.

Figure 2-29 shows the average latitudinal profiles of magnetic fields of both generators in a latitude range from 60° to –60° for 06-12 and 12-18 LT blocks. At the equator, the amplitudes are generally larger in the 06-12 LT block than the 12-18 LT one for both cases. The north-south asymmetry of the amplitudes is clearly seen in the H-component of the 06-12 LT block of the voltage generator (upper right). The asymmetry is not seen in the blocks of the current generator (lower panels). For middle latitudes the difference due to the sources were not definite. The magnetic fields in the late morning at the equator are larger in the current generator than the voltage one, especially in the 06-12 LT block, even taking into account the difference in the total potential drops. This is because the diurnal variation pattern of the electric potential in high latitudes is enforced as a sine curve resulting in the unnatural fittings of the potential contours as can be seen in Figure 2-27(a). I would like to mention that the equatorial magnetic field shown here is different from those obtained by the independent calculations for the solstice conditions; that means the calculation covering both hemisphere is desirable to discuss the ionospheric contribution in low latitudes in the summer or winter seasons.

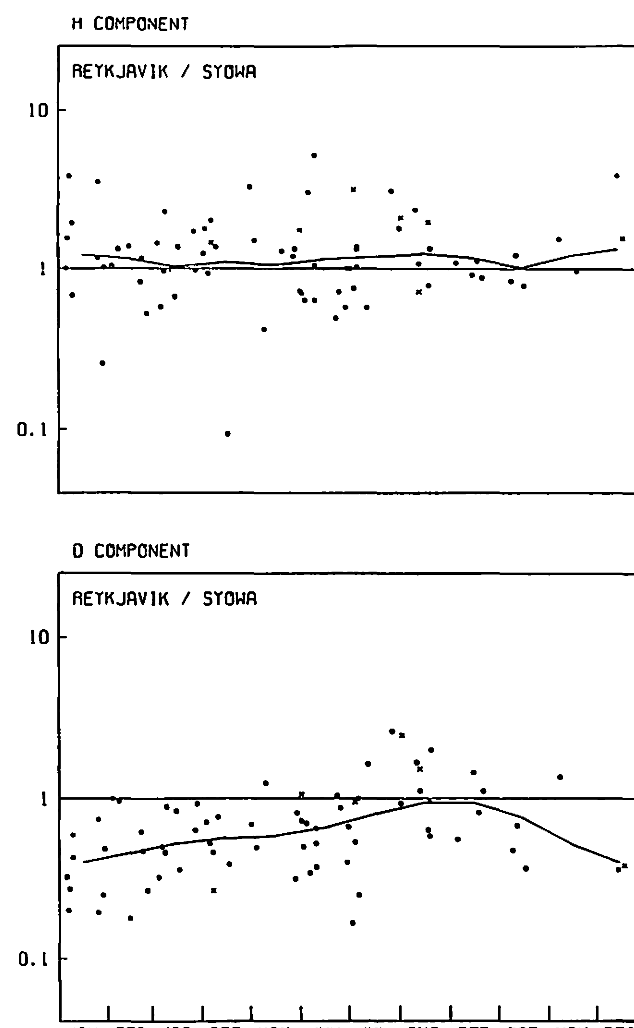

Figure 2-30: Seasonal variations in the ratio of the magnitude of MI of SSC and SI at Reykjavik to that at Syowa. Circles are for SSC and SI+ and crosses for SI-. Fitting lines are three months running average (after Tsunomura, 1989).

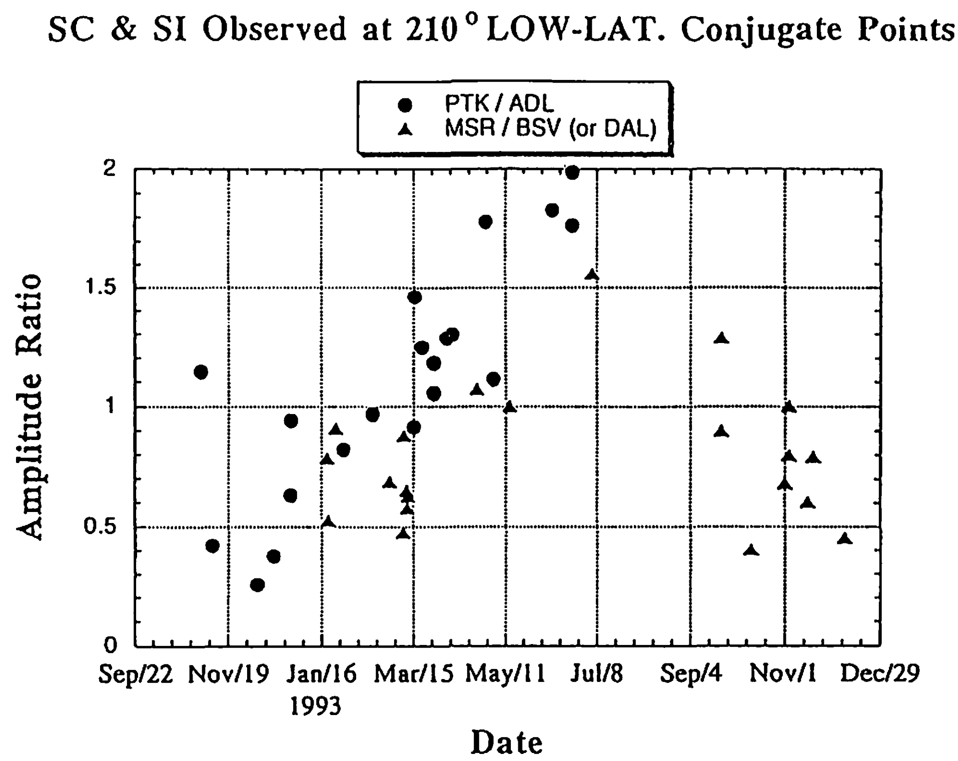

Figure 2-31: Amplitude ratios of SC disturbances observed at low-latitude conjugate point pairs during the interval from November 1992 to December 1993. Solid circles and triangles indicate the ratio of SC amplitudes at Paratunka (L=2.10) in the northern hemisphere to those at Adelaide (2.11) in the southern hemisphere and of those at Moshiri (1.59) to Birdsville (1.55) (or Dalby(1.57)), respectively (after Yumoto and the 210° MM Magnetic Observation Group, 1995).

Comparing SC amplitudes at the conjugate stations in the auroral region, Syowa and Reykjavik, Nagata et al. (1966) showed that the amplitude of the H-component often becomes higher in the winter hemisphere tan the summer. Tsunomura (1989) reexamined the matter using magnetic data at the same station pair and showed that the D-component in the summer hemisphere is a little larger than that in the winter one (Figure 2-30). These relationships in the auroral region seem to fit the current generator feature as shown in Figure 2-28. On the other hand, the amplitude of SC is higher in the summer hemisphere than winter for middle latitude region (Yumoto and the 210° MM Magnetic Observation Group, 1995; Yumoto et al., 1996) (Figure 2-31); that is same as the result of the 12-18 LT block of the voltage generator as shown in Figure 2-29. From these results, it is difficult to decide the source type of the DP_{mi}–field of SC, though it is basically expected to be the voltage generator. The actual process may possibly be the intermediate between the two.

Saito et al. (1989) showed the asymmetry of Pc3-5 magnetic pulsations in the auroral region comparing the data at Syowa with those at conjugate point, Husafell. They showed that the powers of Pc3-5 magnetic pulsations are relatively higher at the winter than the summer and that the ratio of the amplitudes of the pulsations varies in the equinox due to the difference of the local time. They suggested the screening effect of the ionosphere as a cause for these relationships. The complete understanding of this matter should be obtained after the discussion of other matters, such as the horizontal wavelength or the period. The result obtained here (Figure 2-28) may be one of the items to discuss the matter totally. If the amount of field-aligned current associated with the standing oscillation of magnetic field line is thought to be constant, the present result may give the base of the background condition. This is important to prevent the misleading to infer that the ionospheric current contribution 'should' be larger in the summer hemisphere than in the winter one.

2.5.3 Solar Cycle Dependence of the Equatorial Enhancement Rate of SC

Solar cycle dependence in the magnetic variations would also be expected to have some relationships with the ionospheric currents because the ionospheric electron density varies with solar cycle (e.g. Maeda and Fukao, 1972). It was shown that solar diurnal variation at the equator changes its amplitude with sunspot number by many authors (Takeda et al., 1986; Takeda and Yamada, 1987 and references therein).

Jain and Srinivasacharya (1976) showed a solar cycle dependence of the equatorial enhancement of SC amplitude using the magnetic data in the Indian region. They showed the equatorial enhancement rate is greater in high solar cycle period than the low one. Here, the solar cycle dependence of the polar-originating ionospheric current system derived by numerical calculations will be compared with their results.

Figure 2-32 shows the height-integrated conductivity corresponding to the solar minimum (sunspot number = 10 for IRI-90) and maximum (sunspot number = 100) years. The conductivities are larger in the maximum period than the minimum. The ratios of $\Sigma_{\theta\varphi}$ to $\Sigma_{\theta\theta}$ and/or $\Sigma_{\varphi\varphi}$ in middle to low

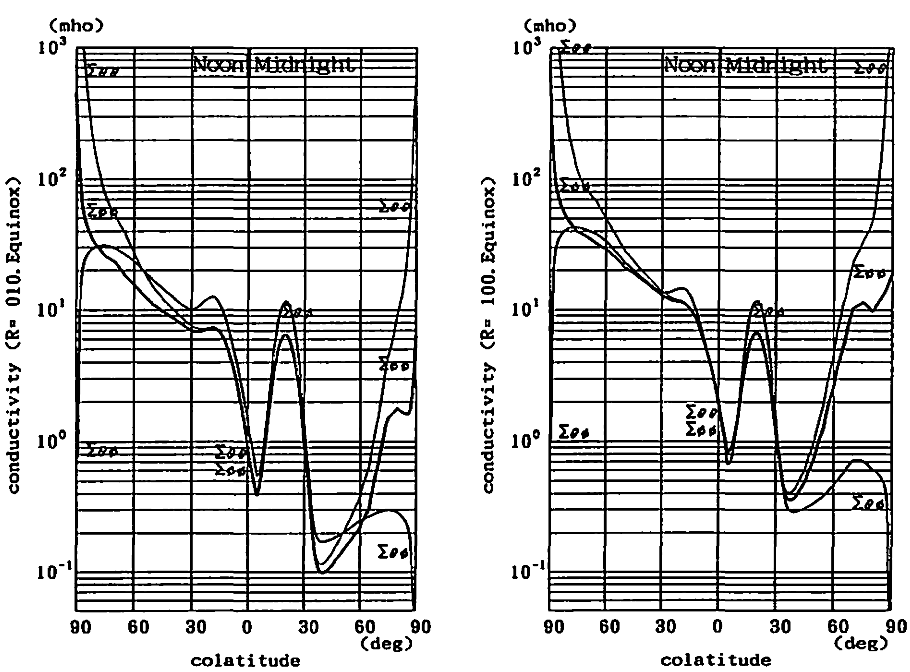

Figure 2-32: Noon-midnight profiles of the ionospheric height-integrated conductivity on equinox and sunspot number = 10 (left) and 100 (right) for the IRI parameters. The meanings of the labels and the style of plot are the same as those for Figure 2-9.

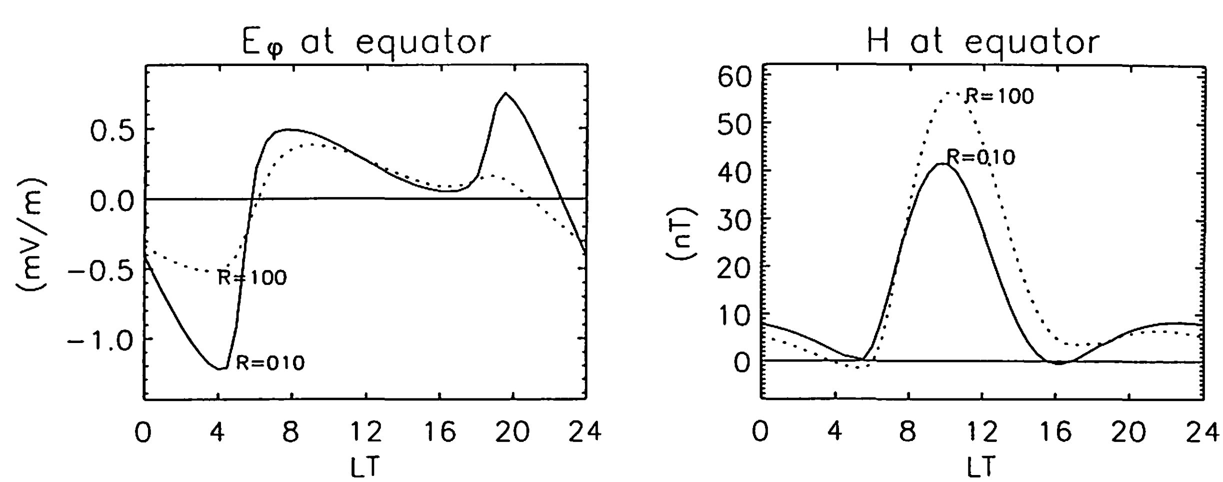

Figure 2-33: Comparison of local time variations of the eastward component of ionospheric electric field (left) and the H-component of magnetic variation (right) at the equator for low (R=010, solid lines) and high (R=100, dotted lines) solar activities.

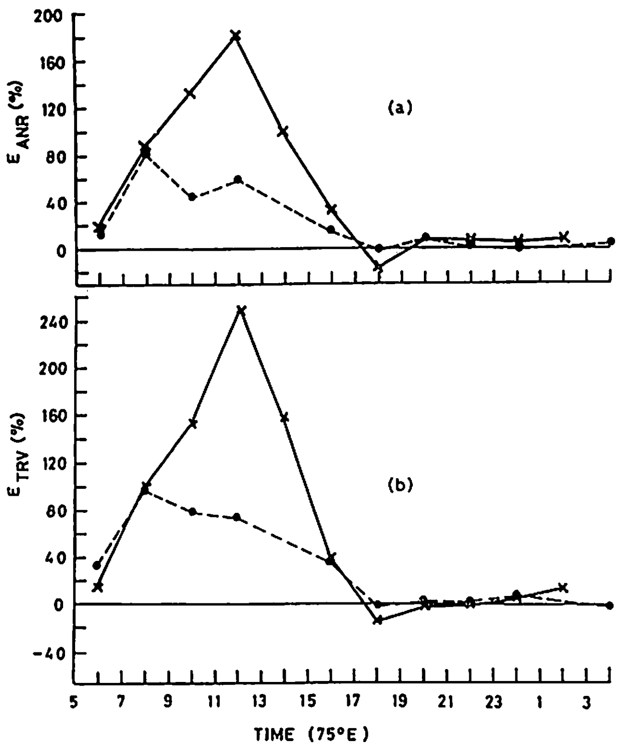

Figure 2-34: Diurnal variation of percentage equatorial enhancement for SC. The dashed line curve is for solar minimum years (1964 and 1965) and solid line is for solar maximum year (1958). (a)ANR, (B)TRV (after Jain and Srinivasacharya, 1974).

latitudes are lower for the maximum period than those for the minimum. This is because Pedersen conductivity becomes higher for the maximum period than the minimum because of the F layer property. It is noted that the nightside conductivity is very high in the solar maximum period compared with low one. This is same as Takeda and Yamada (1987)'s result.

Local time profiles of the electric and magnetic fields at the equator for the sunspot minimum and maximum periods are compared in Figure 2-33. The values are compared equalizing the peak potential drops in the polar region. It is noted that the electric field in the nightside is different for the two models because of the difference in the nightside conductivity. The intensity of the dayside electric field is nearly same for both models, resulting in the stronger electric current in the dayside in the maximum period than the minimum one. The result agrees well with the observational features of SC, that is, the difference in the enhancement rate and the shift of the peak local time (Figure 2-34).

3. Characteristics of SC in Middle and Low Latitudes

3.1 Polarity of the D-component

Locations of the magnetic stations used in this section are shown in Figure 3-1 and listed in Tables 3-1 and 3-2. Here the stations of the 210° magnetic meridian observatory network (Yumoto et al., 1992; Yumoto and the 210° MM Magnetic Observation Group, 1996) are included along with the routine observatories.

Since July, 1957, onset time, amplitude, duration, polarity and other matters for SSC and SI at kakioka (KAK), Memambetsu (MMB) and Kanoya (KNY) have been reported in the tables of magnetic storms and sudden impulses in 'Report of the Geomagnetic and Geoelectric Observations (Rapid Variations) (1957-1984)' and 'Report of Kakioka Magnetic Observatory (1985-1992)'. Those for KAK from 1957 to 1985 were converted to a machine-readable file by Okamoto and Fujita (1987) to make a statistical analysis; the content of the file was updated to 1992 for this study. The polarity of MI for SSC and SI reported in these tables is used to make a statistical analysis.

In Figure 3-2(a), histograms of the occurrence frequency of positive variation (geomagnetically northward and eastward for the H- and D-components respectively and downward for Z) for MI of SSC detected at KAK are presented. The statistics are taken for the events having larger amplitude than 5 nT for MI. It can be seen that the polarity of the H-component is positive in almost all events. This is the expected result, as the most part of MI in the H-component observed in low latitudes is caused by the increase of magnetic field strength due to the global magnetospheric compression.

The polarity of the Z-component is also positive for almost all the events. It is expected that the observed Z-component variation with a short period such as SC is produced by the anomalous distribution of the induced current due to local anomaly in electrical conductivity under the ground (Rikitake and Honkura, 1985, pp. 201 or 297). The Z-component of such an event is thought to be almost shielded by the highly conducting Earth. The anomaly in the ground

Table 3-1 Routine magnetic stations used in this analysis

Station Name	Abbreviation	Geographic* Latitude (Degree)	Geographic* Longitude (Degree)	Geomagnetic* Latitude (Degree)	Geomagnetic* Longitude (Degree)	MLT for 92/09/09 Event	MLT for 93/03/23 Event
Thule	THL	77.48	290.83	88.13	15.03	22.4	18.6
Alert	ALE	82.50	297.50	86.51	160.62	7.9	4.2
Resolute Bay	RES	74.70	265.10	83.08	299.13	16.4	12.7
Mould Bay	MBC	76.30	240.60	79.76	262.00	14.1	10.4
Godhavn	GDH	69.23	306.48	78.94	34.59	23.3	19.6
Cambridge Bay	CBB	69.10	255.00	76.69	300.97	16.8	13.0
Baker Lake	BLC	64.33	263.97	73.49	320.58	18.1	14.4
Narsarsuaq	NAQ	61.20	314.60	70.30	38.81	23.6	19.8
Barrow	BRW	71.30	203.25	69.32	244.80	13.1	9.4
Yellowknife	YKC	62.47	245.53	69.08	297.90	16.6	12.9
Fort Churchill	FCC	58.80	265.90	68.32	327.25	18.6	14.9
Poste-de-la-Baleine	PBQ	55.30	282.25	65.91	351.13	20.3	16.6
College	CMO	64.87	212.17	65.25	260.35	14.1	10.4
Sodankyla	SOD	67.37	26.63	63.76	120.49	5.0	1.3
Lerwick	LER	60.13	358.82	62.05	89.45	3.0	23.2
Meanook	MEA	54.62	246.67	61.78	305.10	17.2	13.4
Sitka	SIT	57.07	224.67	60.36	279.18	15.4	11.7
Glenlea	GLL	46.93	262.90	58.99	326.97	18.6	14.9
Eskdalemuir	ESK	55.32	356.80	57.92	84.08	2.6	22.9
Lovo	LOV	59.35	17.83	57.84	106.72	4.1	0.4
Nurmijarvi	NUR	60.52	24.65	57.75	113.49	4.6	0.8
St. Johns	STJ	47.60	307.32	57.59	23.82	22.5	18.8
Ottawa	OTT	45.40	284.45	56.07	354.79	20.5	16.8
Brorfelde	BFE	55.62	11.67	55.45	98.76	3.6	23.8
Newport	NEW	48.27	242.88	55.05	303.72	17.1	13.4
Victoria	VIC	48.52	236.58	54.28	296.60	16.6	12.9
Hartland	HAD	50.98	355.52	54.02	80.38	2.3	22.6
Belsk	BEL	51.83	20.80	50.18	105.34	4.0	0.3
Chambon-la-Foret	CLF	48.02	2.27	49.94	85.84	2.7	23.0
Fredericksburg	FRD	38.20	282.63	48.84	352.88	20.4	16.7
Boulder	BOU	40.13	254.77	48.70	319.84	18.2	14.5
Nagycenk	NCK	47.63	16.72	46.89	99.74	3.6	23.9
Tihany	THY	46.90	17.90	45.97	100.57	3.7	23.9
Bay St. Louis	BSL	30.40	270.40	40.50	339.26	19.5	15.8
Tucson	TUC	32.25	249.17	40.22	315.30	17.9	14.2
Del Rio	DLR	29.49	259.08	38.64	326.70	18.7	14.9
Memambetsu	MMB	43.90	144.20	34.93	210.78	10.9	7.2
San Juan	SJG	18.38	293.88	29.04	5.74	21.3	17.6
Kakioka	KAK	36.23	140.18	26.94	208.29	10.8	7.0
Tamanrasset	TAM	22.80	5.53	24.80	81.59	2.4	22.6
Honolulu	HON	21.32	202.00	21.56	269.19	14.8	11.1
Kanoya	KNY	31.42	130.88	21.44	200.35	10.2	6.5
M'Bour	MBO	14.40	343.02	20.43	57.21	0.7	21.0
Chichijima	CBI	27.15	142.30	18.11	211.30	11.0	7.3
Bangui	BNG	4.43	18.57	4.36	90.80	3.0	23.2
Papeete	PPT	-17.57	210.43	-15.09	284.90	15.9	12.2
Tananarive	TAN	-18.92	47.55	-23.81	115.22	4.6	0.8
Hermanus	HER	-34.42	19.23	-33.86	83.36	2.4	22.7
Canberra	CNB	-35.30	149.00	-43.10	226.43	12.0	8.3
Martin de Vivies	AMS	-37.83	77.57	-46.75	143.55	6.4	2.7
Crozet	CZT	-46.43	51.87	-51.46	112.36	4.3	0.6
Port aux Francais	PAF	-49.35	70.22	-57.18	131.75	5.6	1.9
Dumont Durville	DRV	-66.66	140.01	-74.79	231.94	12.5	8.8

* The values are reprinted from World Data Center C2 for Geomagnetism DATA CATALOGUE (1996).

Table 3-2 210° magnetic meridian chain magnetic stations used in this analysis

Station Name	Abbreviation	Geographic* Latitude (Degree)	Geographic* Longitude (Degree)	Corrected Geomagnetic* Latitude (Degree)	Corrected Geomagnetic* Longitude (Degree)	MLT for 92/09/09 Event	MLT for 93/03/23 Event
Tixie	TIK	71.59	128.78	65.67	196.88	9.8	5.9
Magadan	MGD	59.97	150.86	53.56	218.66	11.1	7.3
St. Paratunka	PTK	52.94	158.25	46.34	225.91	11.6	7.9
Moshiri	MSR	44.37	142.27	37.61	213.23	10.8	7.1
Onagawa	ONW	38.43	141.47	31.65	212.51	10.8	7.1
Guam	GUA	13.58	144.87	4.57	214.76	11.3	7.5
Biak	BIK	-1.08	136.05	-12.18	207.30	10.8	7.0
Weipa	WEP	-12.68	141.88	-22.99	214.34	11.3	7.5
Darwin	DAW	-12.40	130.90	-23.13	202.68	10.5	6.8
Birdsville	BSV	-25.54	139.21	-36.58	212.96	11.2	7.5
Dalby	DAL	-27.18	151.20	-37.09	226.80	12.1	8.3
Adelaide	ADL	-34.67	138.65	-46.46	213.66	11.3	7.5
Macquarie Is.	MCQ	-54.50	158.95	-64.50	247.84	13.3	9.6

* The values are reprinted from Yumoto et al. (1995).

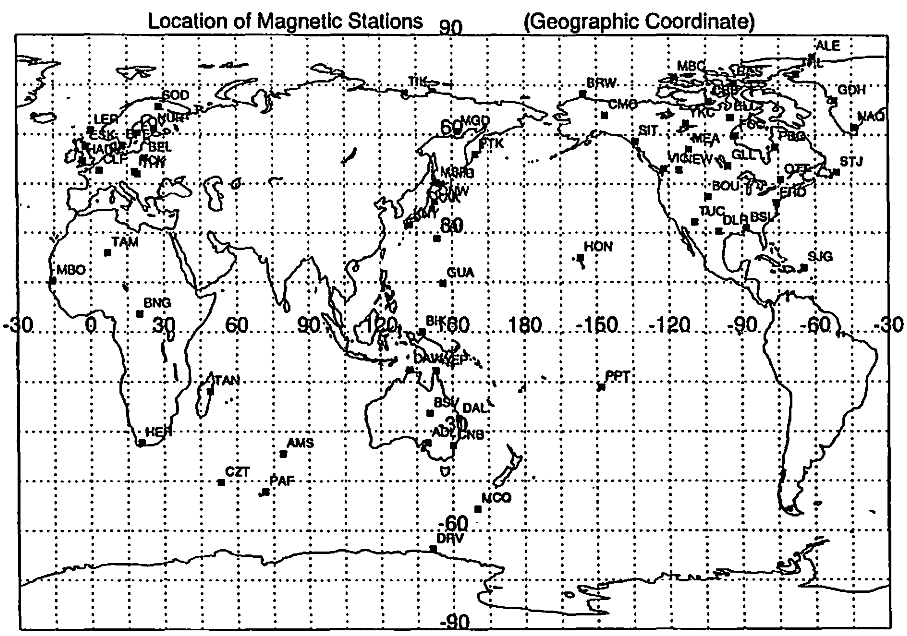

Figure 3-1: Locations of the magnetic stations used in this study.

electrical conductivity is conventionally called CA (Conductivity Anomaly) for short. The CA effect is discussed using CA transfer functions. CA transfer functions or CA coefficients are derived solving equations which describe experimental relationship between the Z-component and the H- and D-components. The equation is,

$$\Delta Z = A \cdot \Delta H + B \cdot \Delta D . \qquad (3\text{-}1)$$

The coefficients A = (Au, Av) and B = (Bu, Bv) are complex functions and depend on frequency of magnetic field variation. A horizontal vector represented by the real parts, (-Au, -Bu), plotted in the directions of the H- and D-components respectively is called an induction arrow to show the rough direction of the gradient in electrical conductivity under the ground. At KAK, Au is much larger than Bu and the induction arrow points nearly southward for wide ranges of period from 10 to 120 minutes (Fujita, 1990; Fujiwara and Toh, 1996). Therefore, the Z-component variation of SSC at KAK is basically caused by the ground current induced by the H-component variation through the CA effect. Because of the positive relationship with the H-component, the Z-component variation of SSC becomes positive

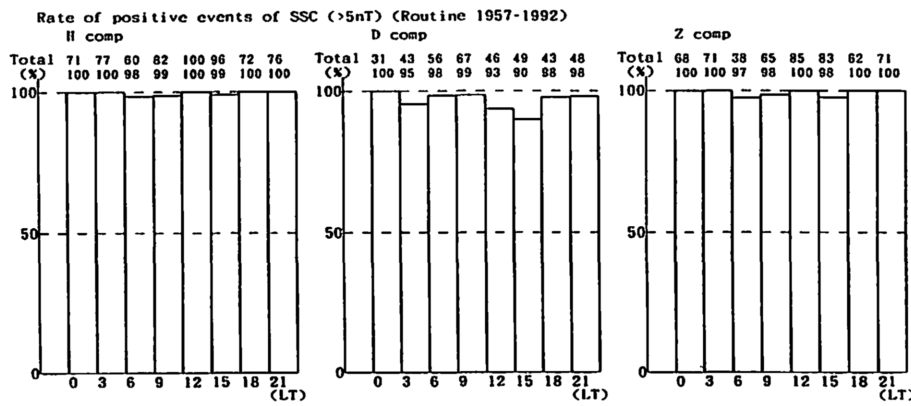

Figure 3-2(a): Local time dependence of occurrence frequency of positive MI of SSC at KAK. The number above each bin is the total number of the events (upper) and the percentage of the number of the positive events to the total (lower) for the local time range between the left and the right side hours shown below.

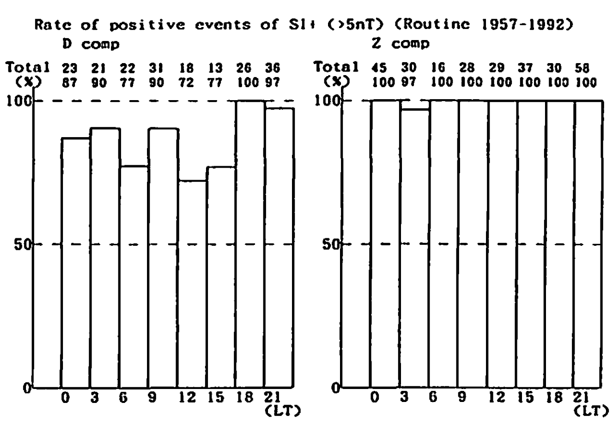

Figure 3-2(b): Same as Figure 3-2(a) for SI+. As the notation '+' already indicate the polarity of the H-component, only the histograms for the D- and Z- components are shown.

together with the H-component.

It is worth to note that there are three events showing negative H-component variations. One of them is the SSC of February 11, 1958 geomagnetic storm during which visible low latitude aurora was observed in Hokkaido district (eg. Tsunomura et al, 1990). The MI of this SSC was reported as a very sharp decrease after a positive PI. As will be discussed in the following sections, this negative MI may possibly be the signature of DP_{mi}–field at this event superposed on the DL-field. In any case, the fact that the negative change due to the DP_{mi}–field surpasses the DL-field is not a common feature of SC observed at KAK. Other two events are difficult to be exactly designated as SSC. Therefore, it may not be a severe mistake to say that MI of SSC in the H- and Z-components are basically positive in low latitudes around KAK.

The polarity of the D-component is also shifted to positive with higher ratio than 90 %, just representing what was pointed out by Fukushima (1994). Similar tendency can be seen for SI+'s (Figure 3-2(b)). In this case the ratio of the positive D-component is a little decreased but remains at higher level than 70 %.

According to the Araki's model, it is expected that the conversion of magnetic field data to the geomagnetic dipole coordinate system will reduce the unbalances seen in Figures 3-2(a) and (b) because the conversion may yield a better indicator to watch the magnetospheric process. Similar conversions are made to derive ASY and SYM indices in 'MID-LATITUDE GEOMAGNETIC INDICES ASY and SYM (PROVISIONAL) No.1 1989-1990' (1992) and its following numbers.

Table 3-3 Difference of dipole meridian and local declination at the stations used in the analysis

Station Name	Abbreviation	Declination Gap (degree)
Chambon-la-Foret	CLF	-13.2
Fredericksburg	FRD	11.5
Tucson	TUC	-2.9
Memambetsu	MMB	16.0
San Juan	SJG	9.1
Kakioka	KAK	13.5
Honolulu	HON	0.3
Kanoya	KNY	10.0
Chichijima	CBI	9.7

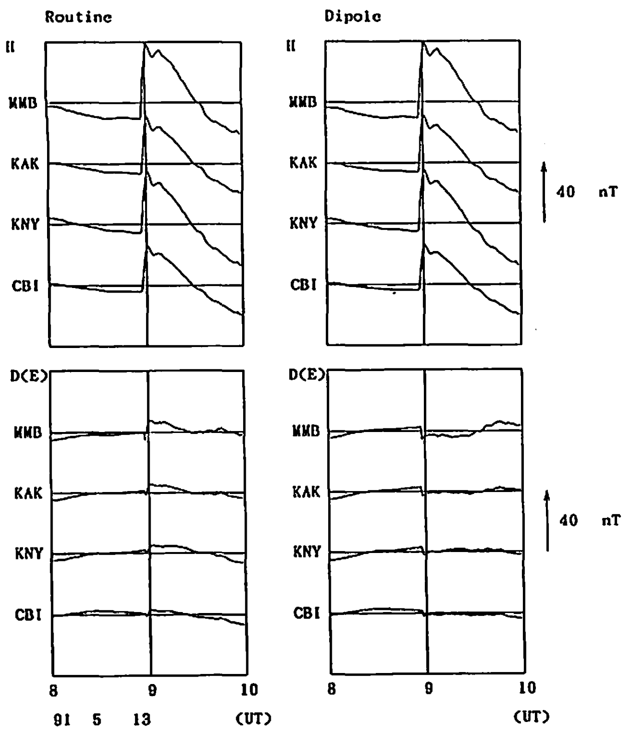

Figure 3-3(a): Comparison of the routine and the converted data for the SC on May 13, 1991.

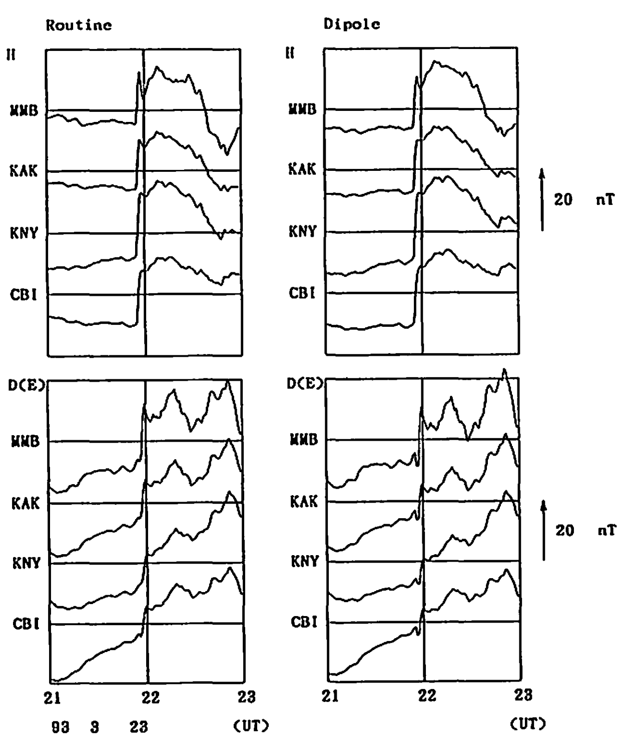

Figure 3-3(b): Same as Figure 3-3(a) for the SC on March 23, 1993.

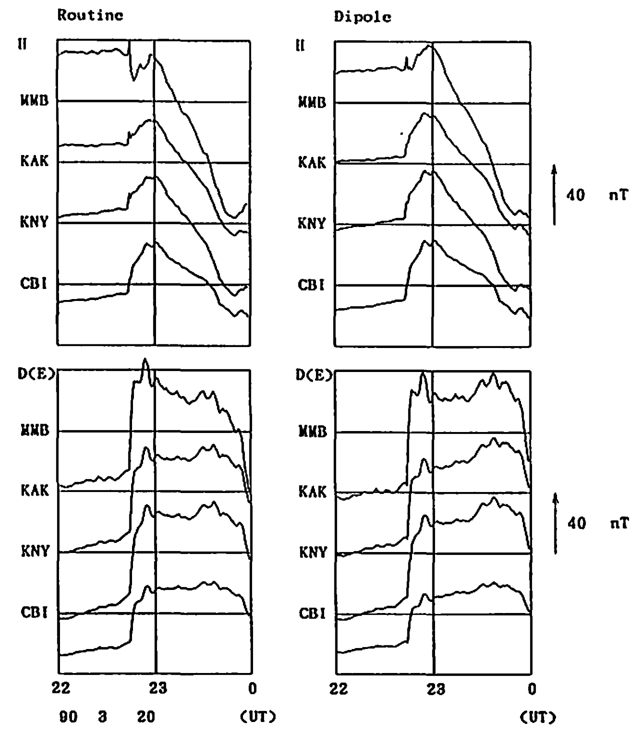

Figure 3-3(c): Same as Figure 3-3(a) for the SC on March 20, 1990.

In the following, the H- and D-component data in the direction of the local geomagnetic north and east are titled 'routine' and the data converted to the geomagnetic dipole coordinate system will be titled 'converted'. The direction of the geomagnetic dipole meridian at a station changes with time because of geomagnetic secular variation but not vary largely in a few tens of years. Here the values averaged for the periods from 1985 to 1992 are used; the values are listed in Table 3-3. The difference of the maximum and minimum values is less than 0.5° at all the stations.

Figure 3-3(a)-(c) are examples of the data comparing the routine and the converted ones. Figure 3-3(a) shows an example that the SC variation in the D-component becomes reverse by the conversion.
The D-component was reported westward for the MI in the routine report but it should be eastward looking the converted data. The conversion often contributes the deformation of the variation form like this. Figure 3-3(b) is an example that PRI in the D-component becomes clear by the conversion. The negative variation just after the onset of SC seen in the H-component in the figure will be precisely discussed in

the subsection 3.4.1. The example of Figure 3-3(c) is a rare case but serious for the routine observation. For this event, the MI in the H-component at MMB was reported as negative. The converted H component looks different and the MI can be reported as positive followed by a negative variation. In these local times, the projection of the large D-component variation on the routine H-component direction affects the apparent negative variation. As can be seen clearly in these figures, the conversion makes a drastic change in some cases. The conversion is necessary to discuss the fine structure of the variation form of SC.

Figures 3-4(a) and (b) are the histograms for the polarity of SSC and SI+ for the converted D-component at KAK respectively. The data period is from 1976 to 1992. The polarity is determined by taking the differences of the converted D-component value at the reported MI peak time from that at the onset. For both cases the occurrence frequencies of positive variations of the D-components are reduced to the level nearly 60 %. It is important that the local time variation of the occurrence frequency is almost parallel as the local time profile curve of the D-component at 30° latitude for the full reduction model (Figure 2-15(b)). The SC polarization for the converted data seems to be consistent with the Araki's model. It can be noted that the local time profile of the D-component polarity seen in Figure 1-13 is almost parallel to the D-component curve in Figure 2-15(b) if the former is shifted lower.

Since the stations MMB, KAK and KNY are located in nearly the same longitude and apart from by less than 15 degrees in latitude (see Table 3-1), the local time is expected to be nearly same for these stations. The correlation coefficients among the magnetic field variations at KAK, MMB and KNY during SC are derived using one-minute magnetic data from 20 minutes before to 40 minutes after the onset of SC. Figure 3-5(a) shows the results of the H- and D-components for the routine data. The data from 1985 to 1992 for SC's are used to calculate the mean correlation coefficients. It can be seen that the correlation coefficients of the H-component between MMB and other stations are relatively low in the morning hours and that the correlation coefficients are generally not high for the D-component comparing with the H-component. Figure 3-5(b) is the results for the converted data. The correlation coefficients

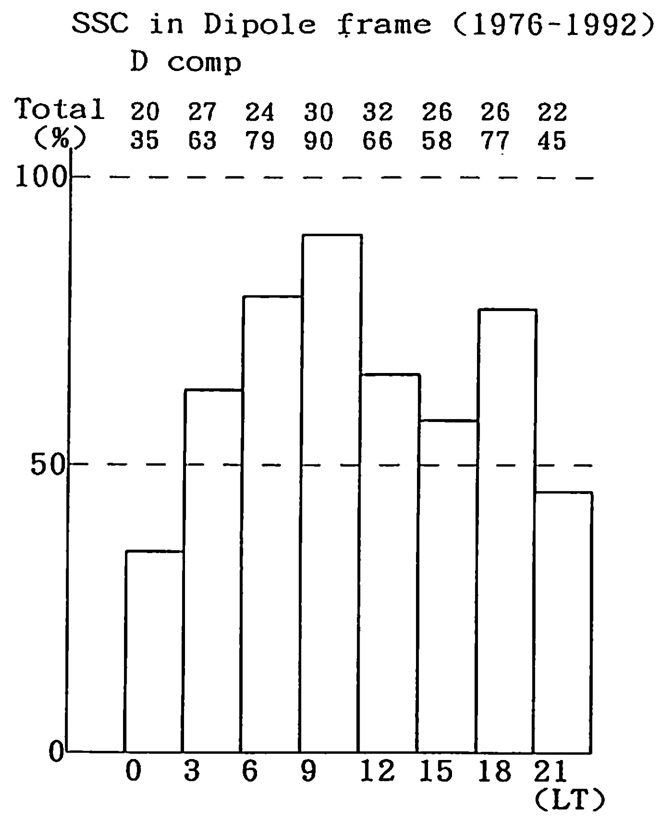

Figure 3-4(a): Local time dependence of occurrence frequency of the positive SSC in the D-component for the converted data.

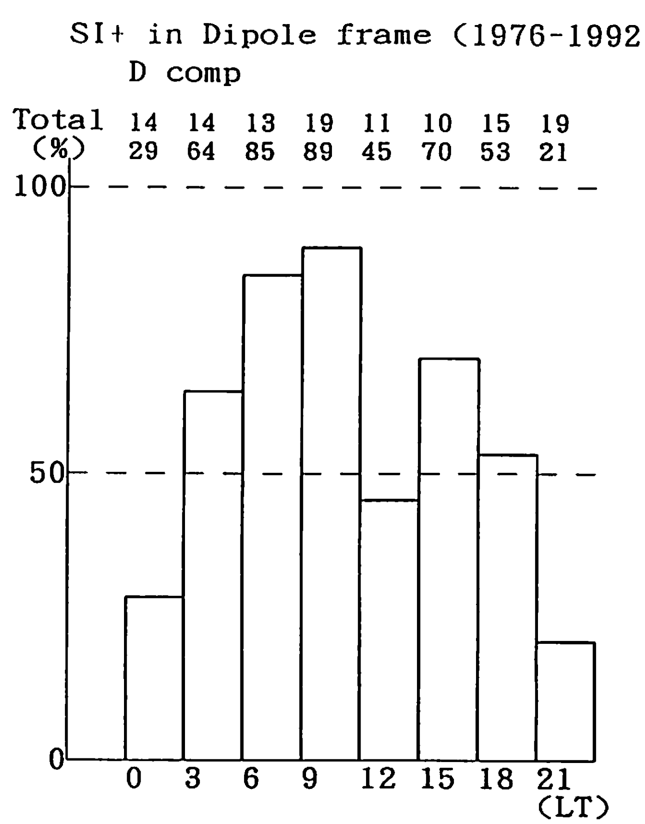

Figure 3-4(b): Same as Figure 3-4(a) for SI+.

become higher for the H-component in the morning hours and a little for D component between KAK and KNY, lower for the D-component between MMB and other stations especially in the nightside, than those of the routine data.

The low correlation coefficients between MMB and other stations (KAK and KNY) for the H-component in the morning hours is not an expected feature. The poor relationship of the converted D-component between MMB and other stations as can be seen in Figure 3-5(b) might be due to the smallness of the variation amplitude of the D-component at KAK and KNY in the nightside. In the morning hours, the correlation coefficient for the D-component becomes high because the ionospheric currents, which are basically same in phase at these stations, will make large magnetic field in the D-component at all the stations. For the routine D-component, the projection of the magnetic field variation due to the enhanced magnetopause current becomes a common bias for the D-component at all the stations. Thus the correlation coefficients of the D-component among the stations become a little higher for the routine data than the converted ones.

As far as the local time dependence of the D-component is concerned, the result of the Araki's model basically agrees well with the observational results for the converted D-component. In the following discussions, the H- and D-components mean the converted ones, if it is not noted especially.

Fukushima (1994) pointed out that there is a tendency that westward declination change at the times of SC is limited only to either in the summer afternoon or in the winter morning. Taking into account of the eastward shift of the scatter points in Figure 1-13, it means that the D-component sometimes becomes strongly westward in those periods. Indeed there are some events in which the converted D-component varies westward in the morning hours as can be seen in the histograms of Figures 3-4(a) and (b). The westward variation in the afternoonside can be reproduced by the present calculation as shown in Figure 2-15(b). To produce the westward variation in the morning hours by the Araki's model, it is necessary to develop the analysis for the solstice condition further.

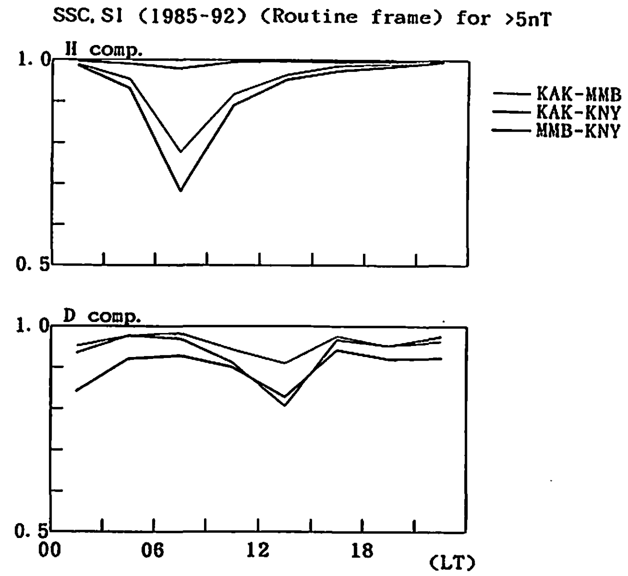

Figure 3-5(a): Local time dependence of the mean correlation coefficients among the magnetic variations of SC observed at MMB, KAK and KNY. The correlation coefficients are calculated for the data with time span of one hour starting 20 minutes before the onset of SC for each event using the routine data.

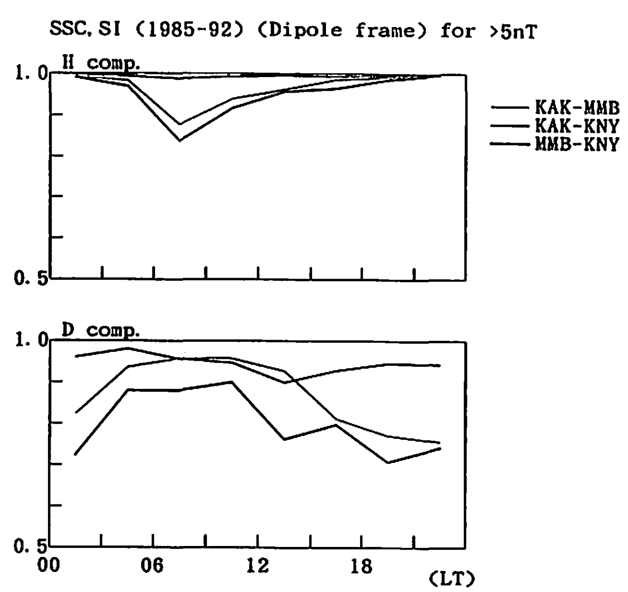

Figure 3-5(b): Same as Figure 3-5(a) for the converted data.

3.2 Anomalous Behavior of the H-component in the Morning Hours

In the previous section, the correlation coefficient becomes low for SC in the H-component in the morning hours. This is an unexpected result and should be examined more precisely. Latitudinal variations in SC amplitudes of the H- and D-components at MMB, KAK, KNY and CBI are shown in Figure 3-6. As these observatories are situated in nearly same magnetic meridian, the data are shown in the order of the magnetic latitude. The value of each point is the average of the normalized SC amplitude at each station to that at MMB, that is, the average of the linear regression coefficients of ten samples of one-minute magnetic data just after the onset of SC at the station to those at MMB. The coefficients are calculated for the events when the amplitude of SC is reported larger than 5 nT at KAK. For CBI, only the data overlapping its period (1989-1992) are used to calculate the values.The results are displayed for four local time intervals.

The tendency that the amplitudes are larger in higher latitude than in lower latitude is clear in the D-component for all local time blocks. For the H-component, the gradient of the latitudinal variation becomes gentler than the D-component except for the 06-12 LT block where the tendency is reversed. Gradients are steeper for the D-component than those for the H-component.

It is expected that the *DL*-field, being caused by the increase of the magnetopause current, produces the northward magnetic field in the geomagnetic dipole coordinate system and that the DP_{mi}–field is responsible for the remaining complicated distribution of the magnetic fields of MI (Araki, 1994). The difference in the gradient between the H- and D-components is due to the mechanism that the MI in the H component is basically the superposition of *DL*- and DP_{mi}-fields, whereas the D-component is basically made by the DP_{mi}-field. Similar difference in the latitudinal profiles between the H- and D-components was also seen in the analysis of Pi2 magnetic pulsation (Yumoto et al., 1994; Yumoto and the 210° MM Magnetic Observation Group, 1995). As the magnetic field variation in the H-component on the ground due to the enhanced magnetopause current roughly decreases with increasing latitude obeying the cosine law, the variation at CBI is expected about 1.16 time as that at MMB. The ratio of the H-component amplitude at CBI to that at MMB in 06-12 LT as shown in Figure 3-6 is a little larger than this value.

The amplitudes seem to be a little enhanced at MMB and KNY except for the 00-06 LT block of the D-component at KNY. The results of magnetotelluric analysis show that electrical conductivity from 2-3 km to 20-30 km depth under the ground at KNY and MMB is about 30-100 ohm•meter and that at KAK is about 10^{3} (Yanagihara, 1965; Owada, 1972; Oshima,1972). It is basically impossible to discuss the effect of induced electric current on the horizontal magnetic variation without precise information of the electrical conductivity under the ground. However, it is reported that the horizontal magnetic variations seem to be enhanced locally at MMB (Mori, 1975), while they are not at KAK (Kuboki and Oshima, 1966). It is suggested that the horizontal magnetic variations of the external origin with the period from several to several hundred seconds are somewhat enhanced through electromagnetic induction at MMB and KNY but not clearly at KAK.

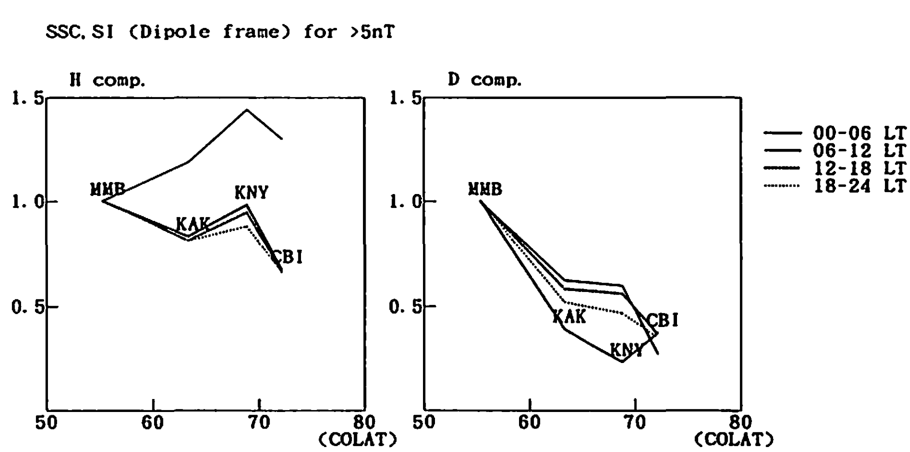

Figure 3-6: Latitudinal variations in the average ratios of MI amplitude at KAK, KNY and CBI to that at MMB for SC's with the amplitude larger than 5 nT at KAK from 1985 to 1992. The graphs are divided for four local time ranges of local time based on JST.

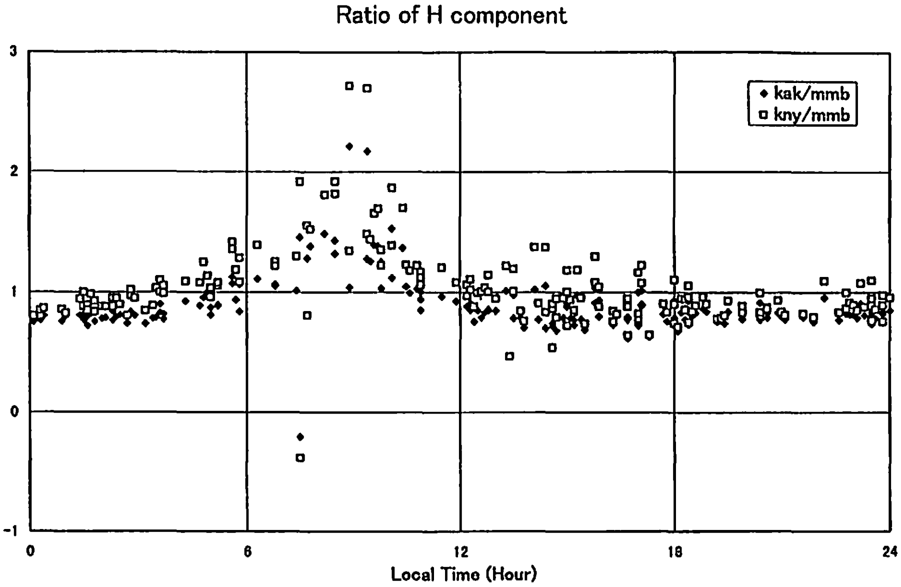

Figure 3-7(a): Local time variation in the ratio of MI amplitude of the H-component at KAK and KNY to that at MMB for SC's same as for Figure 3-6 (after Tsunomura, 1998).

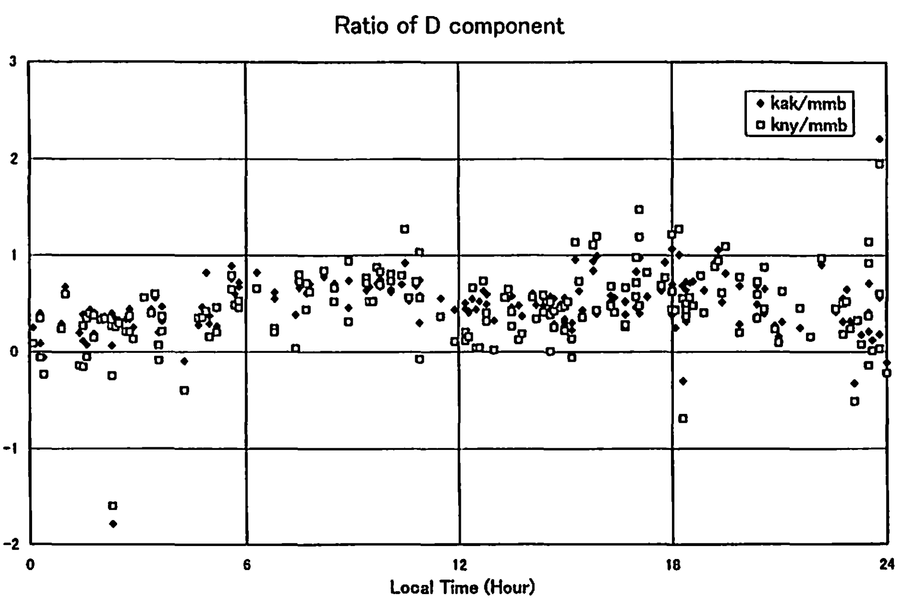

Figure 3-7(b): Same as Figure 3-7(a) for the D-component (after Tsunomura, 1998).

Russell et al. (1994 a, b) mentioned that the variation of the magnetotail current produce a negative variation in the H-component on the ground when the magnetosphere is compressed; the effect is increased for the southward IMF-B_z condition. This is one of the sources to enhance the pattern that the H-component is smaller in lower latitudes than that in higher latitudes. But the facts that the correlation coefficient is low for the H-component only in the morning hours and that the D-component also shows the higher amplitude in higher latitudes cannot be explained by this mechanism.

It is necessary to examine the local time variation of the amplitude ratio more clearly. Figures 3-7(a) and (b) are the scatter plots of the amplitude ratio for each event for the H- and D-components, respectively.

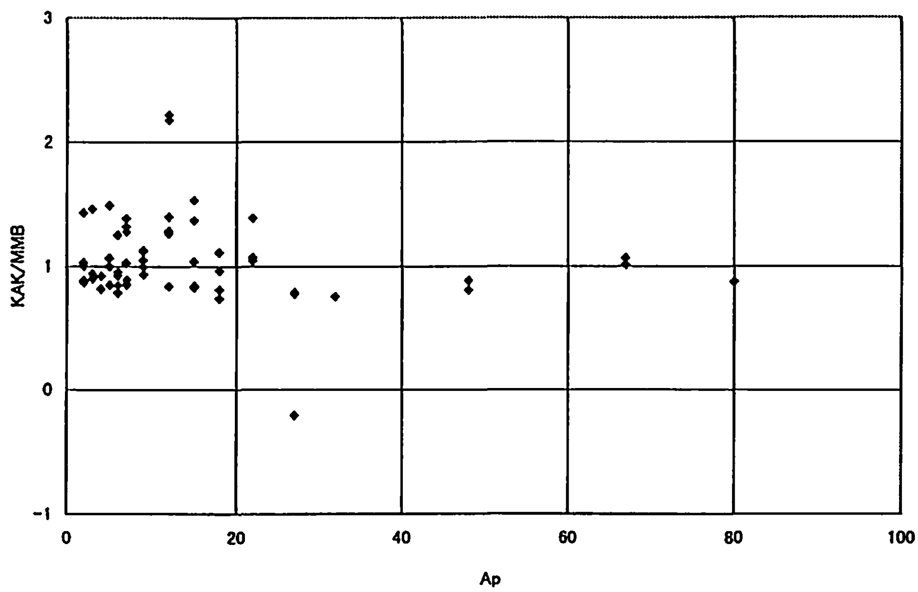

Figure 3-8: Ap dependence of the ratio of MI amplitude in the H-component at KAK to that at MMB for SC's picked up for the local time interval from 03LT to 13LT in JST (after Tsunomura, 1998).

Closed square is for the ratio of SC amplitude at KAK to that at MMB and open one for that of KNY to MMB. The amplitude ratio reveals characteristic change in the H-component in the morning hours near 08 to 10 LT. Such a variation pattern is not seen in the D-component. The dependence of the SC amplitude ratio of KAK to MMB in local time from 03 LT to 13 LT on geomagnetic disturbance is shown in Figure 3-8. Here, Ap index before the onset of SC is used as the parameter of the magnetic disturbance. Any clear relationship between the amplitude ratio and Ap index is not seen from the figure. The situation is same for the result when the Ap index after the SC is used. It is inferred that the anomalous amplitude ratio seen in the H-component in the morning hours is not related with geomagnetic activity before and after the SC.

The characteristics of the SC in the H-component in the morning hours cannot be explained by the Araki's model and/or other models. This matter should be examined extending the area of data analysis wider and using the numerical model in the next section.

3.3 Negative Impulse Associated with SC in the H-component

The average magnetic field variation of SC at CLF, FRD, TUC, MMB, SJG, KAK, KNY and HON using the converted one-minute magnetic data are shown in Figures 3-9(a) and (b), where the data are displayed from high to low geomagnetic latitudes. The events used are same as Figure 3-6. Bars on each curve indicate 95% confidence intervals for the averages as every five minutes. Note that this figure can be used for examining the average variation form at each station for the local time block; it is impossible to compare the amplitudes among the stations.

It can be seen that the H-component at the stations in higher latitudes among the stations in the figure (such as CLF and FRD) in the morning hours show irregular forms of variation; the variation form becomes flat resulting in the reduction of the amplitude. This feature would be related with the statistical result given by Russell and Ginskey (1995) for the subauroral stations. They showed that the H-component shows definite depression in the morning hours in the magnetic stations located from 54 ° to 58 ° geomagnetic latitudes. It seems that a negative impulse is superposed on the main impulse at FRD, TUC and MMB in the 06-12 LT block. At CLF, although it is not clear whether a negative impulse is superposed or not, the amplitude of SC is depressed. Note that the variation forms in the H-component in the 18-00 LT block show positive pulse-like structure especially at CLF, FRD and TUC.

Figures 3-10(a) and (b) are the correlation plot of MMB and FRD for SC's simultaneously observed at

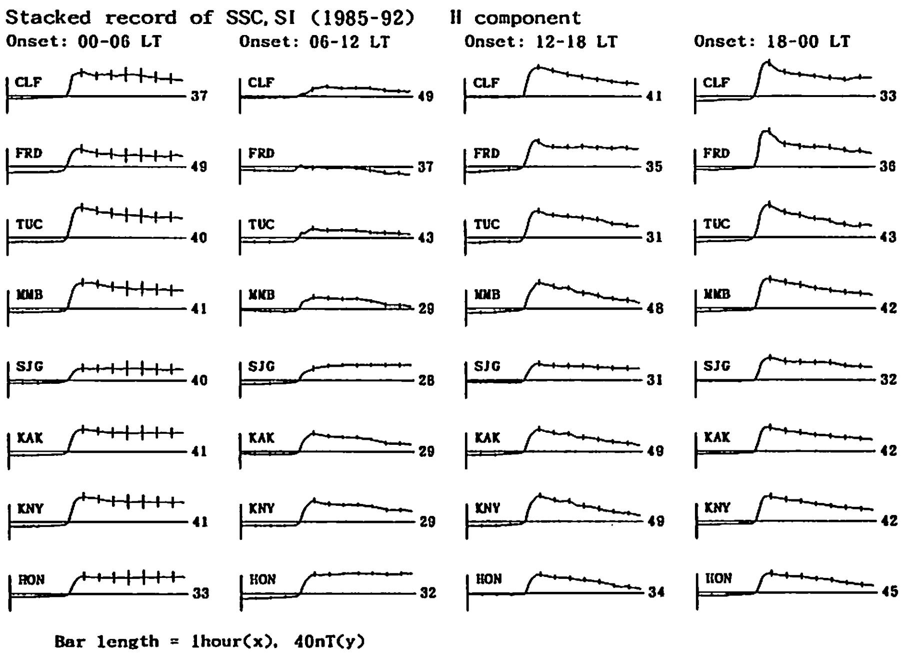

Figure 3-9(a): Average variations of the H-component for SC's from 1985 to 1992 at CLF, FRD, TUC, MMB, SJG, KAK, KNY and HON for four local time blocks at each station. The length of each graph is one hour in time and the length of the bar at the left corresponds to 40 nT magnetic variation. The onset of SC is arranged at twenty minutes after the start of each graph. The numbers of the events to take averages are written to the right of the graphs. The bars on the graphs denote standard errors (after Tsunomura, 1998).

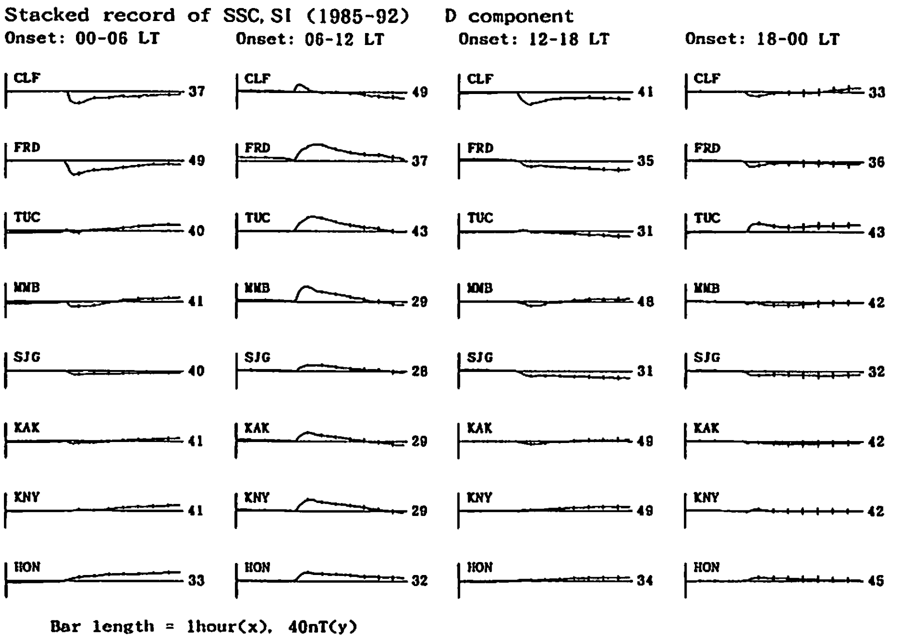

Figure 3-9(b): Same as Figure 3-9(a) for the D-component (after Tsunomura, 1998).

both stations. Figure 3-10(a) is for the events when MMB is in near 06 to 12 LT (that corresponds to near 16 to 22 LT at FRD) and (b) for the events when FRD is in near 06 to 12 LT (that corresponds to near 20 to 02 LT at MMB). It can be seen that the variation patterns are quite different for both stations. The amplitude of the magnetic variation at the observatory in the morning is in general much smaller than that at the observatory in the evening to midnight; moreover, in some events negative variations are observed in the morning. In most cases, a negative impulse is superposed on the MI of SC in the former. The period of the negative impulse seems to be different for each event.

It seems that a negative impulse is usually accompanied with the MI of SC and contributes the decrease of the SC amplitude in the H-component at the stations from subauroral region to middle latitudes in the morning hours. If the superposing negative impulse is originated in high latitudes and is weakened with decreasing latitude, the apparent amplitude ratio of SC in the H-component in lower latitudes to that in higher latitudes would become high. It is interesting that the variation pattern of the SC in the morning hours discussed here is similar to that of PPI (Kikuchi and Araki, 1985). The local time range when this pattern is seen is nearly the same as that of the frequent occurrence of PPI shown by Kikuchi and Araki (1985). In the next section, characteristics of this negative impulse will be investigated on the basis of a case study and a numerical analysis.

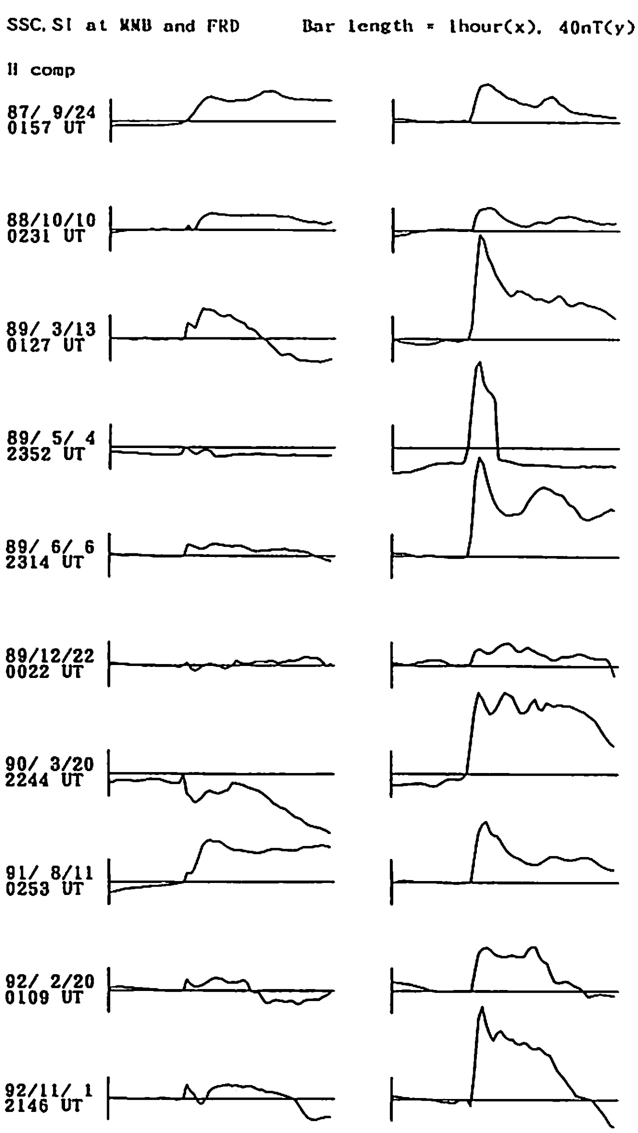

Figure 3-10(a): The H-component variations observed simultaneously at MMB (left) and FRD (right) for the SC's when MMB is in the morning hours (after Tsunomura, 1998).

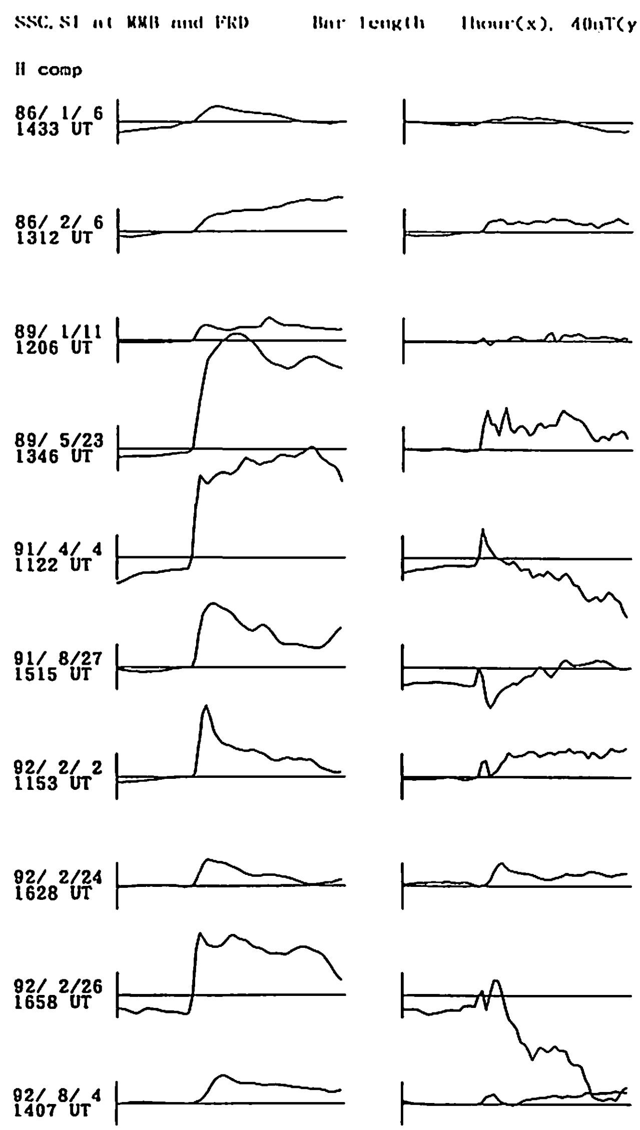

Figure 3-10(b): Same as Figure 3-10(a) for the SC's when FRD is in the morning hours (after Tsunomura, 1998).

3.4 Case Studies for the SC-associated Negative Impulse in the H-component

3.4.1 Typical events

Magnetic records for the SC on March 23, 1993 around 210° magnetic meridian are shown in Figure 3-11(a). Since the absolute measurements are not operated at some of the stations of the 210° magneticmeridian observatory network, the data shown in Figure 3-11(a)-(c) are not the ones converted to the geomagnetic dipole coordinate system. It can be seen that a negative impulse the duration of which is about ten minutes is superposed just after the onset of the SC at the stations form high to low latitudes. The amplitude of the negative impulse is highest at the

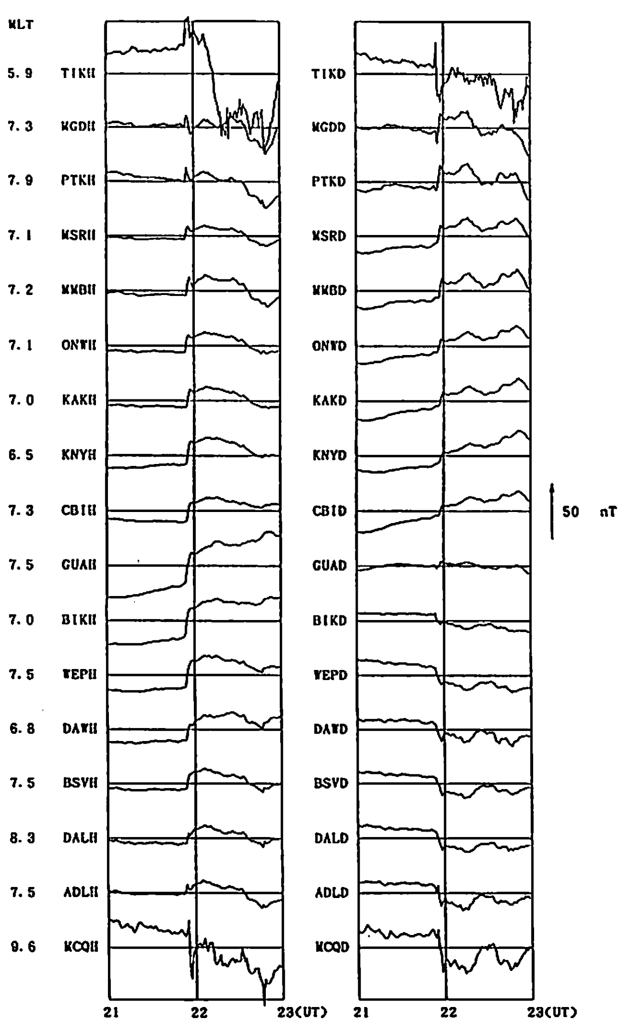

Figure 3-11(a): Correlation plot of the H- or X- (left) and the D- or Y- (right) components of magnetic records for the SC on March 23, 1993 around the 210° magnetic meridian. MLT at each station is noted leftmost (after Tsunomura, 1998).

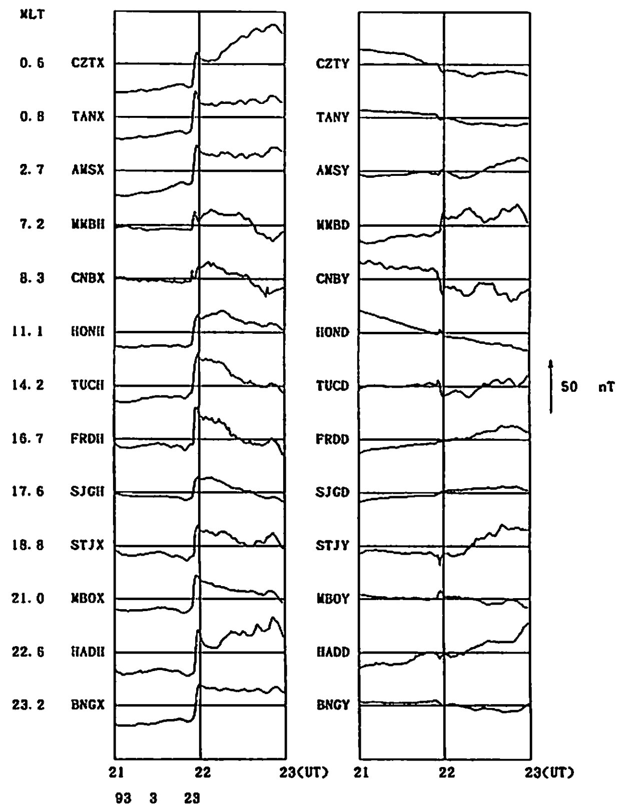

Figure 3-11(b): Same as Figure 3-11(a) for the routine stations in low to middle latitudes (after Tsunomura, 1998).

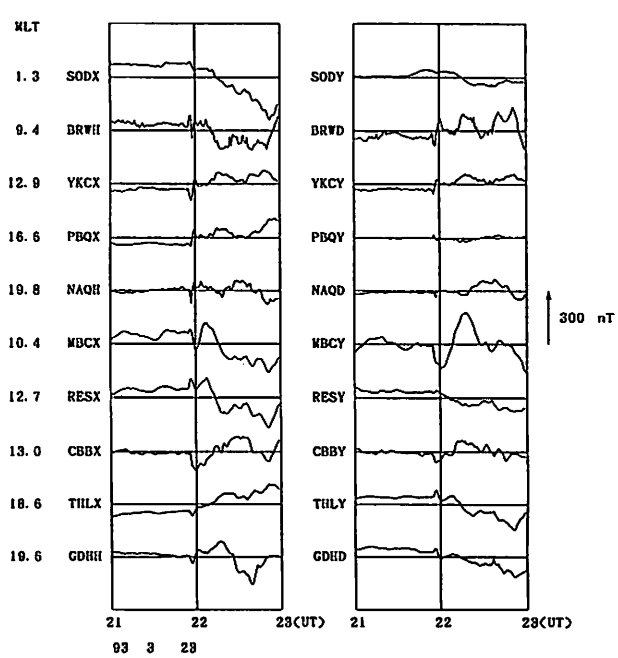

Figure 3-11(c): Same as Figure 3-11(a) for the routine stations in the auroral region (upper five) and the polar cap (lower five) (after Tsunomura, 1998).

station in the highest latitude in both hemispheres (MGD and ADL) and decays rapidly with decreasing latitude. Hence, it is expected that the negative impulse is originated in high latitudes. Negative impulse is not seen in the D-component but it seems that the D-component itself is anti-correlated with the negative impulse of the H-component. The H-component variation accompanied with a negative impulse seen at high and middle latitude stations may be noted as PPI according to the criterion of Kikuchi and Araki (1985). A substorm occurs about twenty minutes after the SC at TIK (Figure 3-11(a)), being clearly after the occurrence of the negative impulse. PRI was seen in the D-component at TIK, MGD, PTK, ADL and MCQ. The duration times of the PRI are definitely different from those of the negative impulses in the H-component. Therefore, it is deduced that the negative impulse is different from PRI. Note that Kikuchi and Araki (1985) mentioned that PPI is different from PRI.

Data at various local times in low to middle latitudes are shown in Figure 3-11(b) and those in high latitudes in Figure 3-11(c), respectively. The upper half of Figure 3-11(c) is for the stations in the auroal region and lower for those in the polar cap. In Figure 3-11(b), the negative impulse is seen only for MMB and CNB; these stations are in the morning hours at the time. The duration time and the variation form of the negative impulse are similar with the H-component at MBC and RES and the D-component at THL and GDH in Figure 3-11(c). From this fact it is expected that the phenomenon is not a localized event in a limited area and that it is a signature of a global process.

Figures 3-12(a), (b) and (c) are similar figures for the SC on September 09, 1992. In this case also a negative impulse of about ten minutes duration is superposed just after the SC at the stations from high to middle latitudes in the morning hours (Figure 3-12(a)). The latitudinal variation of the amplitude of the negative impulse is the same as that of Figure 3-11(a) and it is expected that the negative impulse is originated in high latitudes in this case also. Similar features are seen in the D-component and the variation form of the H-component as those of Figure 3-11(a).

The negative impulse is seen only for AMS and MMB in Figure 3-12(b); these stations are in the morning hours at the time. A substorm occurred just after the SC at NAQ station and soon after at SOD, which were located in the premidnight and morning sectors in the auroral region, respectively (Figure 3-12(c)). Corresponding to the substorm at NAQ, bay disturbance is seen superposed on the MI of SC at the stations in middle and low latitudes in the nightside (HAD, FRD, STJ). As this example show, one should take caution for the triggered substorm in the statistics of SC in the nightside. It is a remaining problem to develop the efficient way to distinguish the effect of substorm from the SC in the nightside. The relationships between the negative impulse in the H-component (or the D-component itself) in the morning hours and the variations in the polar cap are not clear; it may be due to the substorm occurrence. PRI is observed at BRW (Figure 3-12(c)). Considering the difference of duration, it is thought that the PRI and the negative impulse seen in the H-component at the stations in Figure 3-12(a) are different phenomena.

Figures 3-13(a) and (b) are the equivalent current vectors of the negative impulses corresponding to Figures 3-11(a)-(c) and Figures 3-12(a)-(c), respectively; the vectors are drawn for all the available stations in Figure 3-1. The equivalent currents are derived for the time changes of the magnetic variations corresponding to the negative impulse seen in the 210° magnetic meridian chain; the time interval to derive the currents is denoted in the figure. In both figures, a counterclockwise vortex in the afternoon side can be seen, whereas the pattern is not clear in the morning side. The ionospheric current system for the DP_{mi}–field is thought to consist of twin vortices in these region, one is counterclockwise in the afternoon side and the other clockwise in the morning side. The eastward equivalent current due to the *DL*-field may affect the ambiguity of the current pattern in the morning side. The numerically derived equivalent current vectors form the full reduction model is shown in Figure 3-14; here, the equivalent current is derived using Kamide and Matsushita (1979a)'s method, which is based on the theory of Fukushima (1969, 1976). The gross patterns of the current system in Figures 3-13(a) and (b) are basically the same as this and distinctive deformation of the current systems from that of the DP_{mi}-field cannot be found; even for the event on September 09, 1992 when an SC-triggered substorm occurred. Therefore, the pattern of the current system may reveal the nature of development of DP_{mi}-field. From these results, it can be inferred

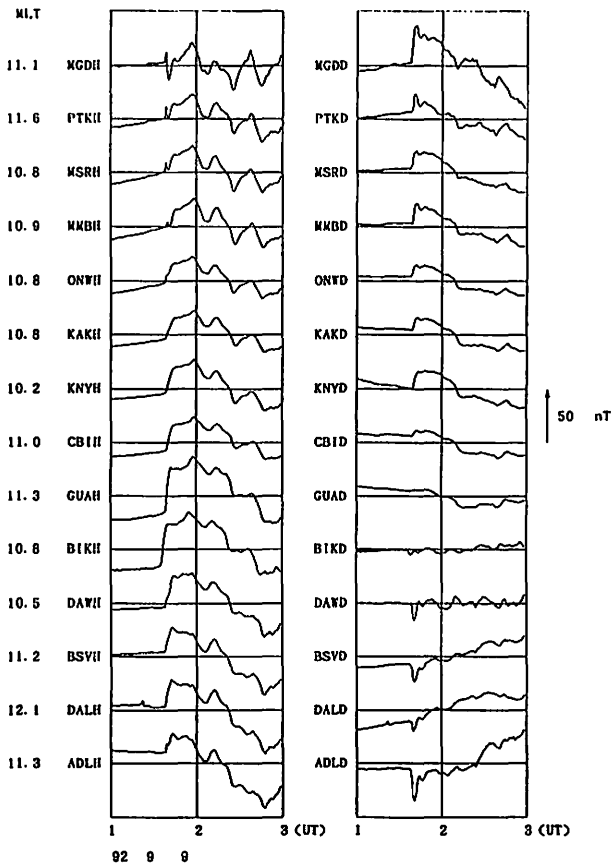

Figure 3-12(a): Correlation plot of the H- or X- (left) and the D- or Y- (right) components of magnetic records for the SC on September 09, 1992 around the 210° magnetic meridian. MLT at each station is noted leftmost.

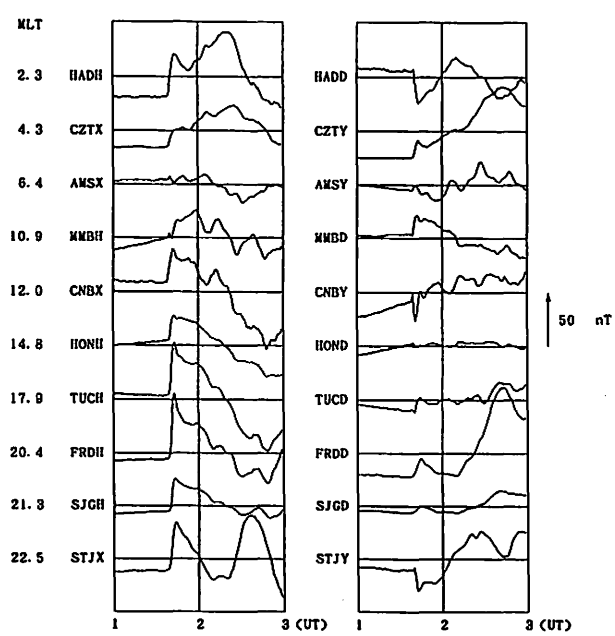

Figure 3-12(b): Same as Figure 3-12(a) for the routine stations in low to middle latitudes.

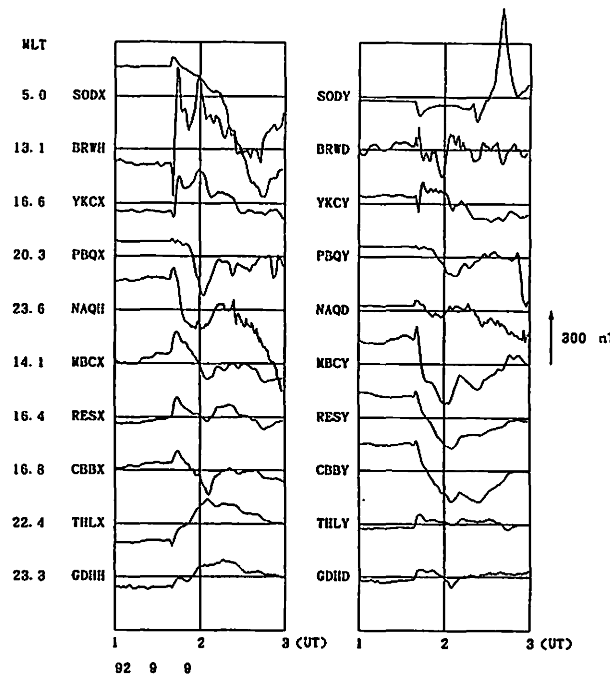

Figure 3-12(c): Same as Figure 3-12(a) for the routine stations in the auroral region (upper five) and the polar cap (lower five).

that the global scale process associated with the negative impulse is the MI of SC itself.

Hence, the negative impulse seen in the H-component in middle and low latitudes in the morning hours cannot be judged as a newly found phenomenon but is most likely the signature of the DP_{mi}–field in that area. This interpretation can explain the resemblance f the D-component with the negative impulse in the H-component as can be seen in Figures 3-11(a) and 3-12(a) and the scattering in its period seen in Figures 3-10(a) and (b).

Local time variations of the H- and D-components at 50, 30 and 5° latitudes derived by the numerical calculation of the full reduction model (Section 2.3.3 and 2.3.4) are shown in Figure 3-15. Negative variations are seen in the H-component in the morning hours in middle latitudes (50°) but not large in low latitudes (30°). The variations of the signs of the D-component are similar to the results in Figure 3-9(b). Note that the calculated variations should be superposed on the DL-field for the H-component, which is expected to show gradual variations in both of latitudinal and local time distributions comparing with those of the DP_{mi}-field. In Figure 3-15, the D-component in the morning hours does not seem to

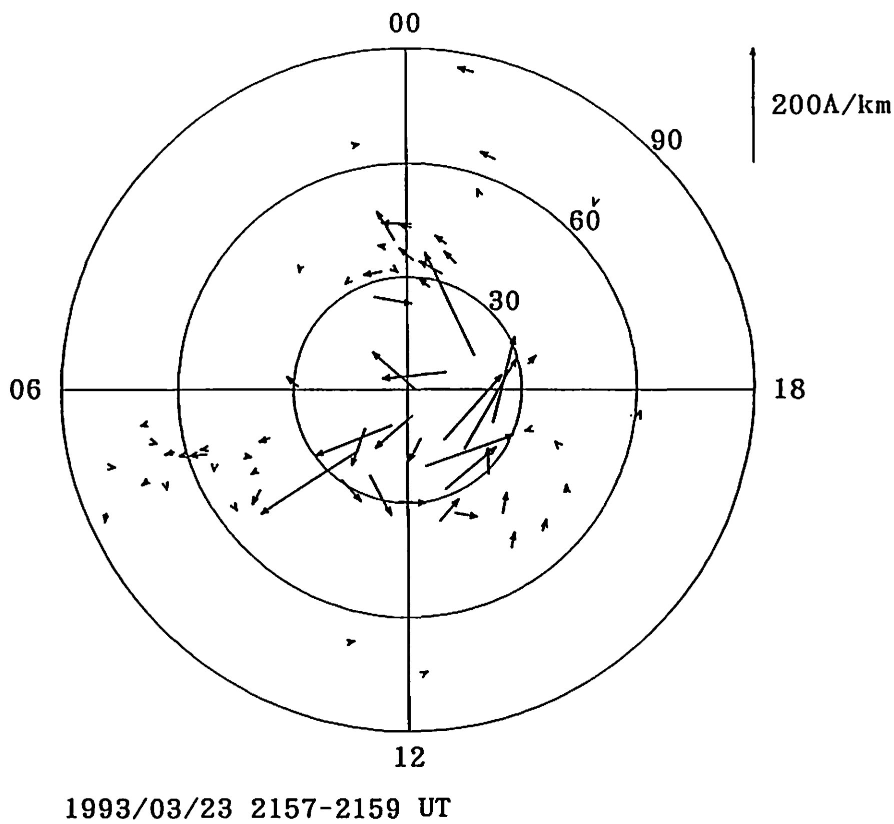

Figure 3-13(a): Equivalent current vectors for the SC on March 23, 1993 (after Tsunomura, 1998).

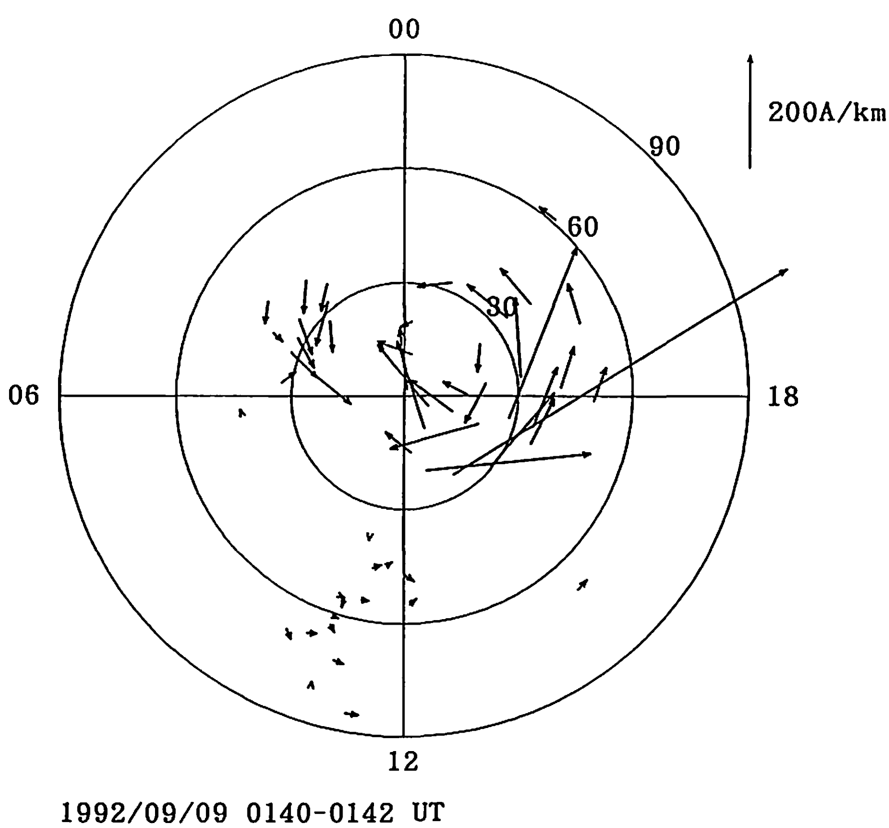

Figure 3-13(b): Equivalent current vectors for the SC on September 09, 1992.

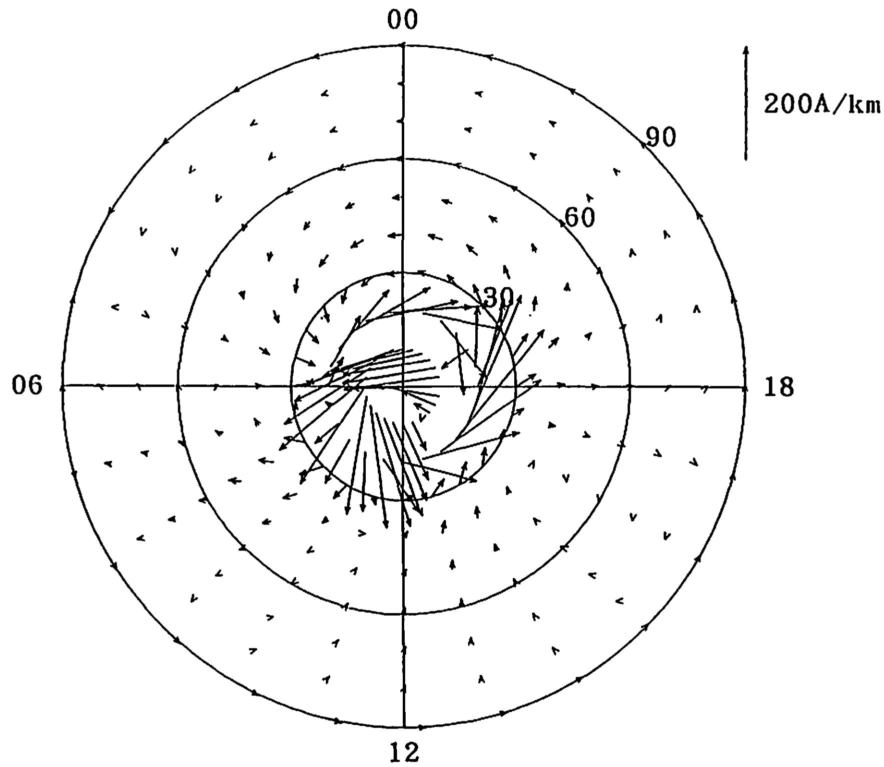

Figure 3-14: Equivalent current vectors given by the full reduction model calculation (after Tsunomura, 1998).

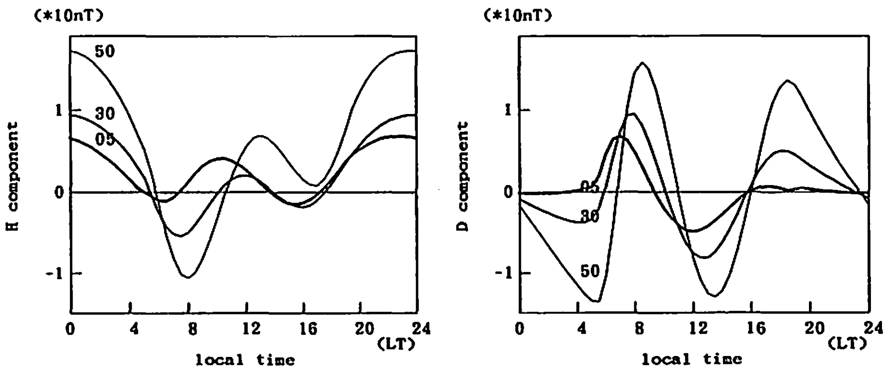

Figure 3-15: Local time variations of the H- (left) and D- (right) components of magnetic variations at 05° (thick), 30° (medium) and 50° (thin) latitudes obtained by the full reduction model calculation (after Tsunomura, 1998).

decrease its amplitude with decreasing latitude not so fast as the H-component in that local time range. This result agrees well with the fact that the amplitude of the negative impulse in the H-component decreases faster with decreasing latitude than the MI of the D-component as seen in Figures 3-11(a) and 3-12(a).

It is worth to note that the variation of the H-component is positive and large in the nighttime. The ionospheric current contributions are negative but small in the nighttime at these latitudes. Most of the positive variation in this local time range is the product of the field-aligned current effects. The variation forms observed in these local time ranges show usually positive pulse-like structures in the H-component (Figures 3-9(a), 3-10(a) and (b)). Yamada et al. (1997) showed that the average polarity of PRI in the night in middle latitudes is negative; this corresponds to the positive MI in that local time range and is consistent with the present result. Therefore some part of the positive variation is certainly caused by the

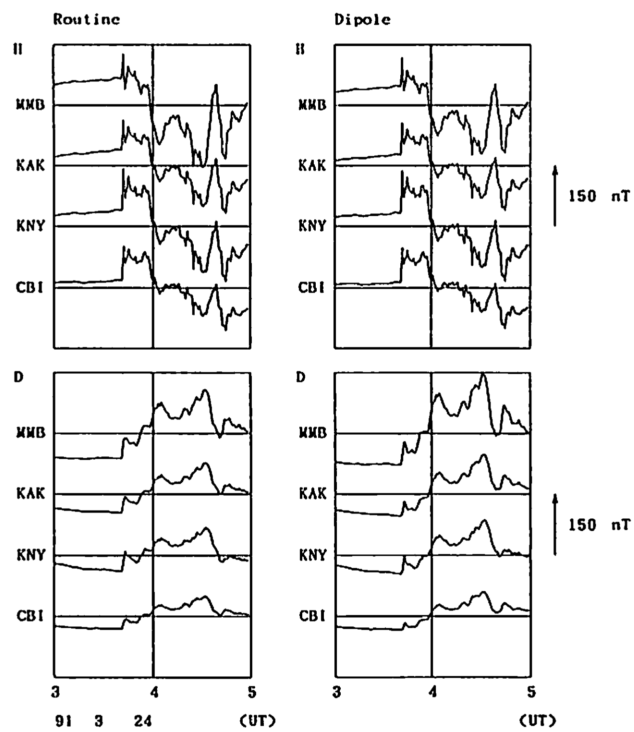

Figure 3-16: Correlation plot of the H- (upper panels) and D- (lower panels) components of magnetic records at Japanese routine stations for the SC on March 24, 1991. The left panels are for the routine data and the right for the converted ones.

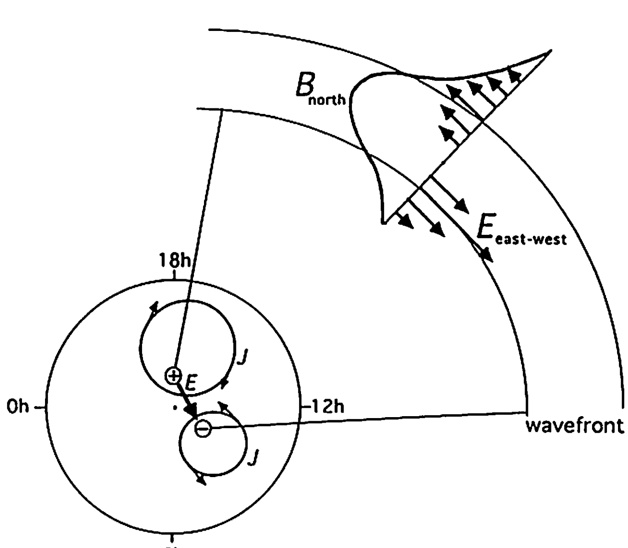

Figure 3-17: Illustration of propagation of the sharp compressional pulse in the afternoon magnetosphere and ionospheric current vortices due to the electric field projected from the wavefront (after Araki et al., 1997).

DP_{mi}-field, though it may include the signature of SC-triggered substorm.

Now a self-consistent interpretation on the basis of the Araki's model is suggested for the local time variation pattern of the SC-associated negative impulse in the H-component. It is added that the signs of the calculated DP_{mi}-fields are almost the same as the remaining part of the ground magnetic variations for the CME event of February 21, 1994 after subtracting the magnetopause current contribution as shown by Petrinec et al. (1996).

3.4.2 The March 24, 1991 Event

As one of the most pronounced events of SC, that of March 24, 1991 0341 UT event is an object of many author's interest. Araki et al. (1997) analyzed the event using many kinds of data and explained it by the existing models of SC successfully. For the extraordinary variation of the D-component, Araki et al. (1997) tried to explain by the observational situation of the routine measurement. They mentioned that the D-component data include the projection of the H-component because of the orientation of magnetometers to the local declination direction, which is for most cases different from the direction of the geomagnetic dipole magnetic meridian.

To examine the validity of their explanation, I tried the actual conversion of the magnetic data in this event to the geomagnetic dipole meridian direction. Figure 3-16 shows the results at MMB, KAK, KNY and CBI; these stations were near the local noon at this event. It is obvious that most of the D-component variation remains after the conversion even the variation form becomes a little sharp. Therefore, the variation pattern of the D-component at these stations is not explained sufficiently by their interpretation. They might overestimate the strength of the *DL*-field and thus underestimate that of the DP_{mi}-field. I would like to try to explain the variation pattern considering the negative impulse discussed so far.

At the time of 0341 UT, Japanese stations are near the noon. As can be seen from Figure 3-15, the calculated D-component near 12 LT is small or negative; that is different from the observation. There is another problem in the comparison of this result with the observation. The observed H-component shows a pair of a sharp increase and a rapid decrease at KAK. According to the previous discussions, the rapid decrease would be the signature of the DP_{mi}-field. However, the calculated H-component of DP_{mi}–field is small negative or rather positive as shown in Figure 3-15. A modification of the calculation is necessary toexplain the observational features in this event.

There is a report that the corresponding solar wind shock attacks the magnetosphere from the evening side (Blake et al., 1992) at this event. That may cause the azimuthal shift of the source current distribution. The situation is illustrated in Figure 3-17. According to the discussion of Blake et al. (1992), I calculated the ionospheric current with the source current shifted such as to make the center at 1600 LT. Figure 3-18 shows the local time variations of the magnetic field as Figure 3-15 but with the center being shifted. The sufficient negative variation in the H-component is expected at the noon and the D-component is positive in the dayside middle latitudes. The direction of the east-west component of the electric field in middle latitudes obtained from the model is eastward (not shown here). This agrees well with the observedfeature of HF Doppler frequency variation (Figure 4 of Araki et al. (1997)). Thus, the variation pattern of March 24, 1991 event can be explained by azimuthally shifting the position of the origin of the DP_{mi}-field.

3.5 The SC-associated Negative Impulse and PPI

Latitudinal variations of the H- and D-components derived by the calculation are shown in Figure 3-19. All components decrease their amplitude almost monotonously with decreasing latitude. This result agrees very well with the observed feature in the latitudinal variation in the D-component amplitude as shown in Figure 3-6. The H-component in the morning hours (06-12 LT block) is negative in middle to low latitudes and grows up large positive value near the equator. Superposing this simply on the *DL*-field, it can be expected that the amplitude of the H-component in this local time range varies similarly with the profile shown in Figure 3-6. Actually, since the variation forms of the *DL*- and DP_{mi}–fields are possibly different, the complicated profiles such as the discrepancy of the ratio of the amplitude at KAK to MMB seen in the morning hours (Figure 3-7(a)) may be apparent.

A substorm is often triggered by SC (Kokubun et

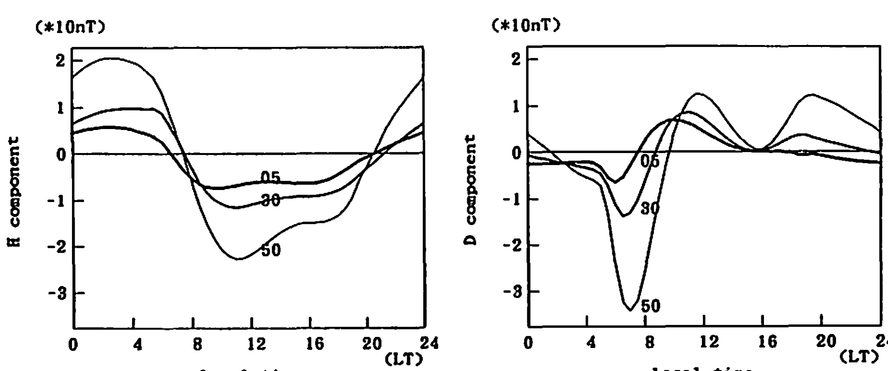

Figure 3-18: Local time variations of the H- (left) and D- (right) components of magnetic variations at 05° (thick), 30° (medium) and 50° (thin) latitudes given by the model calculation shifting the source currents to the evening side (after Tsunomura, 1998).

al., 1977, Iyemori and Tsunomura, 1983). The occurrence of a substorm may accompany additional current systems such as a wedge current and/or the enhanced DP2 type ionospheric current system. There may be a possibility that the negative impulse discussed in the previous sections is caused by these current systems. However, the duration time of the impulse is basically much less than that of a typical substorm and the corresponding substorms are not seen in the case studies in the previous section. As shown in Figure 3-8, the SC amplitude ratio of KAK to MMB does not depend on geomagnetic disturbance before and after the SC. If the negative impulse is caused by the SC-triggered substorm, it should show the dependence on geomagnetic activity. Therefore, it is strongly suggested that the negative impulse is not a signature of the SC-triggered substorm.

Kikuchi and Araki (1985) showed that a positive impulse often precedes the MI of SC and named it PPI. The variation pattern and the dependence of occurrence frequency on local time are same as the negative impulse discussed here. They suggested that the positive impulse is the magnetospheric compression effect after examining the HF Doppler observation associated with PPI. However, the westward electric field to which they mentioned that PPI corresponds can be explained also as the electric field of the DP_{pi}-field. In this viewpoint, the PPI is the apparent positive variation visualized by the succeeding negative impulse. The superposition of the DL- and DP_{pi}-fields, giving rise to the sharp onset signature, promotes the apparent positive variation.

The fact that the PPI at GUA was not much larger than that at MMB (Kikuchi and Araki, 1985) is also explained as follows. As PPI amplitude is basically small and overlapped to the DL-field, the exact amplitude estimation is difficult primarily. Moreover, the present result shows that the magnetic field would not reveal large enhancement at 5° latitude (Figure 3-15). The amplitude grows up rapidly with decreasing latitude towards the equator. The observational fact of Kikuchi and Araki (1985) is not contrary to the DP_{mi}-field model. Hence, it is strongly suggested that PPI is the apparent magnetic variation due to the pair of positive variation made by the DL- and DP_{pi}-fields and the succeeding negative impulse due to the DP_{mi}-field. The pattern would be a basic signature of the DP_{pi}- and DP_{mi}–fields in middle to low latitudes.

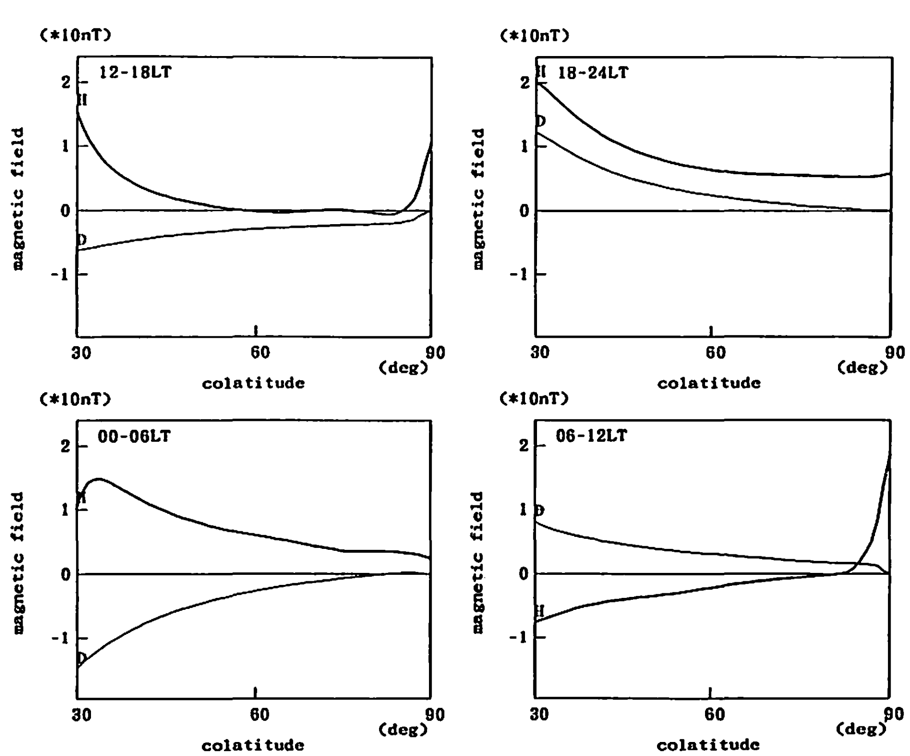

Figure 3-19: Average latitudinal variations of the H- (solid) and D- (thin) components of the magnetic variations from 30° to 90° colatitudes for four local time blocks given by the full reduction model calculation. The abscissa is arranged for colatitude to compare with Figure 3-6 (after Tsunomura, 1998).

This interpretation for the observed magnetic variation is illustrated in Figure 3-20.

Yamada et al. (1997) showed that PRI is often positive in the morning hours in middle latitudes. According to the classification of their positive PRI (Figure 1 of Yamada et al. (1997)), it can be said that their positive judgement corresponds to PPI or the MI with a negative impulse discussed above. Occurrence frequency of the positive PRI mentioned by Yamada et al. (1997) is almost identical with that of the negative impulse discussed here.

There is an observational result that the H-component in the daytime is a little smaller for the southward IMF-B_z condition than that for the northward condition (Russell et al., 1994a, b). This can be interpreted that DP_{mi}-field is larger for the southward IMF-B_z than the northward for the same dynamic pressure change. If the DP_{mi}-field becomes stronger the morning side depression becomes large as shown above. From this viewpoint, the *DL*- and the DP_{mi}-fields should be related with different solar wind parameters respectively. This is partly confirmed that the D-component variation due to sudden solar wind dynamic pressure change is not correlated with the dynamic pressure change of the solar wind as shown by Sitar et al. (1996). They discussed the matter on the basis of the magnetic variation due to the field-aligned current without including the ionospheric current effects. Taking into account of the ionospheric current effects, the pattern may be explained more clearly.

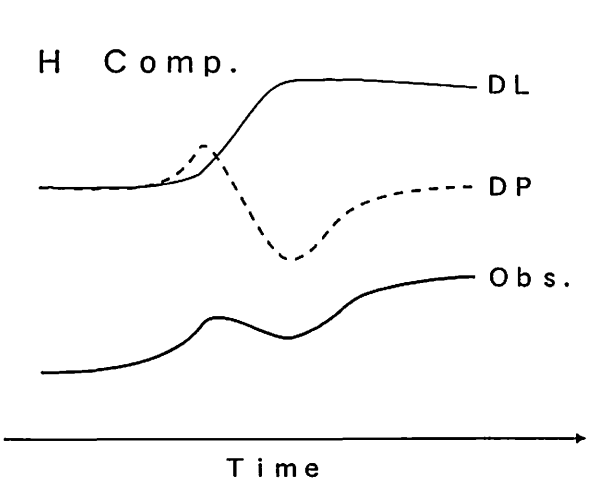

Figure 3-20: Interpretation of the negative impulse seen in the H-component in the morning hours or PPI (after Tsunomura, 1998).

The DP_{mi}-field consists of the effects of the ionospheric current and the field-aligned current. It is important to examine which one contributes the corresponding variation effectively. Figure 3-21(a) shows the magnetic field variations due to the ionospheric current (Ionos), field-aligned current (Fac) and the equivalent current (Sum) separately. It can be seen that the field-aligned current contributes the negative variation in the H-component in the morning and the afternoon hours. Figures 3-21(b) and (c) are the equivalent current vectors from 60° latitude to the equator, corresponding to the ionospheric (Ionos) and field-aligned (Fac) current contributions, respectively. It is clearly seen that the eastward currents at the dayside equator and southward currents in the morningside middle latitudes are large in the former (Figure 3-21(b)). Hence, the D-component in the middle latitude stations in the morningside is expected to have a potential for the usage of monitoring the development and decay of polar-originating ionospheric current systems.

It is interesting and important also how the equatorial enhancement affects this matter. A calculation setting the conductivity values in low latitudes equal from 30° latitude to the equator is operated for this purpose. Figure 3-22 shows the comparison of the result with the full reduction model. The difference is not so large in middle latitudes because the gross pattern of the ionospheric current system is basically controlled by the condition of the conductivity from high to middle latitudes. The negative variation in the H-component is a little reduced because of the stronger H-component due to the ionospheric current. The ionospheric current in low latitudes is enhanced if there is not the equatorial enhancement. This is because the share of the ionospheric current in low latitudes becomes large because of the weakened equatorial current. And then the negative variation in the dayside due to the field-aligned current is counterbalanced by the enhanced ionospheric contribution.

3.6 Availability of the D-component to Monitor the Time Variation of the DP_{mi}-field of SC

It is established that the *DL*-field has a direct correspondence with the solar wind dynamic pressure change, whereas the origin of the DP_{mi}–field has not been exactly clarified. Although the pattern of the

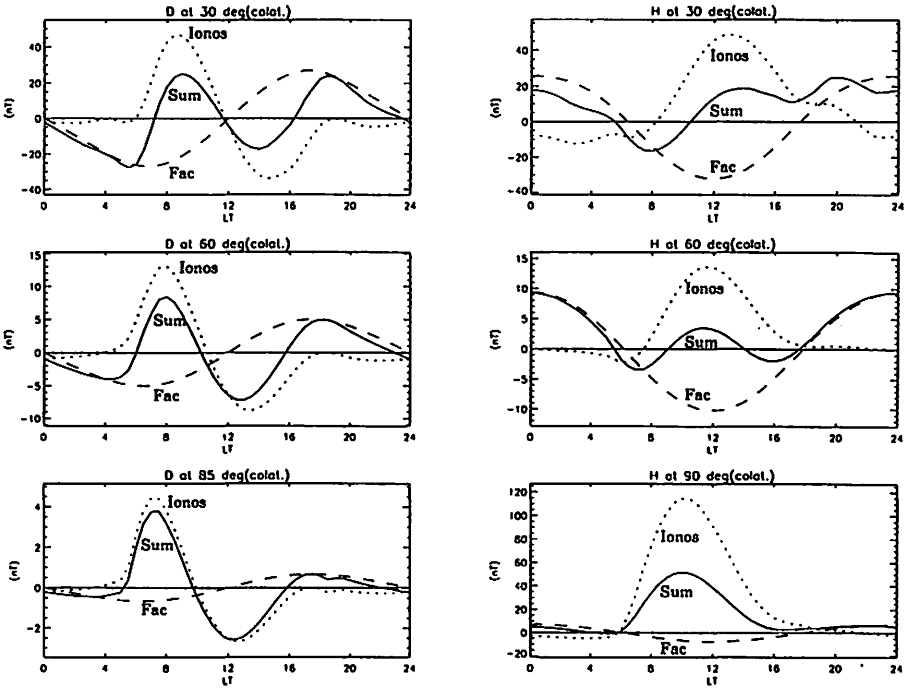

Figure 3-21(a): Local time variations of the D- and H- components of the magnetic fields at 60°, 30° latitudes and the equator for the equivalent (Sum) and ionospheric (Ionos) currents for the full reduction model and the field-aligned currents (Fac). Solid, dotted and dashed lines are for the results for Sum, Ionos and Fac, respectively as labeled on each curve.

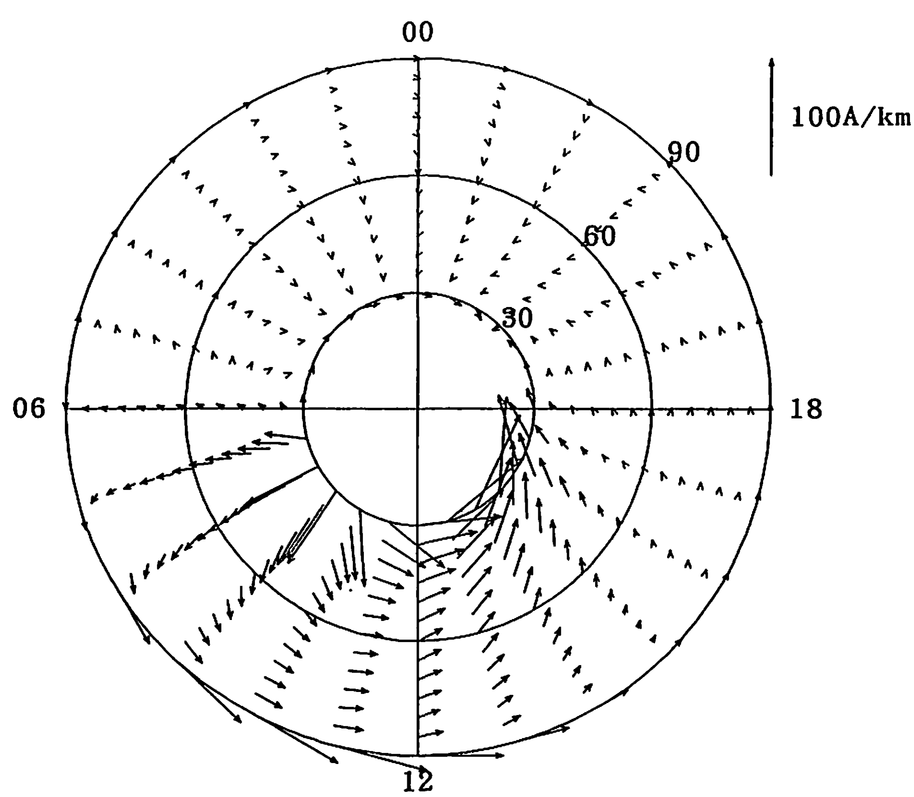

Figure 3-21(b): Equivalent current vectors for the magnetic fields from 60° latitudes to the equator due to the ionospheric currents for the full reduction model, corresponding to the Ionos part in Figure 3-21(a).

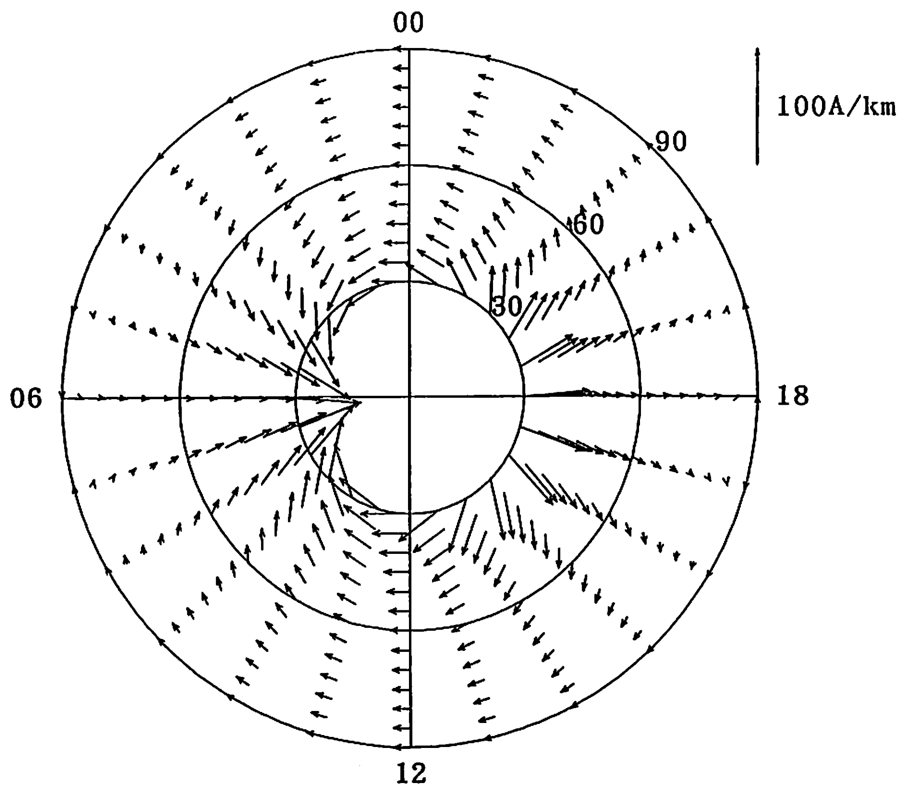

Figure 3-21(c): Equivalent current vectors for the magnetic fields from 60° latitudes to the equator due to the field-aligned currents for the full reduction model, corresponding to the Fac part in Figure 3-21(a).

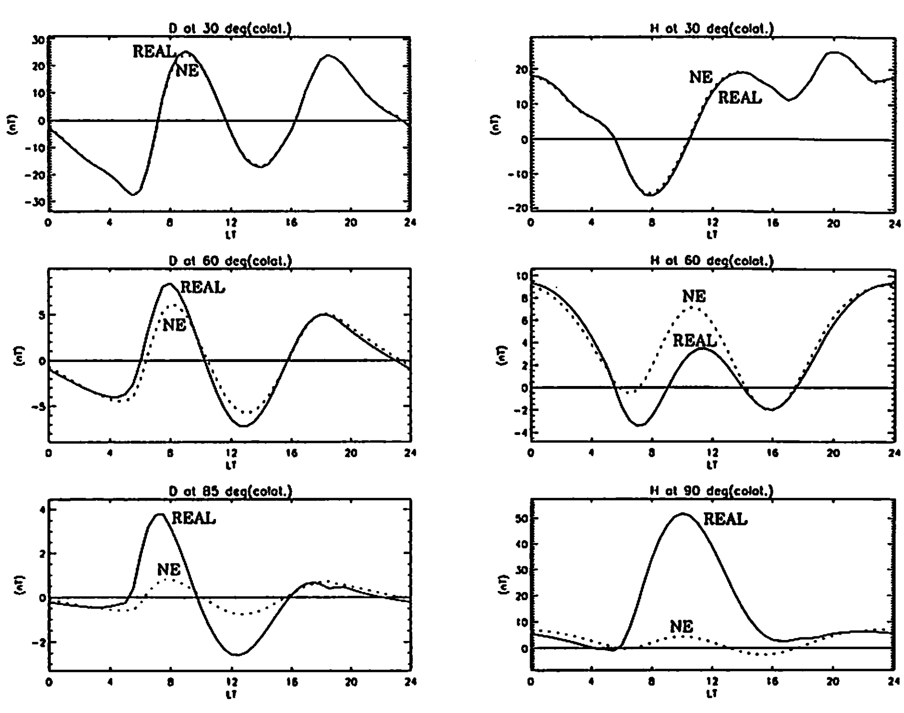

Figure 3-22: Local time variations of the D- and H- components of the magnetic fields at 60°, 30° latitudes and the equator for the full reduction model (REAL) and the model without equatorial enhancement (NE). Solid and dotted lines are for the results for REAL and NE, respectively as labeled on each curve.

equivalent current system of the MI is same as that of the ionospheric convection currents, the whole magnetospheric convection may be difficult to develop sufficiently in a short time range of SC duration (Kikuchi, 1986). As Kikuchi (1986) pointed out, the current system may develop due to a process at the outmost side of the magnetopause. Therefore, an investigation to examine the relationships between the time variations of the solar wind electric field and the DP_{mi}-field is necessary at least to fully understand the matter.

Although the H-component variation usually shows a step like variation corresponding well to the solar wind dynamic pressure, it cannot be used as s pure parameter for monitoring the DP_{mi}-field. For that purpose, it is suggested that the variation of the D-component of magnetic field in the morning hours is a more useful parameter. In this section, I would like to present a speculation for the availability of the D-component as a rough indicator of the DP_{mi}-field.

To see the variation forms of SC in another viewpoint, stacked records of geomagnetic storms starting with an SC at KAK are shown in Figure 3-23. Each graph is a stacked record of each component of the converted one-minute magnetic data for geomagnetic storms starting with the SC at KAK at the local time range denoted in the leftmost. The mean monthly average of the international five quiet days is subtracted to remove the solar diurnal variation pattern. The time span and the sensitivity of the graph are one day and denoted by the bar (50nT) at the left, respectively. The number in the rightmost is that of the events stacked.

The H-component shows nearly the same variation forms with a slight difference due to a diurnal pattern, that is, the minimum in the evening and the maximum in the morning. It can be seen a clearer diurnal pattern in he D-component; the maximum is in the morning and the minimum in the prenoon hours. These diurnal patterns are thought to be different from those of the solar diurnal variation because they are not apparent before the SC; the patterns are similar to those of the SD fields of geomagnetic storm shown by Yokouchi (1958) and Sugiura and Chapman (1960). Hence, these are most likely attributed to the field-aligned and the ionospheric current effects during geomagnetically disturbed periods. It is notable that the diurnal variation pattern resembles the curve of 1.0 in Figure 2-24, that is, the local time variation deduced from the equal mixing of the Region 1 and 2 field-aligned currents.

The diurnal patterns are vanished for the stacked record of all the events as shown in Figure 3-24; the style of the figure is similar to that of Figure 3-23 except for the time span and the sensitivity. In the figure, the average pattern of geomagnetic storm due to the SC and the ring current development is clearly shown in the H-component. The mean duration of the

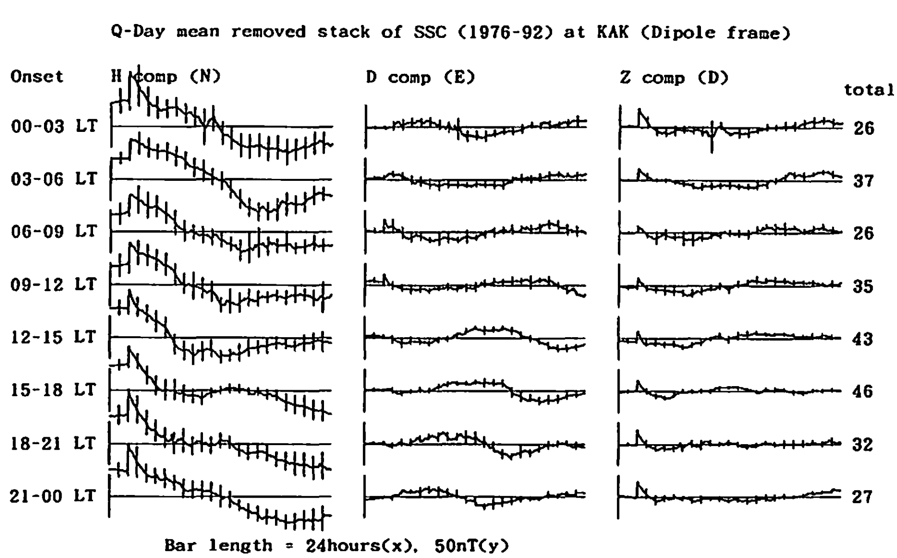

Figure 3-23: Average magnetic variations of geomagnetic storms started with SC in eight local time ranges at KAK from 1976 to 1992. The length of the each graph is 24 hours in time and the length of the bar at the left corresponds to 50 nT magnetic variation. The number in the right is that of the events to take the average. The bars on each graph denote standard errors (after Tsunomura, 1998).

initial phase duration is nearly one hour but it seems that the ring current develops smoothly just after the SC. Therefore, it is again expected that the various effects are included in the H-component during the initial phase. The curve for the D-component becomes almost flat except for the onset (SC).

The Z-component shows at first the local induction effect at KAK. However, the Z-component about ten hours after the onset shows a different form from the local induction pattern due to conductivity anomaly in the crust; the usual variation pattern of the Z-component is nearly parallel to the H-component at KAK. The variation sense of the later part of the Z-component is positive (downward) and same as the magnetic effect of the ring current. That can be seen more clearly at MMB than KAK because the CA effect is smaller at MMB than KAK.

Thus, it is thought that the later part of the Z-component reveals a signature of the direct contribution of the ring current although most of it is reduced by the ground induction (Figure 3-25). The roughly estimated ratio of the internal to external potential strength for the long period (nearly one day) magnetic field variation are 0.35 at KAK and MMB; this is nearly the same as the value, 0.37-039, derived for Dst by Rikitake and Sato (1957).

Taking into account of these gross features of geomagnetic storm as a background, I would like to turn the viewpoint to the initial phase of storm. It is noted that the D-component in 06-09 and 09-12 LT in Figure 3-23 shows clear impulses with somewhat different forms from the H-component of all the local time blocks. The H-component, revealing the broader variation form, is the result of superposition of the *DL*- and DP_{mi}-fields. Moreover, the H-component variation is influenced very much by the succeeding decrease due to the ring current developments as discussed above.

In the previous section it was suggested that the variation in the D-component, showing the anti-correlated pattern with respect to the negative impulse of the H-component, reveals the variation pattern of the DP_{mi}-field during the initial phase clearer than the H-component. In reality, SC's in middle to low latitudes in the morning hours show usually large amplitude in the D-component. Therefore, it is proposed that the D-component in middle and low latitudes in the morning hours can be used as a measure to estimate the magnetospheric electric field variation of SC. The usefulness as a simple measure may have some reality considering the actual condition that there are limited numbers of magnetic

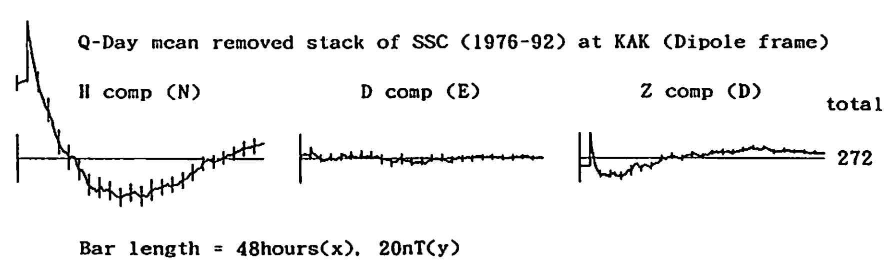

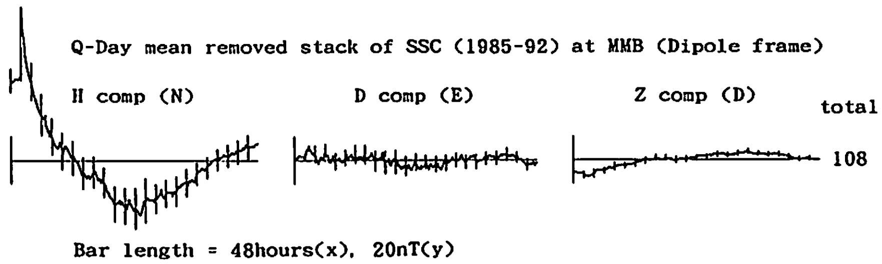

Figure 3-24: The average magnetic variation of geomagnetic storms started with SC at KAK (upper) from 1976 to 1992 and MMB (lower) from 1985 to 1992. The length of the each graph is 48 hours in time and the length of the bar at the left corresponds to 20 nT magnetic variation. The number in the right is that of the events to take the average. The bars on each graph denote standard errors (after Tsunomura, 1998).

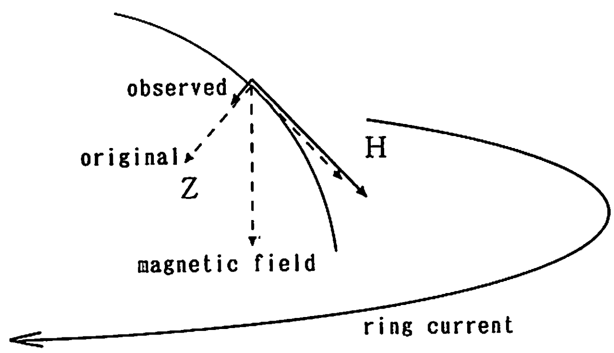

Figure 3-25: Illustration of the modulation of the ring current magnetic field due to the Earth's induction.

observatories in the world. Here, it is assumed that the polar-originating current system and the field-aligned currents vary simultaneously in parallel.

Similar utilization of the D-component in the middle latitudes in the morning hours to estimate the magnetospheric process may be applied to other phenomena, such as DP2, Pi2 and so on. In the actual discussion, however, it is important to convert the routinely observed D-component to the geomagnetic dipole coordinate system in order to exclude the contamination of the H-component.

4. Concluding Remarks

In this paper, characteristics of polar-originating ionospheric current systems relating with geomagnetic disturbances in middle and low latitudes are examined from various viewpoints, that is, a modeling of a numerical analysis, its applications to observational facts and statistical and case studies of the magnetic data. This paper is composed of two main parts. One is for a numerical analysis of polar-originating ionospheric current systems including the equatorial enhancement of the ionospheric conductivity and the other is for investigations of the characteristics of SC in middle and low latitudes. The latter is aimed to clarify the contribution of the polar-originating ionospheric current system for the magnetic variations of SC in middle and low latitudes.

The first part:

A numerical calculation setting some simplifications for a realistic ionospheric conductivity model is made. The result agrees well with the observed magnetic fields of PI of SC from high to low latitudes and an equatorial enhancement signature of the ionospheric current in the dayside equator is obtained. Comparing the result with that of the uniform ionospheric conductivity model, the behavior of the electric field in the dayside low latitudes is clarified. The polar-originating electric field, being weakened by the high conductance in the dayside equator, retains the strength to yield the equatorial enhancement with the aid of the extremely high conductance along the north-south direction.

Then a method to derive a realistic model for the global two-dimensional ionospheric conductivity is proposed after discussions of the effect of the meridional current system on the modification of the equivalent conductivity. Taking into account of the meridional current system, which allows vertical currents inside the ionosphere, an appropriate method to modify the values of the height-integrated conductivity tensor from that of the thin-shell model is proposed. The modification is mainly applied for the components associated with the east-west component of the electric field; it is shown that $\Sigma_{\theta\varphi}$ must be reduced near the equator and $\Sigma_{\varphi\varphi}$ intensified and made to have broarder maximum near the equator than the thin-shell model. The calculated result shows that the modification of $\Sigma_{\theta\varphi}$ influences the profile of the electric field at the equator very much. The model with fully reduced $\Sigma_{\theta\varphi}$ reveals the observed feature of SC best.

The ionospheric conductivity model with the fully reduced $\Sigma_{\theta\varphi}$ was applied for numerical calculations for three matters concerning polar-originating ionospheric current systems as follows.

(1) The latitudinal profile of the DP2 amplitude in the daytime is discussed changing the canceling rate for the dawn-to-dusk electric field due to the Region 2 field-aligned current. It is shown that the equatorial enhancement would not be appeared when the ratio of the total amount of the Region 2 field-aligned current to that of the Region 1 current exceeds 0.5. The result was compared with the observational result of Kikuchi et al. (1996) and it was inferred that the ratio of the Region 2 field-aligned current to the Region 1 might be nearly 0.0 for their case.

(2) Characteristics of the north-south asymmetry of the magnetic fields due to polar-originating ionospheric current systems for the voltage and

current generators are compared; numerical calculations covering both hemispheres simultaneously were performed for this matter. It is shown that the magnetic fields in high latitudes for the voltage generator show the positive relationship with the conductivity. Whereas, the relationship is vague or even reversed for the current generator. The north-south asymmetry of the magnetic fields in middle latitudes is seen only for the afternoon block of the voltage generator.

(3) The solar cycle dependence of the local time profile of the equatorial electric and magnetic fields is examined making calculations with the ionospheric conductivity distributions corresponding to the sunspot numbers of 10 and 100. The result agrees well with the observed feature given by Jain and Srinivasacharya (1976).

As shown by these applications, the new model, being based on the International Reference Ionosphere (IRI) model, and a less technical treatment to construct the conductivity model, is versatile and may be useful to develop quantitative analyses in some aspects of the magnetosphere-ionosphere coupling problems.

The second part:

The polarity of MI of SC observed at Kakioka is statistically examined using the routine reports of SC from 1957 to 1992. It is shown that the polarity of the D-component is positive in most cases as well as the H- and Z-components. It is confirmed that, as pointed out by Fukushima (1994), this shift of the polarity is attributed to the apparent variation caused by the situation of the routine magnetic observation; the magnetic instruments are arranged based on the direction of the local magnetic field, declining from the geomagnetic dipole meridian. In the statistics taken on the basis of the magnetic data converted to the geomagnetic dipole coordinate system, there is not a definite shift in the polarity of the D-component for SC. The local time profile of the D-component polarity for the converted data is almost parallel to that of the numerical calculation; that means that the D-component observation in middle and low latitudes can be explained by the Araki's model. However, the local time profile of correlation coefficients among Memambetsu, Kakioka and Kanoya shows an unexpected feature for the H-component; the correlation coefficient of the H-component becomes low in the morning hours. It is also found that amplitude ratios of SC at KAK and KNY to that at MMB reveal an anomalous local time change for the H-component in the morning hours. These features cannot be explained by the Araki's model straightforwardly.

A data analysis using globally distributed magnetic observations was made to clarify the characteristics of SC in the H-component in the morning hours. It is found that a negative impulse is usually superposed on main impulse (MI) of SC in the H-component just after its onset, at the stations located in low to high latitudes in the local time range from the morning to the early afternoon. The superposition of the negative impulse causes the apparent decrease of SC amplitude in the H-component in this area. The occurrence of the negative impulse does not seem to be dependent on the geomagnetic activity. After case studies and a numerical analysis, it is suggested that this negative impulse is the signature of the DP_{mi}-field of the Araki's model in that area. A possible interpretation for PPI is also given that PPI is an apparent variation due to the combination of the *DL*-field and the negative impulse (DP_{mi}-field). Thus, a self-consistent model for the signature of the SC-associated polar-originating ionospheric current system in middle and low latitudes is presented.

It is also suggested that the D-component data in middle latitudes have a potential to be used as a rough measure to estimate the electric field variation due to the whole magnetospheric process.

There remain some matters concerning SC, which should be investigated in future as follows;

(1) The result shown here exhibits the mean profile and the observed features would be different in each event. The relationship of the time variation pattern of SC and/or DP2 in the D-component in the morning hours in middle latitudes with the solar wind electric field should be examined precisely by case studies.

(2) It is important to examine more precisely the characteristics of PPI and PI using one-second magnetic values.

(3) Effects of ionospheric and field-aligned currents should be clarified for the westward variation of

SC in the D-component in the morning hours.

(4) The characteristics of the generator for the DP_{mi}-field should be exactly clarified.

(5) The theoretical model to derive the dawn-to-dusk electric field for the DP_{mi}-field at the magnetopause should be de developed.

It should be kept in mind that the magnetic data should be converted to the geomagnetic dipole coordinate system to make the analysis exactly. For the conversion, the absolute values of the magnetic fields are used to decide the local declination angle. I would like to note that the absolute measurements in the routine magnetic observations remain to be necessary for the quantitative analysis of the solar wind-magnetosphere-ionosphere relationships.

Acknowledgments

The author thanks Prof. T. Araki, Dr. T. Iyemori and Dr. M. Takeda of Kyoto University, Dr. T. Kikuchi of Communications Research Laboratory and Mr. Y. Yamada of the Kakioka Magnetic Observatory for their encouragements and useful discussions for this study. He also thanks Dr. Takeda of Kyoto University, for supporting to make the ionospheric conductivity model using the computer system of Kyoto University.

The author would like to appreciate Prof. K. Yumoto of Kyushu University, the PI of the 210° magnetic meridian network project, for his courtesy of supplying one-minute magnetic data through Solar-terrestrial Environment Laboratory (STEL) of Nagoya University. The magnetic data in the Siberian region of the 210° magnetic meridian network were contributed by Prof. E. F. Vershinin of Institute of Cosmophysical Research and Radiowaves Propagation (IKIR) and Prof. S. I. Solovyev of Institute of Cosmophysical Research and Aeronomy (IKFIA) in Russia.

The routine observatory data for case studies were copied from the CD-ROMs of INTERMAGNET 'Magnetic Observatory Definitive Data', 1992 and 1993 and those from 1985 to 1992 at CLF, FRD, TUC, SJG, and HON were supplied from WDC-C2 for Geomagnetism of Kyoto University.

The basic part of the list files of SSC and SI at Kakioka was made by Mr. A. Okamoto of the Kakioka Magnetic Observatory and Dr. S. Fujita of Meteorological College. The data processing and a numerical calculation were operated using Data Processing and Analysis System for Geomagnetism of the Kakioka Magnetic Observatory.

References

Ahn, B.-H., Y. Kamide, and S.-I. Akasofu, Electric changes of the polar ionosphere during magnetospheric substorms, J. Geophys. Res., 91, 5737-5754, 1986.

Araki, T., Global structure of geomagnetic sudden commencements, Planet. Space Sci., 25, 373-384, 1977.

Araki, T., A physical model of the geomagnetic sudden commencement, in Solar Wind Sources of Magnetospheric Ultra-Low-Frequency Waves, edited by M. J. Engebreston, K. Takahashi, and M. Scholer, pp. 183-200, Geophysical Monograph 81, 1994.

Araki, T. and H. Ishizaki, Characteristics of SC* in the low latitude region, IAGA Bulletin No. 34, 138, 1973.

Araki, T., T. Iyemori, S. Tsunomura, T. Kamei, and H. Maeda, Detection of an ionospheric current for the preliminary impulse of the geomagnetic sudden commencement, Geophys. Res. Lett., 9, 341-344, 1982.

Araki, T., T. Iyemori, and T. Kamei, Sudden commencements observed by MAGSAT above the ionosphere, J. Geomag. Geoelectr., 36, 507-520, 1984.

Araki, T., J. H. Allen, and Y. Araki, Extension of a polar ionospheric current to the nightside equator, Planet. Space Sci., 33, 11-16, 1985.

Araki, T., S. Fujitani, M. Emoto, K. Yumoto, K. Shiokawa, T. Ichinose, H. Luehr, D. Orr, D. K. Milling, H. Singer, G. Rostoker, S. Tsunomura, Y. Yamada, and C. F. Liu, Aanomalous sudden commencement on March 24, 1991, J. Geophys. Res., 102, 14075-14086, 1997.

Baker W. G. and D. F. Martyn, Electric currents in the ionosphere, I. The conductivity, Phil. Trans. R. Soc., A 246, 281-294, 1953.

Banks, P. M. and G. Kockarts, Aeronomy, Part A, Academic Press, 1973.

Blake, J., W. A. Kolasinski, R. W. Fillus, and E. G. Mullen, Injection of electrons and protons with energies of tens of MeV into L<3 on 24 March 1991, Geophys. Res. Lett., 19, 821-824, 1992.

Brekke, A. and J. Moen, Observations of high latitude ionospheric conductances, J. Atmos. Terr. Phys., 55, 1493-1512, 1993.

Chapman, S. and J. Bartels, Geomagnetism, Vol.1 Geomagnetic and related phenomena, Oxford Univ. Press, London, 1940.

Denisenko V. V., and S. S. Zamay, Electric field in the equatorial ionosphere, Planet. Space Sci., 40, 941-952, 1992.

Fejer, B. G., Equatorial ionospheric electric fields associated with magnetospheric disturbances, in Solar Wind- Magnetosphere Coupling, edited by Y. Kamide and J. A. Slavin, pp. 519-545, Terra Scientific Publishing Company, Tokyo, 1986.

Fejer, B. G., Low latitude electrodynamic plasma drifts: a review, J. Atmos. Solar-Terr. Phys., 53, 677-693, 1991.

Fejer, B. G., The electrodynamics of the low-latitude ionosphere: recent results and future challenges, J. Atmos. Solar-Terr. Phys., 59, 1465-1482, 1997.

Fejer, B. G., and L. Scherliess, Empirical models of storm time equatorial zonal electric fields, J. Geophys. Res., 102, 24047-24056, 1997.

Fejer, J. A., Semidiurnal currents and electron drifts in the ionosphere, J. Atmos. Terr. Phys., 4, 184-203, 1953.

Forbes, J. M., and R. S. Lindzen, Atmospheric solar tides and their electrodynamic effects – I. The global Sq current system, J. Atmos. Terr. Phys, 38, 897-910, 1976a.

Forbes, J. M., and R. S. Lindzen, Atmospheric solar tides and their electrodynamic effects – II. The equatorial electrojet, J. Atmos. Terr. Phys, 38, 911-920, 1976b.

Forbush, W. E. and E. H. Vestine, Daytime enhancement of size of sudden commencements and initial phase of magnetic storms at Huancayo, J. Geophys. Res., 60, 299-316, 1955.

Fujii, R. and T. Iijima, Control of the ionospheric conductivities on large-scale Birkeland current intensities under geomagnetic quiet conditions, J. Geophys. Res., 92, 4505-4513, 1987.

Fujii, R., T. Iijima, T. A. Potemra, and M. Sugiura, Seasonal dependence of Large-scale Birkeland currents, Geophys. Res. Lett, 8, 1103-1106, 1981.

Fujita, S., Monitoring of time changes of conductivity anomaly transfer functions at Japanese magnetic observatory network, Mem. Kakioka Mag. Obs., 23, 53-87, 1990.

Fujiwara, S. and H. Toh, Geomagnetic transfer functions in Japan obtained by first order geomagnetic survey, J. Geomag. Geoelectr., 48, 1071-1101, 1996.

Fukushima, N., Equivalence in ground geomagnetic effect of Chapman-Vestine's and Birkeland-Alfvén's current systems for polar magnetic storms, Rep. Ionos. Space Res. Japan, 23, 219-227, 1969.

Fukushima, N., Generalized theorem for no ground magnetic effect of vertical currents connected with Pedersen currents in the uniform-conductivity ionosphere, Rep. Ionos. Space Res. Japan, 32, 35-40, 1976.

Fukushima, N., Some topics and historical episodes in geomagnetism and aeronomy, J. Geophys. Res., 99, 19113-19142, 1994.

Hanuise, C., C. Mazaudier, P. Vila, M. Blanc, and M. Crochet, Global dynamo simulation of ionospheric currents and their connection with the equatorial electrojet and counter electrojet: A case study, J. Geophys. Res., 88, 253-270, 1983.

Harel, M., R. A. Wolf, P. H. Reiff, R. W. Spiro, W. J. Burke, F. J. Rich, and M. Smiddy, Quantitative simulation of a magnetospheric substorm 1. Model logic and overview, J. Geophys. Res., 86, 2217-2241, 1981a.

Harel, M., R. A. Wolf, R. W. Spiro, P. H. Reiff, C-K. Chen, W. J. Burke, F. J. Rich, and M. Smiddy, Quantitative simulation of a magnetospheric substorm 2. Comparison with observations, J. Geophys. Res., 86, 2242-2260, 1981b.

Hirono, M., A theory of diurnal magnetic variations in equatorial regions and conductivity of the ionosphere E region, J. Geomag. Geoelectr., 4, 7-21, 1952.

Iijima, T. and T. A. Potemra, The amplitude distribution of field-aligned currents at northern high latitudes observed by Triad, J. Geophys. Res., 81, 2165-2174, 1976.

Iijima, T. and T. A. Potemra, Large-scale characteristics of field-aligned currents associated with substorms, J. Geophys. Res., 83, 599-615, 1978.

Itonaga, M., T.-I. Kitamura, O. Saka, H. Tachihara, M. Shinohara, and A. Yoshikawa, Discrete spectral structure of low-latitude and equatorial Pi2 pulsation, J. Geomag. Geoelectr., 44, 253-259, 1992.

Itonaga, M., K. Matsuzono, T.-I. Kitamura, I. Toshimitsu, N. B. Trivedi, R. Horita, T. Watanabe, and J. Riddick, Global structure of low-latitude and equatorial geomagnetic pulsations associated with sudden commencements, J. Geomag. Geoelectr., 47, 441-457, 1995.

Iyemori, T. and S. Tsunomura, Characteristics of the association between an SC and a substorm onset, Mem. NIPR Special Issue No. 26, 139-148, 1983.

Jacobs, J. A. and T. Watanabe, The equatorial enhancement of sudden commencements of geomagnetic storms, J. Atmos. Terr. Phys., 25, 267-279, 1963.

Jacobs, J. A., G. Rostoker, and T. Watanabe, World-wide propagetion of impulse micropulsation activity through the ionosphere, Nature, Lond. 205, 61-62, 1965.

Jain, A. R., and K. G. Srinivasacharya, Equatorial enhancement of SSC amplitudes: Solar activity dependence and effect of electric field, J. Geomag. Geoelectr., 28, 333-341, 1976.

Kamide, Y. and S. Matsushita, Simulation studies of ionospheric electric fields and currents in relation to field-aligned currents 1. Quiet periods, J. Geophys. Res., 84, 4083-4098, 1979a.

Kamide, Y. and S. Matsushita, Simulation studies of ionospheric electric fields and currents in relation to field-aligned currents 2. Substorms, J. Geophys. Res., 84, 4099-4115, 1979b.

Kamide, Y., A. D. Richmond, and S. Matsushita, Estimation of ionospheric fields, ionospheric currents, and field-aligned currents from ground magnetic records, J. Geophys. Res., 86, 801-813, 1981.

Kane, R. P., Equatorial enhancement of SSC magnitudes, J. Geomag. Geoelectr., 30, 631-646, 1978.

Kikuchi, T., Evidence of transmission of polar electric fields to the low latitude at times of geomagnetic sudden commencements, J. Geophys. Res., 91, 3101-3105, 1986.

Kikuchi, T. and T. Araki, Transient response of uniform ionosphere and preliminary reverse impulse of geomagnetic storm sudden commencement, J. Atmos. Terr. Phys., 41, 917-926, 1979a.

Kikuchi, T. and T. Araki, Horizontal transmission of the polar electric field to the equator, J. Atmos. Terr. Phys., 41, 927-936, 1979b.

Kikuchi, T. and T. Araki, Preliminary positive impulse of geomagnetic sudden commencement observed at dayside middle and low latitudes, J. Geophys. Res., 90, 12195-12200, 1985.

Kikuchi, T., T. Araki, H. Maeda, and K. Maekawa, Transmission of polar electric fields to the equator, Nature, Lond. 273, 650-651, 1978.

Kikuchi, T., T. Ishimine, and H. Sugiuchi, Local time distribution of HF Doppler frequency deviations associated with storm sudden commencements, J. Geophys. Res., 90, 4389-4393, 1985.

Kikuchi, T., H. Lühr, T. Kitamura, O. Saka, and K. Schlegel, Direct penetration of the polar electric field to the equator during a DP2 event as detected by the auroral and equatorial magnetometer chains and the EISCAT radar, J. Geophys. Res., 101, 17161-17173, 1996.

Kokubun, S., R. L. McPherron, and C. T. Russell, Triggering of substorms by solar wind discontinuities, J. Geophys. Res., 82, 74-86, 1977.

Kuboki, T., and H. Oshima, The anomaly of geomagnetic variation in Japan (Part 2), Mem. Kakioka Mag. Obs., Suppl. 2, 32-54, 1966. (in Japanese)

Kuwashima, M., Accuracy in geomagnetic measurements of Japanese magnetic observatories, Phys. Earth Planet. Inter., 59, 104-111, 1990.

Maeda, H. and K. Maekawa, A numerical study of polar ionospheric currents, Planet. Space Sci., 21, 1287-1300, 1973.

Maeda, H. and M. Yamamoto, A note on daytime enhancement of the amplitude of geomagnetic-storm sudden commencements in the equatorial region, J. Geophys. Res., 65, 2538-2539, 1960.

Maeda, H., T. Iyemori, T. Araki, and T. Kamei, New evidence of meridional current system in the equatorial ionosphere, Geophys. Res. Lett., 9, 337-340, 1982.

Maeda, K., and S. Fukao, Study on the solar activity dependence of the E-region peak Electron density and some atmospheric parameters, J. Geomag. Geoelectr., 24, 289-301, 1972.

Maekawa, K., Global distribution of electric fields and currents in the ionosphere produced by field-aligned currents of magnetospheric origin - I, J. Atmos. Terr. Phys., 42, 673-682, 1980.

Maekawa,K., and H. Maeda, Electric fields in the ionosphere produced by polar field-aligned currents, Nature, 273, 649-650, 1978.

Marriott, R. T., A. D. Richmond, and S. V. Venkateswaran, The quiet-time equatorial electrojet and counter-electrojet, J. Geomag. Geoelectr., 31, 311-340, 1979.

Matsushita, S., On sudden commencements of magnetic storms at higher latitudes, J. Geophys. Res., 62, 162-166, 1957.

Matsushita, S., On sudden commencements of geomagnetic storms using IGY data from United States stations, J. Geophys. Res., 65, 1423-1435, 1960.

Matsushita, S., On geomagnetic sudden commencements, sudden impulses, and storm durations, J. Geophys. Res., 67, 3753-3777, 1962.

Matsushita, S. and H. Maeda, On the geomagnetic solar quiet daily variation field during the IGY, J. Geophys. Res., 70, 2535-2558, 1965a.

Matsushita, S. and H. Maeda, On the geomagnetic lunar daily variation field, J. Geophys. Res., 70, 2559-2578, 1965b.

MID-LATITUDE GEOMAGNETIC INDICES ASY and SYM (PROVISIONAL) No.1 1989-1990, Data Analysis Center for Geomagnetism and Space Magnetism, Faculty of Science Kyoto University, May 1992.

Mori, T., Conductivity anomalies in the eastern part of Hokkaido, Japan, Mem. Kakioka mag. Obs., 16, 79-93, 1975.

Musmann, G. and E. Seiler, Detection of meridional currents in the equatorial ionosphere, J. Geophys., 44, 357-372, 1978.

Nagata, T., Distribution of SC* of magnetic storms, Rep. Ionos. Res. Japan, 6, 13-30, 1952.

Nagata, T. and S. Abe, Notes on the distribution of SC* in high latitudes, Rep. Ionos. Res. Japan, 9, 39-44, 1955.

Nagata, T., S. Kokubun, and T. Iijima, Geomagnetically conjugate relationship of Polar geomagnetic disturbances –Particularly the distinct geomagnetic conjugacy between Syowa station in Antarctica and Reykjavik in Iceland, JARE 1956-1962, Sci. Rep., Ser. A, No. 3, 1966.

Nisbet, J. S., M. J. Miller, and L. A. Carpenter, Currents and electric fields in the ionosphere due to field-aligned auroral currents, J. Geophys. Res., 83, 2647-2657, 1978.

Nishida, A., Geomagnetic Dp2 fluctuations and associated magnetospheric phenomena, J. Geophys. Res., 73, 1795-1803, 1968a.

Nishida, A., Coherence of geomagnetic DP2 fluctuations with interplanetary magnetic variations, J. Geophys. Res., 73, 5549-5559, 1968b.

Nishida, A. and J. A. Jacobs, Equatorial enhancement of world-wide changes, J. Geophys. Res., 67, 4937-4940, 1962.

Nishida, A., N. Iwasaki, and T. Nagata, The origin of fluctuations in the equatorial electrojet; a new type of geomagnetic variations, Ann. Geophys., 22, 478-484, 1966.

Nopper, R. W., Jr. and R. L. Carovillano, Polar-equatorial coupling during magnetically active periods, Geophys. Res. Lett., 5, 699-702, 1978.

Obayashi, T. and J. A. Jacobs, Sudden commencements of magnetic storms and atmospheric dynamo action, J. Geophys. Res., 62, 589-616, 1957.

Obayashi, T. and A. Nishida, Large-scale electric field in the magnetosphere, Space Sci. Rev., 8, 3-31, 1968.

Okamoto, A., and S. Fujita, Statistics on the geomagnetic phenomena observed at Kakioka, Mem. Kakioka Mag. Obs., 22, 21-42, 1987.

Oshima, H., On the subterranean electric structure near Kanoya, Mem. Kakioka Mag. Obs., 14, 87-92, 1972. (in Japanese)

Owada, S., On the subterranean electric structure near Memambetsu deduced by the magneto-telluric method, Mem. Kakioka Mag. Obs., 14, 77-85, 1972. (in Japanese)

Papamastorakis, I., G. Haerendel, and W. Baumjohann, Local time dependence of the response of the equatorial electrojet to DP2 and SI disturbances, J. Geophys., 54, 213-218, 1984.

Petrinec, S. M., K. Yumoto, H. Lühr, D. Orr, D. Milling, K. Hayashi, S. Kokubun, and T. Araki, The CME event of February 21, 1994: Response of the magnetic field at the Earth's surface, J. Geomag. Geoelectr., 48, 1341-1379, 1996.

PROVISIONAL GEOMAGNETIC DATA REPORTS No. 7 (July-December, 1992), Data Analysis Center for Geomagnetism and Space Magnetism, Faculty of Science Kyoto University, March 1993.

Rastogi, R. G., Equatorial E region electric field changes associated with a geomagnetic storm sudden commencement, J. Geophys. Res., 81, 687-689, 1976.

Rastogi, R. G., Longitudinal variation of sudden commencement of geomagnetic storm at equatorial stations, J. Geophys. Res., 98, 15411-15416, 1993.

Rastogi, R. G., Midday reversal of equatorial ionospheric electric field, Ann. Geophys., 15, 1309-1315, 1997.

Rastogi, R. G. and N. S. Sastri, On the occurrence of SSC (-+) at geomagnetic observatories in India, J. Geomag. Geoelectr., 26, 529-537, 1974.

Reddy C. A. and C. V. Devasia, Equivalent circuit analysis of neutral wind effects on equatorial electrojet, Nature, 273, 195-199, 1978.

Reddy, C. A., V. V. Somayajulu, and K. S. Viswanathan, Backscatter radar measurements of storm-time electric field changes in the equatorial electrojet, J. Atmos. Terr. Phys., 43, 817-827, 1981.

Reiff, P. H., Models of auroral-zone conductances, in Magnetospheric Currents, Geophys. Monogr. Ser., Vol. 28, edited by T. A. Potemra, pp. 180-191, AGU, Washington, D. C., 1984.

Richmond, A. D., Equatorial electrojet - I . Development of a model including winds and instabilities, J. Atmos. Terr. Phys., 35, 1083-1103, 1973.

Richmond, A. D., S. Matsushita, and J. D. Tarpley, On the production mechanism of electric currents and fields in the ionosphere, J. Geophys. Res., 81, 547-555, 1976.

Rikitake, T., and Y. Honkura, "Solid Earth Geomagnetism", Developments in Earth and Planetary Sciences 05, Terra Scientific Publishing Company, Tokyo, Japan, 1985.

Rikitake, T. and S. Sato, The geomagnetic Dst field of the magnetic storm on June 18-19, 1936, Bull. Earthq. Res. Inst., Univ. Tokyo, 35, 7-21, 1957.

Rostoker, G., Propagation of Pi2 micropulsations through the ionosphere, J. Geophys. Res., 70, 4388-4390, 1965.

Russell, C. T. and M. Ginskey, Sudden impulses at subauroral latitudes: Response for northward interplnetary magnetic field, J. Geophys. Res., 100, 23695-23702, 1995.

Russell, C. T., M. Ginskey, S. Petrinec and G. Lee, The effect of solar wind dynamic pressure changes on low and mid-latitude magnetic records, Geophys. Res. Lett., 19, 1227-1231, 1992.

Russell, C. T., M. Ginskey, and S. M. Petrinec, Sudden impulses at low-latitude stations: Steady state response for northward interplanetary magnetic field, J. Geophys. Res., 99, 253-261, 1994a.

Russell, C. T., M. Ginskey, and S. M. Petrinec, Sudden impulses at low latitude stations: Steady state response for southward interplanetary magnetic field, J. Geophys. Res., 99, 13403-13408, 1994b.

Saito, H., N. Sato, Y. Tonegawa, T. Yoshino, and T. Saemundsson, Seasonal and diurnal dependence of Pc 3-5 magnetic pulsation power at geomagnetically Conjugate stations in the auroral zones, J. Geophys. Res., 94, 6945-6948, 1989.

Sano, Y., Morphological studies on sudden commencements of magnetic storms using rapid-run magnetograms (including studies on sudden impulses) (2), Mem. Kakioka Mag. Obs., 11, 1-52, 1963.

Sarma, S. V. S. and T. S. Sastry, On the equatorial electrojet influence on geomagnetic pulsation amplitudes, J. Atmos. Terr. Phys., 57, 749-754, 1995.

Sastri, J. H., J. V. S. V. Rao, and K. B. Ramesh, Penetration of polar electric fields to the nightside dip equator at times of geomagnetic sudden commencements, J. Geophys. Res., 98, 17517-17523, 1993.

Sastri, J. H., Y. N. Huang, T. Shibata, and T. Okuzawa, Response of equatorial-low latitude ionosphere to sudden expansion of magnetosphere, Geophys. Res. Lett., 22, 2649-2652, 1995.

Sastri, J. H., M. A. Abdu, and J. H. A. Sobral, Response of equatorial ionosphere to episodes of asymmetric ring current activity, Ann. Geophys., 15, 1316-1323, 1997.

Senior, C. and M. Blanc, On the control of magnetospheric convection by the spatial distibution of ionospheric conductivities, J. Geophys. Res., 89, 261-284, 1984.

Sitar, R. J., C. R. Clauer, and E. Friis-Christensen, High-latitude ground-based response to sudden changes in solar wind dynamic pressure, J. Geophys. Res., 101, 27001-27013, 1996.

Somayajulu, V. V., L. Cherian, K. Rajeev, G.

Ramkumar, and C. R. Reddi, Mean winds and tidal components during counter electrojet events, Geophys. Res. Lett., 14, 1443-1446, 1993.

Spiro, R. W., R. A. Wolf, and B. G. Fejer, Penetration of high-latitude-electric-field effects to low latitudes during SUNDIAL 1984, Ann. Geophys., 6, 39-49, 1988.

Sugiura, M., The solar diurnal variation in the amplitude of sudden commencements of magnetic storms at the geomagnetic equator, J. Geophys. Res., 58, 558-559, 1953.

Sugiura, M., Compressional hydromagnetic waves in the ionosphere and the reversed impulse of a sudden commencement, SSC*, Program and Abstract for the XV IUGG general Assembly, Moscow, 369, 1971.

Sugiura M. and J. C. Cain, A model equatorial electrojet, J. Geophys. Res., 71, 1869-1877, 1966.

Sugiura, M. and S. Chapman, The average morphology of geomagnetic storms with sudden commencements, Abh. Akad. Wiss. Göttingen, Math.-phys., Kl., Sonderheft, Spec. Issue 4, 1-53, 1960.

Sugiura, M., and D. J. Poros, An improved model equatorial electrojet with a meridional current system, J. Geophys. Res., 74, 4025-4034, 1969.

Takahashi, K., S.-I. Ohtani, and K. Yumoto, AMPTE CCE observations of Pi2 pulsations in the inner magnetosphere, Geophys. Res. Lett., 19, 1447-1450, 1992.

Takeda, M., Three-dimensional structure of ionospheric currents produced by field-aligned currents, J. Atmos. Terr. Phys., 44, 695-701, 1982.

Takeda, M., and Y. Yamada, Simulation of ionospheric fields and geomagnetic field variation by the ionospheric dynamo for different solar activity, Ann. Geopys., 5, 429-434, 1987.

Takeda, M., Y. Yamada, and T. Araki, Simulation of ionospheric currents and geomagnetic field variations of Sq for different solar activity, J. Atmos. Terr. Phys., 48, 277-287, 1986.

Tamao, T., A hydromagnetic interpretation of geomagnetic SSC*, Rep. Ionos. Space Res. Japan, 18, 16-31, 1964.

Tarpley, J. D., The Ionospheric wind dynamo - I Lunar tide, Planet. Space Sci., 18, 1075-1090, 1970.

Tsunomura, S., On the conjugate relationships of the amplitudes of SSC's and SI's observed at Reykjavik and Syowa, Mem. Kakioka Mag. Obs., 23, 7-16, 1989.

Tsunomura, S., On the polarity of SSC and SI observed in low latitudes, Mem. Kakioka Mag. Obs., 26, 15-36, 1995.

Tsunomura, S., Characteristics of geomagnetic sudden commencement observed in middle and low latitudes, Earth, Planets and Space, 50, 755-772, 1998.

Tsunomura, S., Numerical analysis of global ionospheric current system including the effect of equatorial enhancement, Ann. Geophys., 17, 692-706, 1999.

Tsunomura, S. and T. Araki, Numerical analysis of equatorial enhancement of geomagnetic sudden commencement, Planet. Space Sci., 32, 599-604, 1984.

Tsunomura, S., T. Uwai, Y. Yamada, K. Hasegawa, F. Fukui, S. Toyodome, and M. Kuwashima, Characteristics of geomagnetic variations associated with low latitude auroras, Mem. Kakioka Mag. Obs., 24, 25-38, 1990.

Tsunomura, S., A. Yamazaki, T. Tokumoto, and Y. Yamada, The new system of Kakioka Automatic Standard Magnetometer, Mem. Kakioka Mag. Obs., 25, 3-32, 1994.

Untiedt, J., A model of the equatorial electrojet involving meridional currents, J. Geophys. Res., 72, 5799-5810, 1967.

Vasyliunas, V. M., The interrelationship of magnetospheric processes in Earth's Magnetospheric Processes, edited by B. M. McCormac, pp.29-38, D. Reidel, Norwell, Mass., 1972.

Vickrey, J. F., R. C. Livingston, N. B. Walker, T. A. Potemra, R. A. Heelis, M. C. Kelley, and F. J. Rich, On the current-voltage relationship of the magnetospheric generator at intermediate spatial scales, Geophys. Res. Lett., 13, 495-498, 1986.

Williams, D. J., E. C. Roelof, and D. G. Mitchell, Global magnetospheric imaging, Rev. Geophys., 30, 183-208, 1992.

WORLD DATA CENTER C2 FOR GEOMAGNETISM, Data Book Special Issue, No. 2, Kyoto Univ. and Inst. Of Space and Astronautical Sci., Japan, 1990.

Yamada, Y., M. Takeda, and T. Araki, Occurrence characteristics of the preliminary impulse of geomagnetic sudden commencement detected at middle and low latitudes, J. Geomag. Geoelectr., 49, 1001-1012, 1997.

Yanagihara, K., Estimate of the deep layer resistivity near Kakioka, Mem. Kakioka Mag. Obs., 12, 115-122, 1965. (in Japanese)

Yasuhara, F., Y. Kamide, and S.-I. Akasofu, Field-aligned and ionospheric currents, Planet. Space Sci., 23, 1355-1368, 1975.

Yokouchi, Y., Development of SD field with storm-time at Kakioka, Mem. Kakioka Mag. Obs., 8, 13-32, 1958.

Yumoto, K and the 210° MM Magnetic Observation Group, Initial results from the 210° magnetic meridian project-Review, J. Geomag. Geoelectr., 47, 1197-1213, 1995.

Yumoto, K and the 210° MM Magnetic Observation Group, The STEP 210° magnetic meridian network project, J. Geomag. Geoelectr., 48, 1297-1309, 1996.

Yumoto, K., Y. Tanaka, T. Oguchi, K. Shiokawa, Y. Yoshimura, A. Isono, B. J. Fraser, F. W. Menk, J. W. Lynn, M. Seto, and 210° MM Magnetic Observation Group, Globally coordinated magnetic observations along 210° magnetic meridian during STEP period: 1. Preliminary results of low latitude Pc3's, J. Geomag. Geoelectr., 44, 261-276, 1992.

Yumoto, K., H. Osaki, K. Fukao, K. Shiokawa, Y. Tanaka, S. I. Solovyev, G. Krymskij, E. F. Vershinin, V. F. Osinin, and 210° MM Magnetic Observation Group, Correlation of high- and low-latitude Pi2 magnetic pulsations observed at 210° magnetic meridian chain stations, J. Geomag. Geoelectr., 46, 925-935, 1994.

Yumoto, K., H. Matsuoka, H. Osaki, K. Shiokawa, Y. Tanaka, T. Kitamura, H. Tachihara, M. Shinohara, S. I. Solovyev, G. A. Makarov, E. F. Vershinin, A. V. Buzevich, S. L. Manurung, O. Sobari, M. Ruhimat, Sukmadradjat, R. J. Morris, B. J. Fraser, F. W. Menk, K. J. W. Lynn, D. G. Cole, J. A. Kennewell, J. V. Olson, and S.-I. Akasofu, North/south asymmetry of sc/si magnetic variations observed along the 210° magnetic meridian, J. Geomag. Geoelectr., 48, 1333-1340, 1996.

中低緯度における地磁気擾乱への極起源グローバル電離層電流系の寄与について

角村悟

概　　　要

極起源電離層電流系の特性を調べることは，中低緯度における地磁気擾乱の研究にとって重要である。この論文の目的は中低緯度で観測される地磁気擾乱に関わる極起源電離層電流系の性質を定量的に明らかにすることである。この論文は二つの部分で構成される。一つは赤道増加を含んだ極起源電離層電流系の数値解析，他方は中低緯度における地磁気急始部（ＳＣ）の特性調査にあてられる。後者は中低緯度におけるＳＣの地磁気変化への極起源電離層電流系の寄与を明らかにすることを目的としている。

第一部：

最初に，現実的な電離層電気伝導度モデルをいくらか簡略化して２次元球殻上での電離層電流の連続の方程式を数値的に解くことにより，グローバル極起源電離導電流への電気伝導度赤道域増加の影響が見積もられる。赤道域で電気伝導度が増加することによる遮蔽効果で電場が弱められるものの，はっきりした昼間側電離層電流の赤道増加が見られる。計算された電離層電流プロファイルはＳＣの preliminary impulse （ＰＩ）の観測された特性とほぼ良く合う。

次に，極起源電離層電流系の数値シミュレーションの現実的な解を得るのに適する２次元電離層層状伝導度を導出するモデル化手法が開発される。そのモデルは伝統的な薄層伝導度モデルを修正することにより導出される。赤道付近における伝導度テンソルの非対角成分の一つである$\Sigma_{\theta\phi}$を修正することが非常に重要であることが示される。その項は赤道における電離層電場のプロファイルに著しく影響する。提案されたモデルはＳＣの観測される電場・磁場の特長を良く再現する結果を出す。次に，新しいモデルが極起源電離層電流系に関わる３つの事項に応用される。はじめに，昼間の時間帯におけるＤＰ２振幅の緯度プロファイルが，Region 2 沿磁力線電流による電場キャンセル率を変えて調査される。Region 2 沿磁力線電流の総量が Region 1 のそれの０．５倍を越えると赤道増加が見られなくなることが示される。二番目に，夏至における電離層伝導度条件で両半球をカバーするグローバル電離層電流を計算することにより，磁場変化の南北非対称性が調査される。電流源として定電圧源が与えられたときに高緯度における磁場と伝導度との間に正の相関がはっきり見られることが示される。その関係は，電流源が定電流源であるとはっきりしないかむしろ逆の関係になる。最後に，太陽活動極大期および極小期における伝導度モデルによる結果を比較することにより，極起源電離層電流系の赤道での電場・磁場の太陽活動依存性が調べられる。結果はＳＣの赤道増加のＬＴプロファイルにおける太陽サイクル依存性の観測事実と良く合う。International Reference ionosphere （ＩＲＩ）モデルに基づく新しいモデルは磁気圏－電離圏結合問題の定量的調査にさらに応用することが可能である。

第二部：

１９５７年から１９９２年におけるＳＣの現象報告を使用して柿岡で観測されたＳ

Ｃの極性について統計解析が行われる。地磁気東向き成分（Ｄ成分）が地磁気北向き成分（Ｈ）下向き成分（Ｚ）と同様にほとんどの場合で正であることが示される。地磁気双曲子座標系に変換された磁場データに基づく統計ではＳＣにおけるＤ成分極性の明確なシフトはなかった。この結果は，Araki (1977) によって与えられたＳＣの極起源電離層電流系モデルと合う。しかしながら，女満別・柿岡・鹿屋の間の相関係数が，地磁気双曲子座標系への変換で常により高くなるわけではない。柿岡・鹿屋の女満別に対するＨ成分振幅比が午前の時間帯で異常な地方時変化をすることも示される。

午前の時間帯におけるＨ成分の変化特性を明らかにするために，中低緯度における定常磁場観測を用いた重ね合わせ解析が行われる。午前から午後の早い時間帯の中低緯度観測点でＳＣのＭＩの開始直後にＨ成分に負のパルスが重畳することが見出される。事例解析及び数値解析を行った後で，この負のパルスがＳＣのＭＩを起こす極起源電離層電流系による磁場変化であることが示唆される。ＳＣに関連する preliminary positive impulse （ＰＰＩ）が磁気圏圧縮による北向き磁場変化にこの負のパルスが重なることによって視覚化される見かけの変化であるという形態的解釈が提案される。高緯度電流源を夕方側に４時間ずらした数値計算で，１９９１年3月２４日のＳＣの変化形について可能な解釈が与えられる。最後に，中低緯度における磁場Ｄ成分がＳＣに関連する磁気圏－電離圏結合過程を大まかに見積もるのに使える可能性が提案される。